A STUDY OF LASER-BASED ULTRASONIC WAVE PROPAGATION IN COMPOSITES WITH METAL INSERTS USING WAVELET TRANSFORM

A Thesis Submitted

in Partial Fulfillment of the Requirements

for the Degree of

MASTER OF TECHNOLOGY

by

SANJAYA KUMAR SAHOO

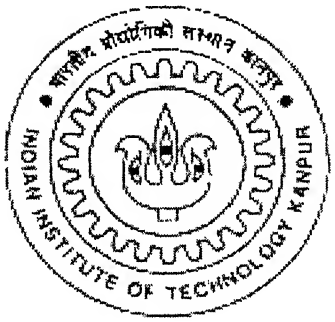

to the

DEPARTMENT OF MECHANICAL ENGINEERING

INDIAN INSTITUTE OF TECHNOLOGY, KANPUR

AUGUST 2002

CERTIFICATE

It is certified that the work contained in the thesis entitled "**A STUDY OF LASER-BASED ULTRASONIC WAVE PROPAGATION IN COMPOSITES WITH METAL INSERTS USING WAVELET TRANSFORM**" by **Mr. Sanjaya Kumar Sahoo** has been carried out under our supervision and that this work has not been submitted elsewhere for a degree.

(Dr. V. Raghuram)
Department of Mechanical Engineering
Indian Institute of Technology, Kanpur.

(Dr. N. N. Kishore)
Department of Mechanical Engineering
Indian Institute of Technology, Kanpur.

August 2002

DEDICATED

TO

MY BELOVED PARENTS

ACKNOWLEDGEMENTS

At the outset, I would like to express my deepest regards and most sincere gratitude to my teachers and thesis supervisors Dr. N. N. Kishore and Dr. V. Raghuram for their earnest involvement, active guidance and impetus, without which this work could not have seen the light of day. Their inspiration and support made my work successful.

I wish to express my special thanks to Dr. V. B. Shenoy and Mr. T. Sriram for their invaluable suggestions and constant encouragement towards the completion of my work.

I wish to thank especially Suraj, Chandan, Himanshu, Sanjib, Bhanu, Pradipta, Daliraju, Sarinji and Sarat sir who had always been so kind to me and took special interest to solve my problems. Perhaps words are not enough to acknowledge their help during my stay at IITK. I appreciate and extend my thanks to my other labmates, Nitesh, Samuel, Ashish and Ramkrishna for helping me to overcome my inadequacies with respect to computing and computational packages. I specially acknowledge them, who were always been source of my energy at IITK

I would like to thank Atul sir, Maya bhai, Rana bhai, Badjena, Saswat, Prafulla and all my batchmates for making my stay at Hall-V very enjoyable and memorable. I will really miss their company when I go out of campus.

I am very much thankful to Shri S. K. Trivedi, who prepared all test specimens and experimental fixtures in a very short time and professionally.

I remember with reverence the encouragement and moral support from my parents, brothers, sisters and sisters-in-law, who always remain behind the scene, but stood by me and provided support and inspiration through out this work, without which I would not have been able to reach this stage.

Sanjaya Kumar Sahoo

ABSTRACT

The non-homogeneous nature of composite materials induces a very high level of structural noise, which greatly complicates the interpretation of the NDE signals. Many researchers of ultrasonic testing (UT) view wave dispersion as noise when performing ultrasonic tests. However, significant information is present in the dispersion characteristics. Measurement of dispersion has the potential to separate the effects of inhomogeneities and damage or defects because of differences in structural level. Wavelet transform (WT) based time-frequency analysis makes it possible to investigate the dispersive character of structural waves. In this study, the thermoelastic waves induced in glass/epoxy composites with metal inserts by laser-based ultrasonics (LBU) are considered. The Morlet wavelet has been used as the analyzing wavelet. Changes in the appearance of wavelet scalograms and changes in the density of contour lines indicate the wave propagation through different regions of composites. In addition, the peaks of the time-frequency distribution indicate the arrival time of waves. By utilizing this fact, various defects can be identified by identifying the dispersion relation of the group velocity for a wide range of frequencies.

Keywords: Composites; Laser-based ultrasonics; Signal processing; Wavelet transform; Time-frequency analysis; Dispersive wave

CONTENTS

List of Figures

List Of Symbols

E_i	Energy levels
ν_p	Pumping frequency
T	Sampling period
Ω_S	Sampling frequency
$f(t)$	Signal in time-domain
t	Time
ω, ν	Frequency
F(ω)	Signal in frequency-domain
$w(t-b)$	STFT window function
a	Scaling parameter
b	Time-shift parameter
$\psi(t)$	Mother wavelet function
ω_0	Central frequency
$C(a,b)$	Wavelet coefficient
$s(t)$	Ultrasonic signal
$f(t)$	De-noised signal
$n(t)$	Noise
k_i	Wave numbers
c_p	Phase velocity
c_g	Group velocity

Chapter 1

INTRODUCTION

1.1 INTRODUCTION

Non-destructive testing (NDT) may be defined as the science of examining objects, materials or systems, in order to determine their fitness for certain purposes, without impairing their future usefulness or their desirable properties. The term is generally applied to non-medical investigations of material integrity. Non-destructive evaluation (NDE) of material plays a vital role in quality assurance of structural members during manufacturing stage and operating life. In general, the various NDE techniques can be placed into two categories: active and passive. The active techniques are those where something is introduced into or onto the specimen and a response is expected if a defect is present where as passive techniques are those that monitor or observe the item during either a typical load environment or a proof cycle and attempt to determine the presence of a defect through reaction of specimen. Magnetics, Ultrasonics, radiography fall in the category of active NDE and acoustic emission, noise analysis, leak testing etc. are the examples of passive NDE. Being one of the most commonly used non-destructive testing (NDT) methods, ultrasonic testing (UT) is rapidly developing in recent years. Ultrasonic inspection involves impinging a low energy, high frequency stress pulse into the material under inspection and examining the subsequent propagation of this energy. It not only detects bulk and surface flaws, but also obtains information on material microstructure to determine engineering properties, such as elastic moduli and ultimate tensile strength. However, traditional ultrasound requires liquid or contact coupling for its transmission, making it difficult or impossible to apply in many industrial situations. This occurs in particular on curved parts and on parts at elevated temperature, a situation widely found in industrial products and during the processing of industrial materials.

In conventional method, a piezoelectric transducer (or probe) generates ultrasonic waves, which propagate in the elastic medium and are detected either by the same (pulse-echo) or by a different transducer (through transmission). Although piezoelectric

transducers are commonly used for non-destructive testing, several problems are associated with the requirement that they have to be bonded to the test material with an acoustical impedance matching coupling medium. For velocity measurements, which are necessary for material thickness measurements and to locate the depth of defects, the coupling medium can cause transit time errors. Due to the partial transmission and partial reflection of the ultrasonic energy in the couplant layers, there may be a change of shape of the waveform, which can further affect the accuracy of the velocity measurement. This can also lead to serious errors in absolute attenuation measurements, which is the reason that so few reliable absolute measurements of attenuation are reported in the scientific literature. Therefore, a method of non-contact generation and detection of ultrasound is of great practical importance. Several such techniques are presently available in various stages of development, namely capacitive pick-ups, electromagnetic acoustic transducers (EMATS), laser beam optical generators and detectors, and more recently air (or gas) – coupled ultrasonic systems. However, as the name implies, capacitive pick-ups cannot be used as ultrasonic generators and, even when used as detectors, the air gap required between the pick-up and test structure surface is extremely small, which in essence causes the device to be very nearly a contact one. The problem with EMATS is that the efficiency of ultrasound generation and detection rapidly decreases with lift-off distance between the EMATS face and the surface of the test object. They can obviously be used only for examination of electrically conductive materials. Because of the physical processes involved they are much better detectors than generators of ultrasound. Laser-based ultrasound (LBU) generation and detection overcomes all of these problems and make truly non-contact ultrasonic measurements in both electrically conductive and non-conductive materials, in materials at elevated temperatures, in corrosive and other hostile environments, in geometrically difficult to reach locations, and do all of these at relatively large distances from the test object surface. Furthermore, lasers are able to produce simultaneously shear and longitudinal bulk wave modes, as well as Rayleigh and Lamb wave modes. LBU system uses a pulsed laser to generate ultrasound and a continuous wave (CW) laser interferometer to detect the ultrasound at the point of interrogation to perform ultrasonic inspection. Some of the important areas of application of LBU are:

- Medical field
- Microwave electronics
- Defect identification in a wide range of materials, including metals concrete, ceramics and composites etc.
- Aerospace industry
- Steel industry
- Nuclear reactors
- Microstructure analysis of ferrous and non-ferrous materials

An additional benefit of laser techniques is that they are capable of a high degree of absolute accuracy, since measurements can in principle be calibrated against the wavelength of light. There may be sensitivity penalties for using lasers rather than piezoelectric transducers or probes, and certainly they are likely to be more costly and complex to use. Nevertheless they are beginning to make a small but significant impact in a limited number of applications where their benefits over other probes outweight their disadvantages.

The various pops and bursts that appear in sensor output have physical causes, and in ultrasonic observations, the physics of the causes is typically well understood. Signal processing must exploit this understanding of new and relevant sensor output data, and to provide an indication of confidence in the results. Once the signature of interest is separated from everything else in the sensor signal, the identification of defects in a work piece is straightforward. Typically the work piece is scanned across a physical range by the sensor. Continuity of the mathematical properties of the signature across scans suggests a non-defective work piece. The appearance of an abrupt discontinuity suggests the presence of a defect.

The time-frequency analysis of time domain signals using wavelet transform has been started since early nineties. As far as the laboratory applications are concerned, the possibility of applying time-frequency analysis using wavelet transform in ultrasonic non-destructive application is providing the best results. The wavelet transform divides the signal into different frequencies/scales/levels in terms of basis functions obtained by dilation and translation of mother wavelet. Compared to other time-frequency representations like short-time Fourier transform (STFT) and Wigner-Ville distribution

(WVD), the wavelet transform (WT) provides spectral representations and temporal order of the signal component simultaneously. Another important property is that the signal reconstruction does not involve global averaging in time or frequency domains because of good localization of the wavelet coefficients in both domains.

1.2 LITERATURE SURVEY

Non-destructive evaluation of advanced composite materials poses a challenge to researchers and applied technologists. Ultrasonic methods, however, are most common and practiced widely because of the low cost, relative ease in their use and the amount of information that can be obtained from them. In this section, an overall review of processing of ultrasonic signals to enhance the confidence of identification of defects in composite materials is presented.

In ultrasonic techniques, information on defect characterization requires more evolved techniques than classical methods. Modern non-destructive testing of materials has to provide the highest possible detection probability, the correct size and exact orientation of defects in the specimen. The simplest acoustical characterizations of materials deal with velocity measurements. Some well-known techniques of calculating wave speed by measuring the time-of-flight are described in Krautkramer and Krautkramer [1]. Neslroth et al [2] introduced the idea of using various features of ultrasonic signal to detect various types of defects, flaws or anomalies in composite materials. Rose [3] introduced a concept of feature mapping. The basic concept is based on the fact that different types of defect are expected to interact distinctively with different features of ultrasonic signal. He proposed the Fischer linear discriminant function as a classifier, which uses linear combination of useful features to detect anomalies. Datta [4] proposed a methodology to experimentally detect defects using a two-dimensional automated Ultrasonic C-scan system. Both time and frequency domain features were extracted from the digitized data during scanning procedure. Multi-dimensional cluster analysis was used for effective grouping of datasets in a systematic manner leading to automatic image generation. Detection of ultrasound by optical means were motivated by the need to visualize and image the ultrasonic field. Sarin [5] and Daliraju [6] have developed an experimental set-up using an Nd: YAG pulsed laser for

generation of ultrasound in specimens and a He-Ne continuous laser based heterodyne optical interferometric probe for detection of the same. They have proposed a methodology for inspection of composite specimens using LBU and evaluation of effectiveness of different features of ultrasonic signals in detecting different types of defect. Scruby and Drain [7] in their introductory book on this subject have elaborated on the principles underlying generation and reception processes of all techniques used. Monchalin [8] has given an elaborate review on discussion of different techniques with reference to exploitation of the laser ultrasonic generation. The review covers knife-edge techniques, optical heterodyning, differential interferometry, and velocity (time-delay) interferometry methods. Corbel et al [9] have applied laser-generated ultrasound for the inspection of carbon-epoxy composite laminates. Transient elastic waves were launched thermo elastically in half cylindrical composite samples using a Q-switched Nd: YAG laser. The waves were detected with an optical heterodyne interferometer. Huang et al [10] showed that a laser-based ultrasonic system consisting of a tunable narrowband laser line array ultrasound generator and fiber-optic dual probe heterodyne interferometer can be used for detection of cracks and for tomographic imaging in thin plates. Castegnede et al [11] reviewed some advances dealing with the characterization of composite materials by using laser-based ultrasound techniques. They discussed laser interferometer detection and the determination of theoretical displacement fields. Jeong [12] has presented a new approach for the analysis of transient waves propagating in anisotropic composite laminates. He has applied wavelet transform using the Gabor wavelet to the time-frequency analysis of dispersive flexural waves in these plates. He has developed a method to obtain the group velocity of the flexural mode as a function of frequency. Legendre et al [13] have proposed a wavelet-based method to perform the analysis of NDE ultrasonic signals received during the inspection of reinforced composites. By combining the time domain and the classical Fourier analysis, the wavelet transform provides simultaneous spectral representation and temporal order of the signal decomposition components. To construct a C-scan image from A-scan signals, they have proposed a selection process of wavelet coefficients, followed by an interpretation procedure in the time-frequency domain. Cho et al [14] carried out an evaluation of sub-surface lateral defects using SAW (surface acoustic waves) generated by a Q-switched

YAG laser and monitored by a heterodyne laser interferometer. This fundamental work was carried out in thin metallic foil; the material's properties of the bonded layer can be estimated by the velocity dispersion of the Rayleigh wave, and the bond quality can be estimated by an analysis of the generalized lamb wave. Yamawaki [15] et al also demonstrated the applicability of LBU technique for a microscopic material evaluation in imaging experiments using specimens, which contain artificial sub-surface defects. Independent component analysis and feature extraction techniques for NDT data have been compared by Carlo [16] in his paper, which also proposes a combination of various types of features to cope with different situations. Monchalin et al [17] have demonstrated the applicability of laser ultrasonics to the steel industry: on line thickness gauging of seamless tubes and to the aeronautic industry: inspection of the composite structure of aircrafts. Rathore et al [18] have employed LBU and ray acoustics for establishing a criterion to identify the ray tangential to the defect boundary and evolve a method of reconstruction of the defects to estimate the size and location of the defect.

The analysis of wave propagation in structures is a fundamental issue related to a wide range of engineering problems such as analysis of impact response of structures, characterization of structures-borne noises, and ultrasonic identification of material properties. The Fourier transform has been extensively used for the analysis of dispersive signals. Recently, the wavelet transform has been introduced to the time-frequency representation of transient waves propagating in a dispersive medium. There has been intense research activity in the application of wavelets in various fields of science and engineering [19-22]. Kishimoto et al [23] applied the wavelet transform using the Gabor wavelet to the time-frequency analysis of flexural waves induced in beams by lateral impact. They have presented a new approach for investigating the dispersive character of structural waves. Suzuki et al [24] correlated the wavelet transform of AE signals to the fracture modes of fiber-reinforced composites. Abbate et al [25] utilized the wavelet transform to improve ultrasonic flaw detection in noisy signals as an alternative to the split-spectrum processing technique. Safizadeh et al [26] applied the time-frequency analysis for detection and measurements of the material loss due to corrosion in aircraft fuselage lap splices. Gaul et al [27] have developed a model experiment to identify the exact source location on the surface using synthetic acoustic emission (AE) signals. The

recorded signals are analyzed by wavelet transform in order to determine the arrival time of waves for several frequency levels. These arrival times are used to quantify the location of AE source in the surface as well as the velocity of the most dominant feature, the Rayleigh wave, and the time lag between the instant of AE and the recording of the signal. Peterson et al [28] have applied wavelet transform to study the material inhomogeneities and damage state in concrete. In their study, two complex wavelet functions, the Paul and Morlet have been investigated.

1.3 PRESENT WORK

The present investigation involves a study of ultrasonic wave propagation for non-destructive evaluation (NDE) of glass/epoxy composite specimens implanted with artificial inclusions like metal inserts. Brass, mild steel and aluminum have been used as inserts. In the present work, an Nd: YAG pulsed laser has been used for generation of ultrasound in specimens and a He-Ne continuous laser based heterodyne optical interferometric probe for detection of the same. The experimentation includes verification of calibration of the LBU set-up, and interfacing of the manual scanning set-up for scanning composite specimens and pure metals also.

Specimens were prepared with known defects such as metal inserts. Then A-scan signals were recorded for both defective and non-defective regions of specimens using LBU set-up. The wavelet transform using the Morlet wavelet as the mother wavelet has been applied to the time-frequency analysis of transient waves propagating in non-homogeneous and anisotropic composite specimens. A method is shown to identify the defect present in composites using the information extracted from wave data by the wavelet transform.

1.4 THESIS ORGANIZATION

The various chapters in this thesis deal with the following aspects.

Chapter 2 deals with the various aspects of laser-based ultrasonic technique.

Chapter 3 deals with the details of experimental set-up and data acquisition procedure.

Chapter 4 deals with different signal processing techniques and time-frequency analysis.

Chapter 5 presents results and discussion of the present work.

Chapter 6 finally concludes the present work and gives suggestions for future work.

Chapter 2

BASICS OF LASER ULTRASONICS

2.1 INTRODUCTION

Laser (Light Amplification by Stimulated Emission of Radiation) is a device that generates or amplifies light, just as transistors generate and amplify electronic signals at audio, radio or microwave frequencies. Here, light must be understood broadly, since lasers have covered radiation at wavelengths ranging from infrared range to ultraviolet and even soft x-ray range. The term ultrasonics is used to describe mechanical wave propagated in gases, liquids or solids at frequencies above the upper limit of human hearing i.e. 20KHz and up to 400MHz. Because the characteristics of these waves are influenced by the mechanical properties of any medium through which they pass, one can use ultrasonics to investigate the properties of that medium.

The laser-based ultrasonics (LBU) is the technique, in which laser beam interaction with the surface of the test sample is substituted for piezoelectric transducers for launching and probing elastic waves. Since they do not require any mechanical contact, these techniques are very attractive. For example, in the field of NDT, the association of laser generation with optical detection provides a completely remote ultrasonic system. Other fields of applications are: material evaluation, acoustic emission photo thermal microscopy and acoustic field imaging. According to the intensity of the laser, the impact generation method may be classed in two main categories: thermoelastic regime and ablation régime. In the field of NDT, surface damage is avoided by means of specific techniques. In concrete testing, the structure can tolerate some surface imperfection. There are different methods applied; for example, one uses shock waves, which are generated by laser impact on the sample and optical detection (interferometrics or non-interferometrics), which monitors the induced surface. Other methods are used incorporating contact ultrasonic probes working as receivers or transmitters. Hence, this method needs no contact medium and the source can be some meters away; it is used especially for applications such as NDT of systems at high temperature.

2.2 MAIN PROPERTIES OF LASER LIGHT

Lasers are characterized by a number of key optical properties, most of which play an important role in the interaction with ultrasonic fields. Their four major optical properties are:

(1) Monochromaticity
(2) Coherence
(3) Directionality
(4) High Intensity or Brightness

2.2.1 Monochromaticity

Monochromatic means the same frequency. Light from sources other than lasers covers a range of frequencies. True single-frequency operation of a gas laser can be achieved by careful design. Monochromaticity is reduced by multimode operation of a laser. A small He-Ne laser generally has three or four longitudinal modes excited with a spacing of a few hundred MHz, depending on the cavity length. This still gives a bandwidth of a few parts in 10^6. Solid-state lasers tend to have rather large frequency spreads.

Monochromaticity is important for some ultrasonic applications, in particular the interferometric measurement of ultrasonic fields. Firstly, it is necessary in order to obtain high coherence, and secondly, it enables accurate absolute measurements of ultrasonic displacement to be made, since calibration is against the wavelength of the light. Monochromaticity is of less importance for the generation of ultrasound by laser.

2.2.2 Coherence

Coherence means the same order or as a copy of the other photon and in phase with the other photon. Coherence is an important property when it comes to building an optical system to detect ultrasonic waves. In simple words, coherence is used to describe how well a wave disturbance at one point in space or time correlates with the disturbance at another point. If there is a well defined phase relationship between the light at two different points in space (i.e. two light beams), or at two different times (i.e. one beam split into two with a delay between the parts, as is typical in an interferometer) then the two light disturbances can be brought together to produce a predictable interference

pattern. If the light is completely incoherent so that there is no predictable relationship (i.e. random phase) between the two disturbances, no interference fringes will be formed. Fig.2.1 shows the comparison between the ordinary light and laser light.

Coherence is important to the reception of ultrasonic waves by laser. Most techniques involve some form of interferometer, in which good coherence between probe and reference beam is essential. Coherence length is the distance of the origin of the beam to the farthest point at which the wave disturbance can be effectively correlated with the disturbance at its starting point. Conventional monochromatic light cannot be used because their coherence length is only of the order of millimeters. The use of a gas laser however enables use of a longer probe than reference beam. This means that a compact instrument (incorporating all except the probe beam) can be built, and that the distance to the sample is not critical.

2.2.3 Directionality

Directionality is a function of the spatial coherence of the beam of light. Laser beam is highly directional which implies laser light is of very small divergence because of the parallelism of the beam. The radiation produced by a laser is confined to a narrow cone of angles. The beam of divergence for a typical gas laser is of the order of 1 milliradian, although some commercial He-Ne lasers are available with divergences of a few tenths of a milliradian. Comparable beam divergences are now available from pulsed solid-state laser systems. It is only possible to attain such low beam divergence from conventional light sources by severe collimation, which leads to extremely low intensities. The diameter of the beam is typically about 1mm for a gas laser such as helium-neon, and in the range 1-20 mm for a pulsed solid-state laser.

The light from gas and solid state lasers thus forms a highly collimated beam which is extremely valuable for laser ultrasonics since it enables the beam to be focused to a very small spot. This means not only high spatial resolution, but also, in the case of ultrasonic displacement measurement by interferometer, the ability to collect a larger fraction of the scattered light from a rough surface, thereby increasing sensitivity. For laser generation it indicates that very high incident power densities are attainable. Low beam divergence also means that the beam can travel distances of the order of several

meters from the laser to the specimen without appreciable spreading and losses. Thus both laser generation and reception of ultrasound can be made genuinely remote techniques.

2.2.4 High Intensity or Brightness

Intensity or brightness of a light source is defined as the power emitted per unit area per unit solid angle. A laser beam is extremely intense, more intense than any other light source. This is perhaps the property for which lasers are best known outside the field of optics. Although the optical power output from a small helium-neon (He-Ne) laser may only be say 2mW, a beam diameter of 0.5mm leads to a power density of about 1 W cm^{-2}. Such a beam can readily be focused by a simple lens to a spot of diameter 0.05 mm because it is monochromatic and coherent. The incident power intensity is then 100 W cm^{-2}. Focusing optics produces a beam of sufficient intensity to melt, cut or weld structural materials.

Intensity is a most important property for laser reception of ultrasound, as sensitivity of a single mode laser interferometer system (defined as signal to noise ratio for a fixed bandwidth) increases with the square root of light intensity, provided other conditions remain constant. The limiting factor becomes the intensity at which the specimen is damaged or otherwise adversely affected by intense irradiation. Increase in power also brings penalties like increase in noise and multimode interference. Intensity is also a crucial factor in the generation of ultrasound by laser since incident power intensities typically in the range of 10^4-10^6 Wcm^{-2} are needed to act as a thermoelastic source of ultrasound. The laser energy per pulse largely controls the ultrasonic amplitude in the thermoelastic regime. The limiting factor is not the power that is available from commercial lasers, but rather the threshold for damage in the irradiated sample. Indeed, many pulsed lasers are too powerful for ultrasonic applications, and must be used at reduced power if the technique is not to be destructive.

2.3 BASIC PRINCIPLE OF LASER OPERATION

The laser is a device, which amplifies the intensity of light by means of a quantum process known as stimulated emission. A practical laser needs a means of amplification

(i.e. stimulated emission) and a means for feeding the energy back into the system to build up sustained oscillation. The operation of the simplest type of laser can be most readily understood in terms of a quantum mechanical model having say three energy levels E_0, E_1, E_2, such that $E_2>E_1>E_0$ (Fig.2.2). In reality, there may be more than three levels, but for present purposes, other levels are neglected. The ground state E_0 is well populated, whereas the intermediate and upper states are more sparsely populated. Suppose now the atom absorbs a quantum of incident radiation such that the atom is excited into the upper state. From quantum theory, the radiation must have a frequency ν_p such that

$$h\nu_p = E_2 - E_0 \tag{2.1}$$

Where h is the Planck's constant. In laser terminology this process of absorption is known as 'pumping', so that ν_p is the 'pumping frequency'. Pumping tends to equalize the population of two states so that E_2 becomes well populated. This reverses the normal occupancy of E_2 and E_1 and is known as population inversion. Emission (i.e. stimulated emission) can now occur in response to incident radiation, at a frequency ν given by

$$h\nu = E_2 - E_1 \tag{2.2}$$

It can be noted that necessarily $\nu_p \geq \nu$, so that the pumping frequency must always be equal to or higher than that of the radiation to be amplified. In order to obtain light of sufficient intensity for practical use, there has to be some mechanism for feeding the energy back into the laser system and thereby building up the amplitude of oscillations in a resonant system. The usual way of obtaining sustained oscillations is to site a high performance mirror at each end of the lasing medium. In the simplest system, both mirrors are plane, and accurately aligned perpendicular to the axis of the laser. Thus, the light can be reflected backwards and forwards through the lasing medium. On each pass it stimulates further emission from the medium and is thus amplified in intensity.

2.4 LASERS FOR ULTRASOUND GENERATION

The simple laser arrangement will operate in a pulsed mode if it is pumped for example by a pulsed flash tube. Depending on the type of laser, pulses of duration typically 100 μs to 1ms can be obtained. Although high-energy pulses can be produced in this way, the normal mode is not particularly useful for laser ultrasonics because the pulse duration is

too large. An additional technique, known as Q- switching or Q-spoiling, is needed to obtain pulses in the required 1-100ns range. The Q (quality) factor of a cavity resonator is the energy stored in the cavity divided by the energy lost from the cavity per round trip of the light within the cavity. Thus, if Q is low, the cavity oscillations are suppressed and the stored energy builds up within the lasing medium. When the Q is high, the cavity can support oscillations into which energy is supplied from the medium. Thus switching from low to high Q results in the rapid extraction of power from the laser cavity. Practical Q-switches are in the form of elements with variable absorption that are inserted between the mirrors. Two commonly used Q switches are the Pockels cell and bleachable (saturable) dye. Also of potential importance to non-contact ultrasonics are lasers that can be pulsed repeatedly. Adequate cooling in pulsed solid-state lasers is a problem. Hence gas lasers are preferred. However solid-state lasers can store higher individual pulse energies than gas medium lasers. Conventional ultrasonic inspection often uses repetition rates as high as 1-10 kHz for signal averaging purposes or for speed.

Laser generation of ultrasound does not impose very stringent conditions on the source laser. All that is required is the ability to deliver a reasonably high-pulsed energy density to a small area of the specimen, where the pulse length is in the range of 1-100 ns. As already mentioned, wavelength is not critical, nor is monochromaticity or coherence. Most researchers have employed a solid state laser, either ruby or Nd: YAG. The Nd: YAG laser has proved itself to be a versatile system under Q-switched conditions. Adequate pulse energy can be obtained from Nd: YAG lasers of modest size, while the pulse lengths are close to ideal for ultrasonic studies in metals. However, the fundamental wavelength (1064nm) is in the near infrared, which makes alignment more difficult than with a visible laser, in addition to increasing the risk of accidental eye damage. The Nd: YAG laser is available with frequency doubling to give several harmonics of the fundamental frequency. The frequency-doubled wavelength of 532 nm is in the middle of the visible spectrum, while the harmonics of 266nm and 355nm are in the ultraviolet zone.

2.5 LASERS FOR INTERFEROMETRY

For applications like interferometry, where wavelength purity and coherence are important, continuous wave lasers are to be designed with special optical components. The main problem is that a simple laser will excite a number of longitudinal and transverse modes. The result is that energy is amplified over a narrow range of frequencies instead of the desired single frequency, giving rise to intermode beat frequencies, and there is a variable distribution of energy across the beam. The generally preferred transverse mode (usually the lowest order mode with circular symmetry, TEM_{00}) can be selected, and higher order modes suppressed, by the use of at least one curved (concave) mirror at the end of the cavity and/or a suitable aperture within the cavity. A multi-mode laser can be employed to minimize the multi-mode problem of longitudinal wavelengths in interferometry and then a balanced detection system and adjustment of the path difference between the two arms of the interferometer can be used to minimize the effects of intermode beats if necessary.

The reception of ultrasound by laser is dependent upon all the fundamental properties of the laser: monochromaticity, coherence, directionality and high power density. Because of its ready availability and excellent optical characteristics, notably monochromaticity and coherence, the He-Ne laser has dominated much of the work. This system is however somewhat limited with regard to maximum power which controls sensitivity. The other choice is the argon ion laser, which not only can deliver higher power, but also inherently more sensitive because of its shorter wavelength. Argon ion lasers are however very bulky and noisy. The CW Nd: YAG laser is also available as a solid-state option, although it suffers from a number of drawbacks including bulk.

2.6 LASER-IRRADIATED ULTRASOUND MODES

Laser ultrasonics are based on the phenomenon that laser irradiation onto a solid surface generates ultrasonic waves in the solid. Fully non-contact generation and detection of ultrasonic waves can be realized by combining with optical (laser) interferometer for ultrasonic detection. Thus, laser ultrasonic NDE could be applied to materials and structures in hostile environments, such as very high temperatures, or to components having complex geometries. A laser emits a beam of coherent radiation, whose

wavelength may be in the infrared, visible or ultraviolet part of the electromagnetic spectrum. When this is incident on a solid sample, in general some of the energy is absorbed by various mechanisms, depending upon the nature of the sample and the frequency of the radiation, while the remainder is reflected or scattered from the surface. Three basic mechanisms have been illustrated below:

(I) The Thermoelastic Regime: At lower incident powers, electromagnetic radiation from the laser is absorbed in the surface region of a sample, causing localized heating as shown in Fig.2.3. Thermal energy then propagates into the specimen as thermal waves. The heated region undergoes thermal expansion and thermoelastic stresses generate elastic waves (ultrasound), which propagate deep within the sample. For typical Q-switched laser pulse durations, the thermal wave field only extends a few micrometers even in good conductors. Contrast the incidence of low frequency modulated light where the thermal field extends millimeters or centimeters and is itself useful for materials characterization.

(II) The Constrained Surface Source: Constrained surfaces include coating the surface with a thin solid layer of, for instance, paint or rust and roughness, covering the surface with a transparent solid such as glass, covering the surface with a transparent liquid, and finally constraining a thin layer of liquid between a transparent solid and the sample. All these four techniques for modifying the surface of the sample introduce large stresses normal to the surface, as shown in Figs.2.4 (a-d), which are otherwise absent for the thermo elastic source at a free source. The form of the ultrasonic source is thus substantially modified. The different combination of stresses generates a different ultrasonic sound field, with considerable enhancement in compression-wave amplitude, especially propagating normal to the surface. The constrained surface source generates a sound field more akin to that of ablation, but at lower power densities and without any damage. However, the need to constrain with for instance a liquid, reduce the usefulness of the laser ultrasonic source for many non-destructive applications.

(III) The Plasma Regime: At higher incident powers, surface melting and evaporation occurs, resulting in material ablation and the formation of plasma above the sample surface as shown in Fig.2.5. The momentum of the evaporated material exerts an opposite force on the sample, causing a reactive stress at the surface. This generates an intense broadband ultrasonic source, whose strongest components are, directed normal to the surface. The effects caused by the plasma generated in association with ablation in case of Q-switched lasers are:

- The plasma exerts a high pressure on the surface, which in turn suppresses vaporization of the material by raising the boiling point of the material well above its normal value.
- It absorbs light from the laser pulse, acting as a shield, but also becoming extremely hot.
- As it expands it produces an impulse reaction on the surface.
- It radiates some of its heat back on to the surface, maintaining its high temperature for some time after the incident laser pulse power has started to fall.

2.7 PRINCIPLE OF LASER INTERFEROMETRY

Optical interferometry is a very sensitive way of measuring displacement, but to be practicable for general use, it requires a highly monochromatic light source and thus the use of lasers is virtually essential. Interferometers for the detection of ultrasonic movements of waves may be divided into two main types. In the first type, light scattered or reflected from a surface is made to interfere with a reference beam, thus giving a measure of optical phase and hence instantaneous surface displacement. The second type of interferometer makes use of interference between a large number of reflected beams. This is designed as a high-resolution optical spectrometer to detect changes in the frequency of the scattered or reflected light. It thus gives an output dependent on the velocity of the surface. The first type is the more widely used and the most practical at lower frequencies and with reflecting surfaces. The second type offers a potentially higher sensitivity with rough surfaces, particularly at higher frequencies.

For the detection of ultrasonic waves at a surface, the techniques are admittedly insensitive compared with piezoelectric devices. They do, however, offer a number of advantages.

(1) They are non-contacting and thus do not disturb the ultrasonic field. The point of measurement may be quickly moved and there are no fundamental restrictions on surface temperature.

(2) High spatial resolution may be obtained without reducing sensitivity. The measurements may be localized over a few micrometers if necessary.

(3) As the measurements may be directly related to the wavelength of the light, no other calibration is required.

(4) They can have a flat broadband frequency response, something difficult to achieve with piezoelectric transducers, particularly at high frequencies.

2.8 HE-NE LASER HETERODYNE INTERFEROMETER

2.8.1 Working of Optical Heterodyne Probe

The system consists of a compact optical head and an electronic signal-processing unit. The optical layout is shown in Fig. 2.6. The laser beam emitted by the laser source, horizontally polarized, is directed in the interferometer by two deflecting mirrors. The laser beam is split into two parts by the beam-splitting cube. The *reference* beam is reflected by the beam-splitting cube and goes through the Dove prism. It is then transmitted by the polarizing beam-splitting cube and deflected by the mirror on the photodetector. The *probe* beam is transmitted by the beam-splitting cube and is horizontally polarized. Its optical frequency is shifted in the Bragg cell, and transmitted by the polarizing beam-splitting cube. A quarter wave plate transforms the horizontal polarization into circular polarization. The lens focuses the beam on the surface of the sample.

The probe beam is then phase modulated upon reflection on the sample by the mechanical displacement. After the second pass in the quarter wave plate, the direction of polarization becomes vertical. The probe beam is reflected by the polarizing beam-splitter on the photodetector. Just after the polarizing beam-splitter, the polarization of the probe

and reference beam are respectively vertical and horizontal. These two beams can therefore not interfere. The analyzer selects a common component at 45° of the two polarizations, thus allowing interference. The photodetector delivers a beat signal at the frequency of the Bragg cell phase modulated by the mechanical displacement of the object.

2.8.2 Principle of Detection

The complex amplitude of a laser beam of frequency f_L can be written as:

$$L = e^{2i\Pi f_L t} \tag{2.3}$$

This is divided in the interferometer into a reference beam and a signal beam, whose complex amplitude is:

$$R = r.e^{2i\Pi f_L t} \tag{2.4}$$

The reference beam does not experience any perturbation, however the signal beam experiences a frequency shift f_B in the Bragg cell. Upon reflection on the object, its phase is modulated by the displacement of the sample:

$$\varphi(t) = 4\pi.d(t)/\lambda \tag{2.5}$$

where, λ is the wavelength of the laser beam and d (t) the mechanical displacement of the object. The complex amplitude of the signal beam is therefore:

$$S = s.e^{2i\Pi f_L t + 2i\Pi f_B t + i\varphi(t)} \tag{2.6}$$

The interference of the two beams on the photodetector produces an electrical signal at frequency f_B, phase modulated by the displacement of the object:

$$I(t) = I_0 + i(t) \tag{2.7}$$

$$I(t) = k\cos(2\pi f_B t + \varphi(t)) \tag{2.8}$$

The useful signal is contained in the signal delivered by the photodetector as a phase modulation of the carrier frequency. The signal processor delivers an electric signal proportional to the displacement of the object. Half of the current i(t) is filtered at the frequency f_B, and phase shifted by 90°. It is then mixed with the other half, non perturbed, and yields a current:

$$j(t) \propto \cos(2\pi f_B t + \varphi(t)) \times \cos(2\pi f_B t + \pi/2) \tag{2.9}$$

$$j(t) \propto 1/2[\cos(4\pi f_B t + \varphi(t) + \pi/2) + \cos(\varphi(t) + \pi/2)] \tag{2.10}$$

The signal at the frequency $2f_B$ is filtered, to give:

$$s(t) \propto \sin \varphi(t) \tag{2.11}$$

If the displacement is very small compared to the optical wavelength, this signal can be written as:

$$s(t) = k.4\pi.\, d(t)/\lambda \tag{2.12}$$

The final electrical signal is therefore directly proportional to the displacement of the object.

2.8.3 Sensitivity

Laser ultrasonics suffers from a lack of sensitivity relative to conventional ultrasonics as the photon structure imposes a fundamental limit on the change in light levels during generation / detection of lasers.

Overall sensitivity to flaws is given by:

$$\text{Sensitivity} = T \times f(\sigma, A) \times R \tag{2.13}$$

Where T, $f(\sigma, A)$, R are terms related to the transmitted sound, the focal or imaging properties of the system determined by the flaw scattering σ and the focal aperture A, and the receiver sensitivity. The generated signal can be improved using tailored surface coatings or by increasing the power of the generating source. However, this approach is limited by the onset of ablation in the target.

2.9 CLOSURE

In this Chapter, the basic theory of generation of ultrasonic waves by lasers and their detection using laser-based interferometers has been presented. Some of the important properties of lasers related to aspects of generation and detection of ultrasonic waves have been discussed. Advantages of using laser-based detectors despite poor detectivity and sensitivity have also been explained.

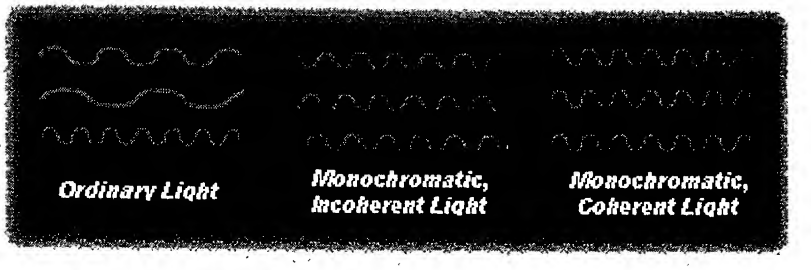

Fig.2.1 Comparison of ordinary light and laser light.

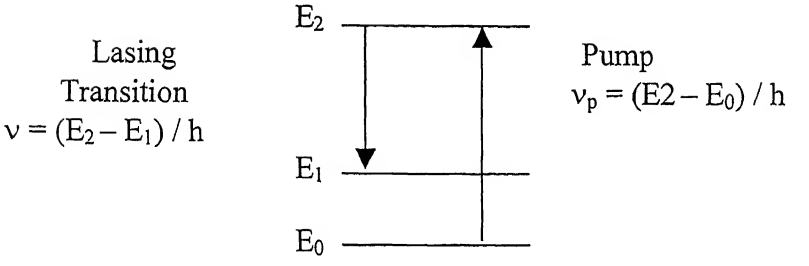

Fig.2.2 Simplified energy level diagram for a laser medium

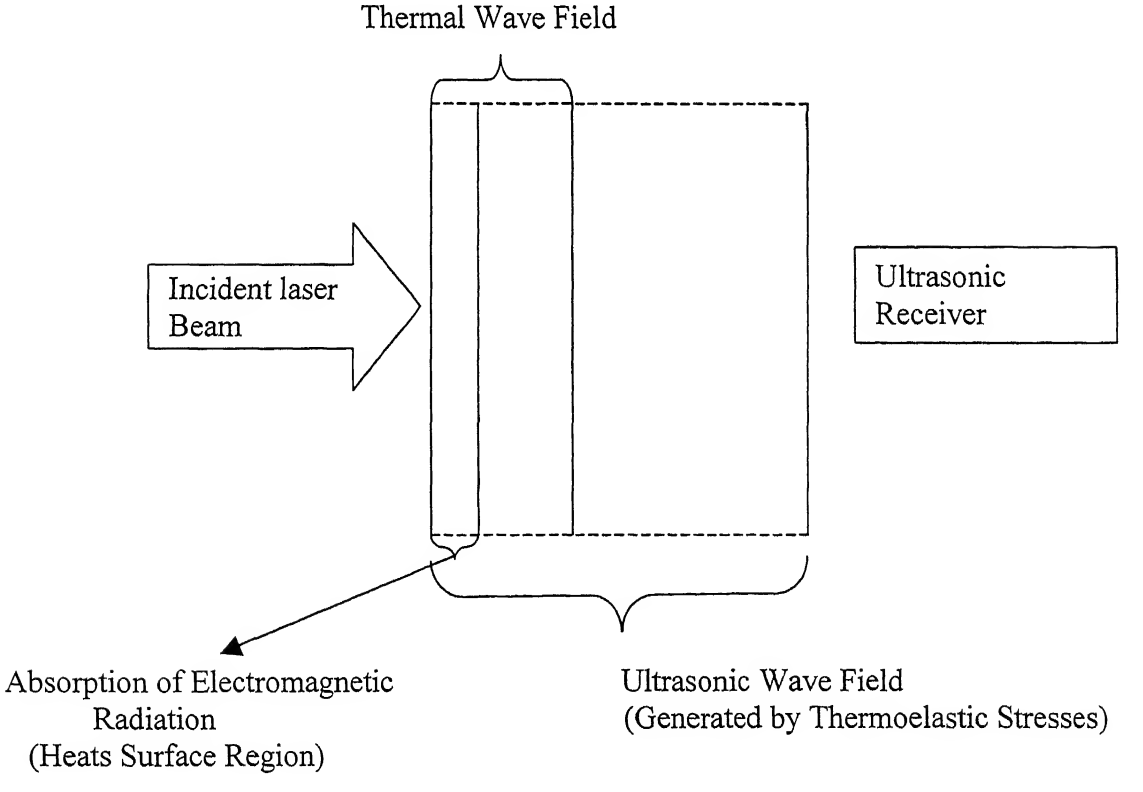

Fig.2.3 Thermoelastic regime

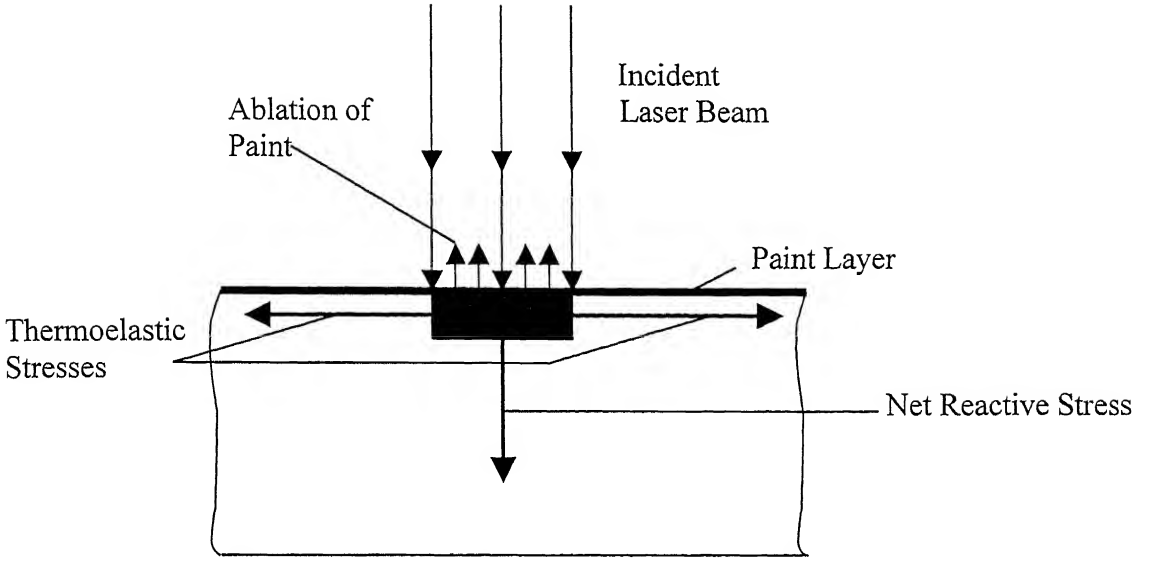

(a) Paint Layer

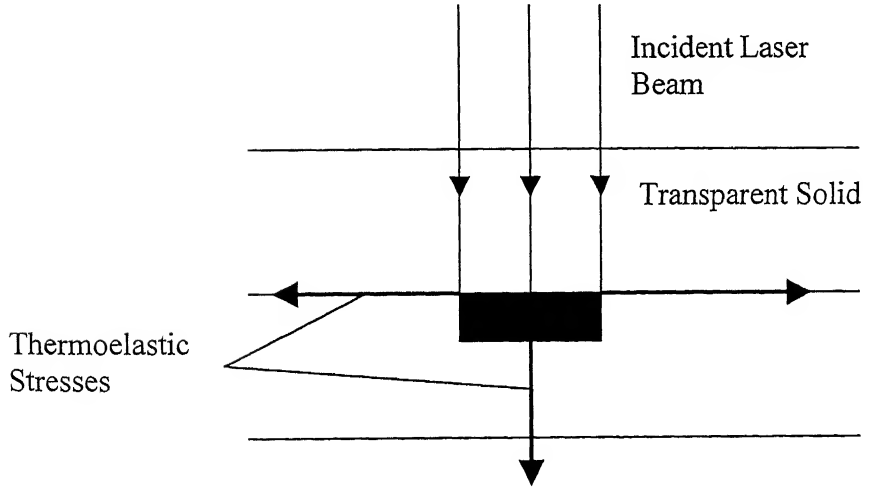

(b) Solid constraining layer

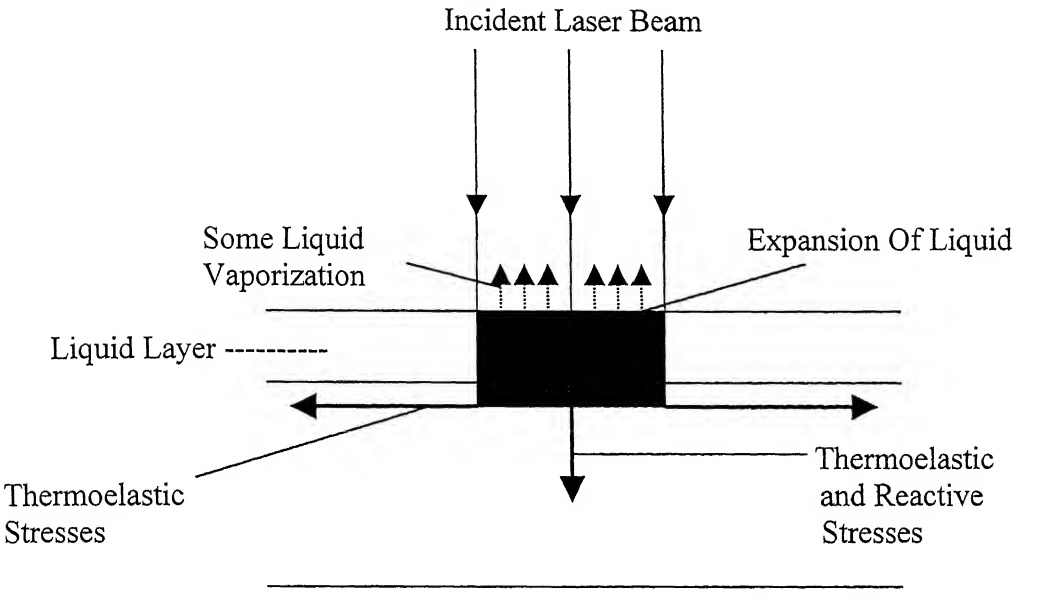

(c) Liquid Layer

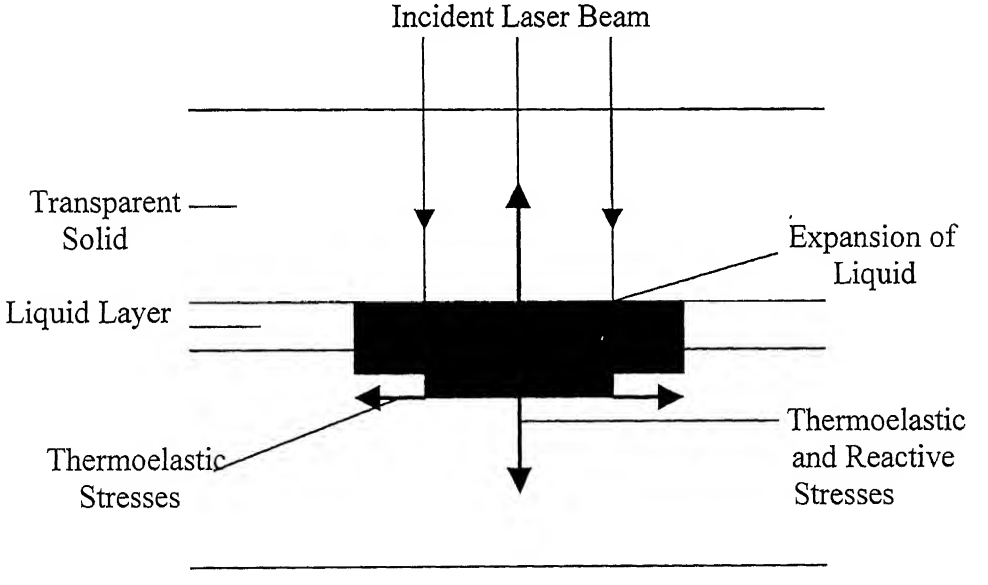

(d) Constrained Liquid Layer

Fig.2.4 Schematic diagram showing stresses induced when a laser pulse is incident on a sample surface covered by (a) a thin layer of paint, (b) a thick transparent solid (c) a layer of liquid (d) a layer of liquid constrained by a transparent solid.

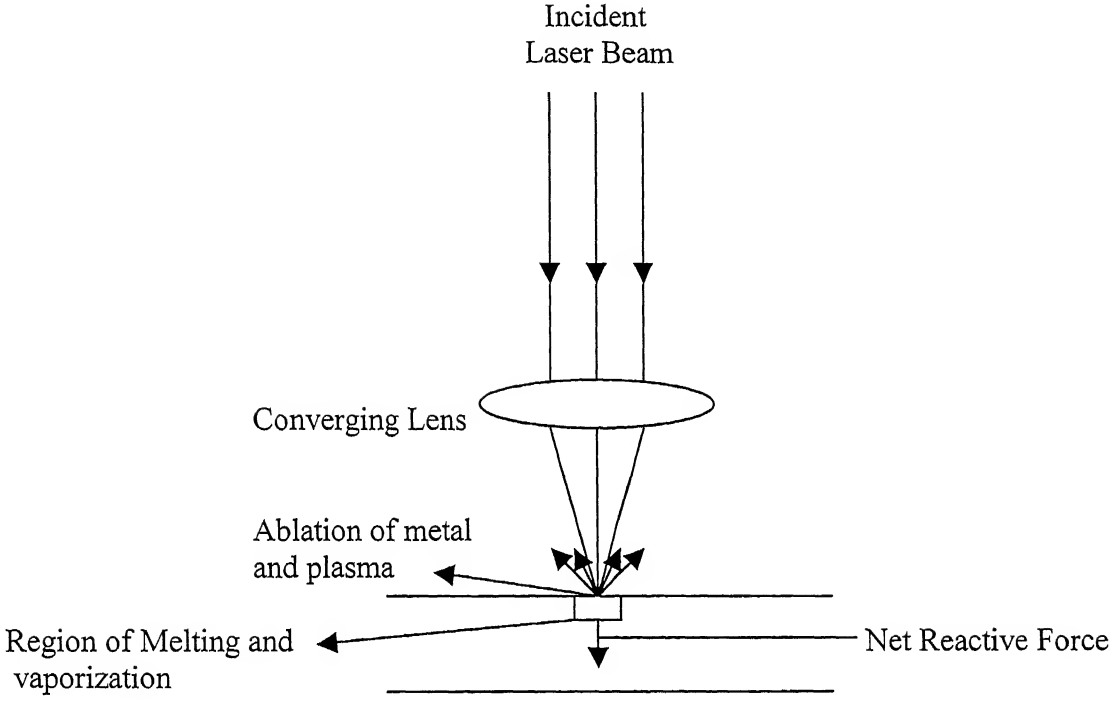

Fig.2.5 Schematic diagram to show ablation of surface material and net reactive force on sample.

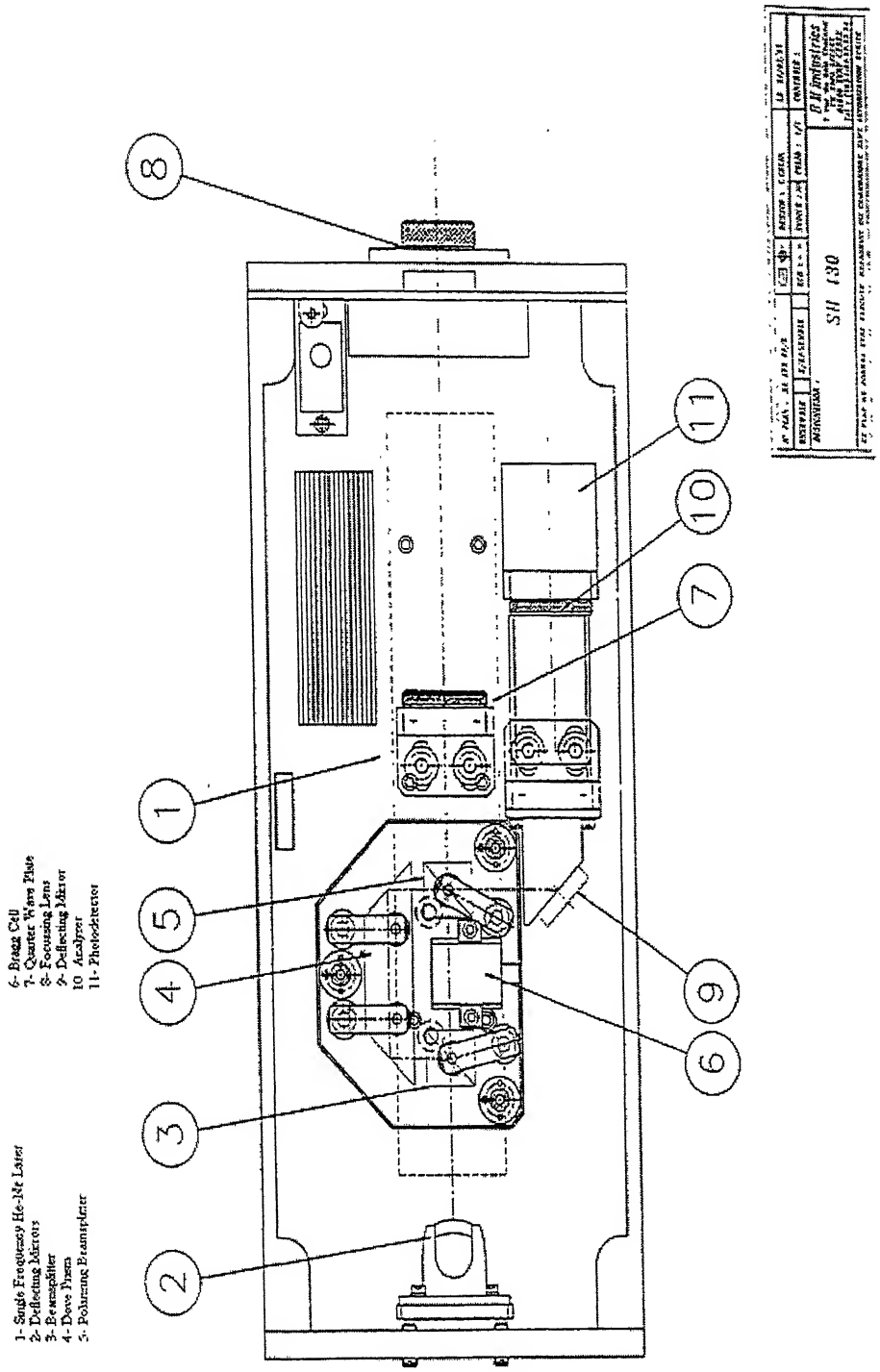

Fig.2.6 Optical Layout of Heterodyne Interferometer

Chapter 3

EXPERIMENTAL SET-UP AND PROCEDURE

This chapter briefly describes the details of laser-based ultrasonic (LBU) set-up, developed for non-destructive evaluation (NDE) of composite materials and data acquisition procedure.

3.1 EXPERIMENTAL SET-UP: LASER-BASED ULTRASONICS

Nd: YAG pulsed laser is used to generate ultrasonic waves in materials or objects to be inspected. Heterodyne type laser interferometer is used to detect the transmitted wave through the material; the signals are then amplified and digitized using a Yokogawa DL1740 Digital Storage Oscilloscope (DSO). The oscilloscope is triggered using a synchronization signal from the pockels cell of the pulsed laser. The recorded waveforms through DSO are transferred to a HP Pentium III computer over an USB/Ethernet interface for subsequent storage and analysis. The schematic layout of experimental set-up is shown in Fig.3.1 and photographs of the same are shown in Figs.3.2 (a) and (b). The scanning is done manually using two single axis micrometer controlled XYZ translator mounted on the Optical Test Bench. A brief description of the components of the present set-up is given in the following paragraphs.

3.1.1 Nd: YAG Pulsed Laser Ultrasonic Generator

The 5000 DNS series pulsed Nd: YAG laser is built on a modular concept. The optical configuration allows variable setting of the optical parameters. It consists of three major components, the laser-head, the power supply and the cooling unit. The heart of the system is the pumping structure, which houses the Nd: YAG rod and the flash lamp. The lasers are built on an electro-optically Q-switched oscillator. This oscillator uses a pockels cell Q-switch to produce pulses of high intensity and short duration (i.e. in the order of 5-7 ns). Q- Switched lasers are often used as a non-contact ultrasound source in non-destructive testing (NDT) of materials. Q-switched lasers typically have nanosecond

(ns) pulse durations and generate broadband ultrasound waves, though longer laser pulses of 100 microseconds or greater have been used for NDE. A variable reflectivity output coupler allows the extraction of high energy on a single spatial transverse mode. This leads to laser beams of low divergence, and to high conversion efficiencies in the harmonic wavelengths (1064, 532, 355, 266 nm). Different harmonic generators extend the wavelength range to the second, third and fourth harmonics.

The active medium of the laser operates on transitions of triply ionized Neodymium atoms (Nd3+), which take place of another ion (Yttrium) in the host: Yttrium Aluminum Garnet known by the acronym YAG. The laser operates as a 4-level system. The intense broad-spectrum light of the flash lamp populates the upper level. Once in the higher energy level, the Neodymium ions drop to a metastable level, producing a population inversion. The lower level decays by a fast non-radiative process to the ground state. The strongest Neodymium line is 1064 nm.

3.1.2 Optical Heterodyne Laser (He-Ne) Probe.

The SH-130 probe is designed to measure transient mechanical displacements of very low amplitude. It is specially devoted to measure displacements generated by the propagation of an acoustic or ultrasonic wave. The system consists of a compact optical head and an electronic signal-processing unit. The optical head integrates high stability, low power laser source for fast detection with a high spatial resolution.

The electronic signal processor delivers a response proportional to the displacement of the target, with a high bandwidth. The output signal is automatically calibrated to give the absolute value of the measured displacement. The principle of detection (heterodyne interferometry) makes the system insensitive to external vibrations. The compactness of the system allows for a wide range of operating conditions.

3.1.3 Digital Storage Oscilloscope

The set-up utilizes a Yokogawa DL1740 (four channel, one GSa/sec, 500 MHz) Digital Storage Oscilloscope, having built in Zip drive, Ethernet, USB, GPIB and Serial Ports for communication with external PC's/ systems.

3.1.4 Computer

The DSO is interfaced to a Pentium III based PC and the data is transformed on-line using communication ports (Ethernet).

3.2 EXPERIMENTAL PROCEDURE (LBU)

3.2.1 Calibration of Set-up.

The system was checked for calibration before scanning the specimen .The procedural steps involved to check for calibration are as follows:

(1) Alignment of the SH-130 Optical Probe: This involved optimizing the control signal by adjusting the orientation of highly reflective mirror and fine-adjustment of its distance from the focusing lens. (The focal length of the focusing lens is around 215 mm.)

(2) The photodetector output was measured without going through the signal processor. This was found to be 310 mV (as per specifications). The DSO image is shown in Appendix 'A'.

(3) The output was then taken through the signal processor with the automatic gain control switched on. The measured signal was found to be in excess of the stipulated signal level of 630 mV peak to peak on 50Ω (found to be 730 mV). This was adjusted using the adjustments available in the signal-processing unit. The DSO image is shown in Appendix 'B'.

3.2.2 Preparation of Specimens

The present ultrasonic non-destructive evaluation was done on composite specimens implanted with artificial inclusions like metal inserts. The specimens were prepared by hand lay up technique, using woven glass fabric as the reinforcing material and epoxy resin as the matrix material. Resin used being LY556, hardener HT976 and accelerator XY73 all manufactured by Ciba Geigy (India). The curing was done at 120° C and 5 atm pressure for one hour followed by one hour at 150° C and 5 Atm pressure and left to cool to room temperature at same pressure overnight.

The dimensions of the finished specimens were 50 x 50mm^2. Model specimens were prepared with a central aluminum, brass and mild steel insert to simulate presence

of flaws or defects. The metal inserts, square in shape, about 1mm in thickness was introduced centrally in the thickness direction (in between plies 16 and 24). All the specimens were cast with 40 plies with a final thickness of around 5 mm.

3.2.3 Scanning Procedure

The specimen to be investigated was cleaned and the area under investigation was marked. To get good signals, the portion of the specimen facing to the Ne-He laser was pasted with retro-reflective tape. The He-Ne laser was switched on to align the CW laser beam with the marked point of investigation to obtain good information regarding the wave propagation. Then the Nd: YAG laser was focused onto the specimen using an arrangement of optical mirrors and lenses (as shown in figure 3.1) so that it acts as a point source and is perpendicular to the irradiated face of the specimen. The alignment of Nd: YAG and He-Ne laser was ensured by focusing the Nd: YAG laser on the marked point of investigation on the opposite face of the specimen. The power level of the laser was adjusted to ensure thermoelastic region so that there was no ablation of the specimen. The scanning was performed at setting corresponding to 1064nm wavelength for the Nd: YAG laser. The He-Ne laser was focused on the opposite side of the specimen at the focal length of the collection lens (approx 215mm). The output of the Optical probe was fed to the electronic signal-processing unit. The electronic signal processor delivers a response proportional to the displacement of the target, with a high bandwidth. The output signal was automatically calibrated to give the absolute value of the measured displacement. This was fed to the Digital Storage oscilloscope (DSO) where it was displayed and storage of the data was carried out on-line in the PC interfaced to the DSO.

3.3 CLOSURE

In this Chapter, the details of experimental set-up and scanning procedure are presented for the Laser-Based Ultrasonic (LBU) set-up. Experimental procedure for data acquisition is also explained.

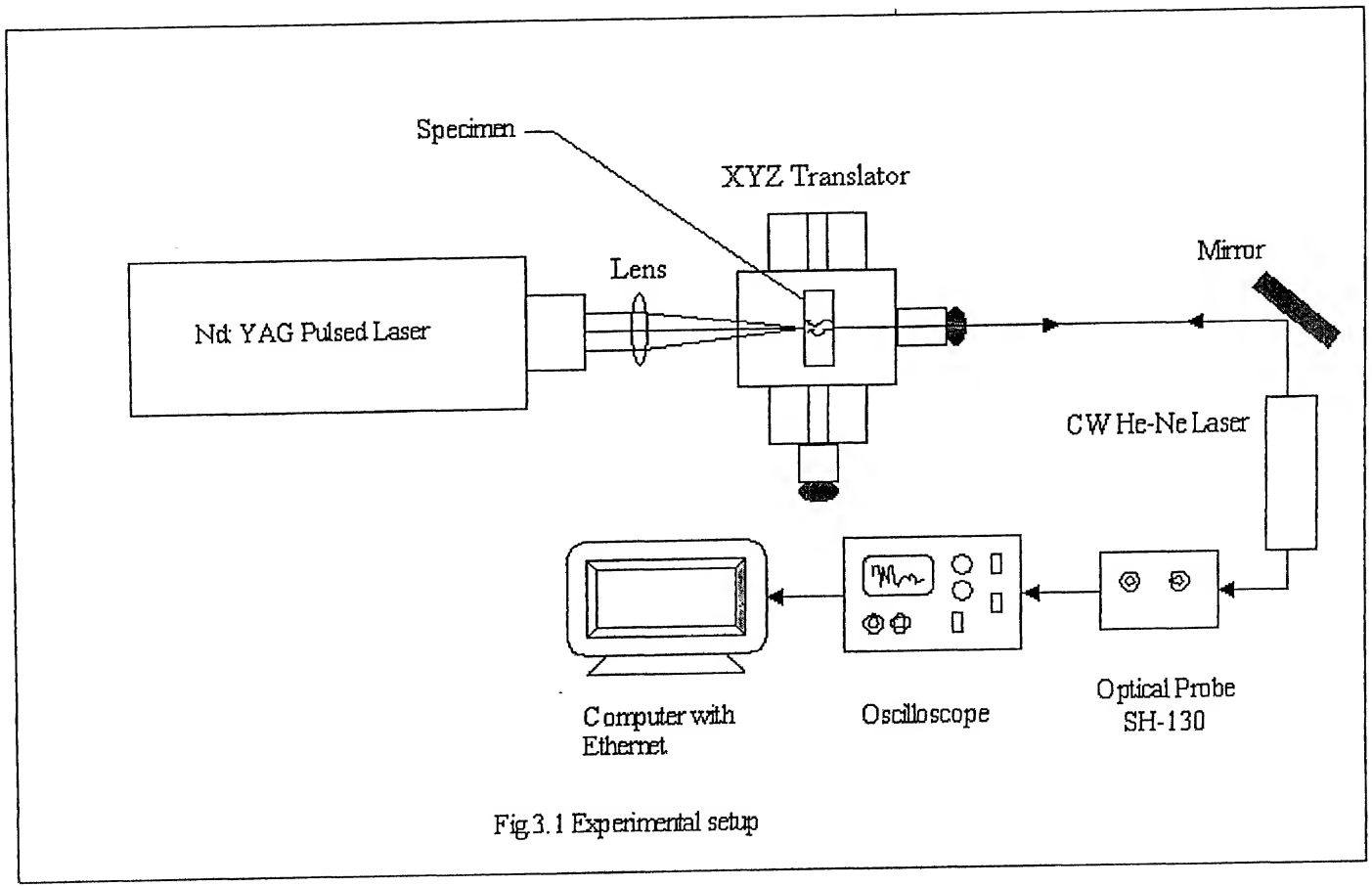

Fig.3.1 Experimental setup

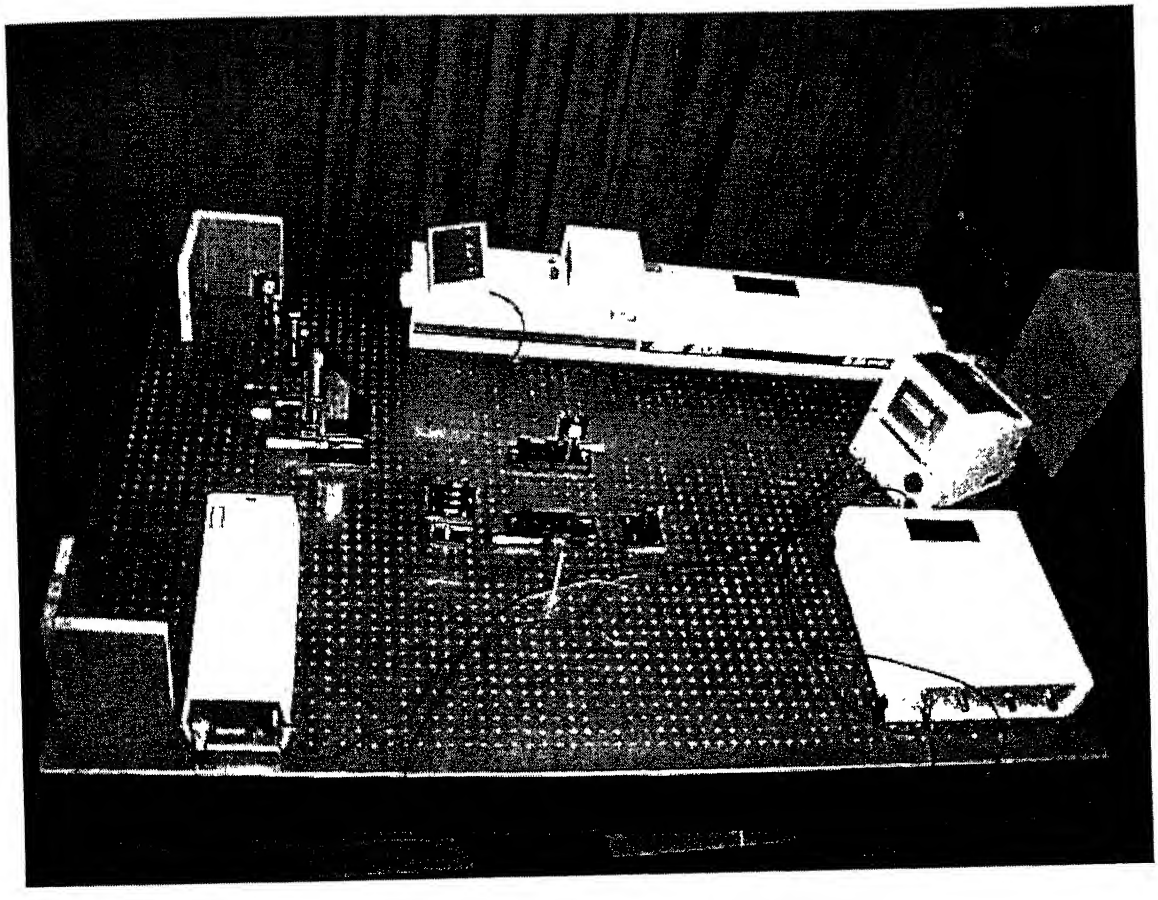

Fig.3.2 (a) Photograph of experimental set-up

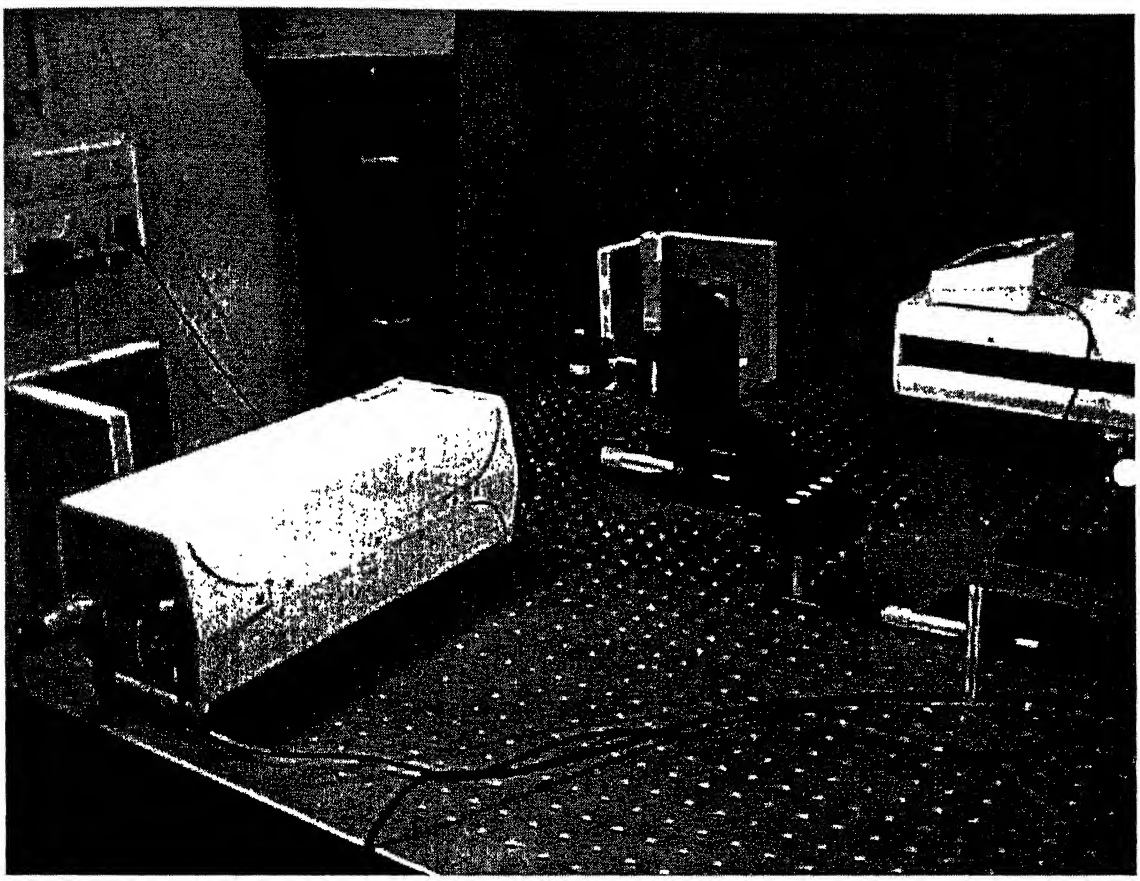

Fig.3.2 (b) Photograph of experimental set-up

Chapter 4

BASICS OF SIGNAL PROCESSING AND WAVELET TRANSFORM

4.1 INTRODUCTION

Composites may contain many types of damage modes, such as delamination, debonding, resin richness, fiber breaks, matrix cracking etc. either individually or in combinations. The variations in the type of flaw, local heterogeneity in the composite materials and other instabilities, cause statistical variation in the signal. To identify a particular damage type, specific information in the form of features, must be extracted from the signal. Each type of damage interacts with the signal in a unique way causing certain changes in the relevant features of it. These variations must be detected and quantified for being used in the identification process. In relation to ultrasonics, peak amplitude, time-of-flight, rise time, pulse duration, fall time, may be some of the time domain features and amplitude of different frequency components or harmonics, phase values may be the frequency domain features.

The Non-destructive testing aims to have the highest possible probability of detection, the most exact size and the exact orientation of defects. The possibility to acquire some information to characterize defects in nature, size and orientation has necessitated the development of techniques more evolved than those that are regrouped under the general technical term of ultrasonic imaging. In the present work, an algorithm has been used based on wavelet transform in order to enhance flaw visibility. Wavelet transforms have generated much interest in various applications such as speech coding, pitch detection, image compression, multi-resolution analysis and estimation of multiscale processes. The idea of examining signals at various scales and analyzing them with various resolutions has, in fact, emerged independently in many fields of mathematics, physics and engineering. Wavelet decomposition introduces the notion of scale as an alternative to frequency and maps a signal into a time-scale plane. Each scale

in the time-scale plane corresponds to a certain range of frequencies in the time-frequency plane. By combining the time domain and the classical Fourier analysis, the wavelet transform provides simultaneous spectral representation and temporal order of the signal decomposition components. Dispersion relation of the group velocity has been studied by using information extracted from wave data by the wavelet transform.

4.2 DIGITAL SIGNAL PROCESSING

Digital Signal Processing (DSP) concepts were introduced many years ago and later emerged as the primary means of detecting, conditioning and automatically classifying a variety of signal types. Unfortunately Ultrasonic Non-destructive Evaluation (UNDE) and UNDE Instrumentation development have not exploited the advantages offered by DSP implementations as much as one would expect. This is in spite of the fact that compared to analog signal processing systems; digital systems have the following advantages:

- Greater Signal Transmission Fidelity
- Large Non-volatile Storage capabilities
- Processing/calculation/classification capabilities, and
- More sophisticated filtering and signal analysis methods

4.2.1 Digitizing the Time Axis

A continuous time analog signal $x_a(t)$ has to be converted into a sequence of discrete time signals, represented by a sequence of numbers x, denoted x[n], with n being the n^{th} number in the sequence. Such a sequence is the result of periodic sampling of the continuous time analog signal $x_a(t)$,

$$x[n] = x_a(nT) \tag{4.1}$$

T is the sampling period, and 1/T the sampling rate or sampling frequency. For ultrasonic applications this is typically in the MHz range. The sampling frequency, $\Omega_S = (1/T)$, has

to be greater than the bandwidth Ω_N of the signal being sampled. More precisely, according to the Nyquist Sampling Theorem, for a correct representation of a digitized signal, the sampling frequency Ω_S has to be at least twice as high as the bandwidth Ω_N:

$$\Omega_S = 2\pi/T > \Omega_N \tag{4.2}$$

Under-sampling, or sampling at rates less than the Nyquist requirement will cause "aliasing", which results in "shadow frequency images" of the original signal.

4.2.2 Digitizing Signal Amplitude

The A/D converter performs the initial amplitude discretization for the input analog ultrasonic signal prior to further conversion needed during processing by either a fixed or floating-point signal processor. This conversion process quantizes the signal amplitudes into a sequence of finite-precision samples. The precision or quantization error is determined by the number of amplitude quantization levels. This quantization error can be represented as an additional noise signal component.

4.2.3 Time and Frequency

Fourier analysis is well known technique of signal processing, which breaks down the signal into constituent sinusoids of different frequencies. The *Fourier Transform* (FT) is a technique to transform time-domain signal f(t) into frequency- domain signal F(ω). Fig.4.1 shows an example of the *Fourier Transform*. Mathematically the *Fourier Transform* is given by

$$F(\omega) = \int_{-\infty}^{\infty} f(t) e^{-i\omega t} dt \tag{4.3}$$

and its inverse,

$$f(t) = \int_{-\infty}^{\infty} F(\omega) e^{i\omega t} d\omega \tag{4.4}$$

where, ω is the frequency. In *Fourier Transform,* the main drawback is that the time information is hidden. When looking at a FT of a signal, it cannot be seen when the particular spectral components appear exactly in the signal.

4.2.4 Short-Time Fourier Transform (STFT)

Short-Time Fourier Transform (STFT) is a modification of the Fourier transform. STFT analyzes a small section of the signal at a time. This technique is known as *windowing* of a signal. Fig. 4.2(a) shows transformation of a signal into two-dimensional function of time and frequency. Mathematically the STFT, with window function *w(t-b)* is expressed as

$$STFT(\omega) = \int_{-\infty}^{\infty} f(t) w(t-b) e^{-i\omega t} dt \tag{4.5}$$

where, w*(t-b)* is the analysis filter or analysis window. The STFT represents a compromise between the time-domain and frequency-domain views of a signal. It provides information about frequency content in the window of the signal at the given time. However, this information is obtained with limited precision, and that precision is determined by the size of the window. The drawback is that once a particular size is chosen for the time window, that window is the same for all frequencies. Many signals require a more flexible approach, where the window size can vary to determine more accurately in either time-domain or frequency-domain.

4.3 WAVELET TRANSFORM (WT)

Wavelet Transform, similar to the STFT, is the next logical step in which the windowing technique with variable sized regions is used. Wavelet transform allows both low frequency information with long time intervals and high frequency information with shorter regions. Fig. 4.2(b) shows that wavelet transform does not use a time-frequency region, but rather a time-scale region. Mathematically, the *Wavelet Transform* (WT) of a signal is defined as follows:

$$C(a,b) = \int_{-\infty}^{\infty} f(t) \frac{1}{\sqrt{a}} \psi^* \left(\frac{t-b}{a} \right) dt \tag{4.6}$$

where, $\psi(t)$ is a mother wavelet, b is a time shift parameter and a is a scaling parameter. By definition, the WT is the correlation between the signal and set of basic *Wavelets*.

Wavelet analysis produces a time-scale view of a signal, with scaling and shifting. *Scaling* a *Wavelet* means stretching (or compressing) it. Fig. 4.4 shows wavelets with different scaling parameters. Shifting a Wavelet simply means delaying (or hastening) its onset. Mathematically, delaying a function *f(t)* by *b* is represented by $f(t-b)$. Fig. 4.5 shows wavelets with different shift factors.

Wavelet analysis is capable of revealing aspects of data that other signal analysis techniques miss such as trends; break down points, discontinuities in the higher derivatives and self-similarity. Wavelet analysis can *compress or de-noise* a signal without appreciable degradation.

The wavelet transform comes in three different forms:

1. Continuous Wavelet Transform (CWT)
2. Discrete Wavelet Transform (DWT)
3. Wavelet Packets

4.3.1 Continuous Wavelet Transform (CWT)

The continuous wavelet transform (CWT) is developed as an alternative approach to the short time Fourier transform to overcome the resolution problem. The wavelet analysis is done in a similar way to the STFT analysis, in the sense that the signal is multiplied with the wavelet function ψ, similar to the window function in the STFT, and the transform is computed separately for different segments of the time-domain signal. However, there are two main differences between the STFT and the CWT:

1. The Fourier transform of the windowed signals are not taken, and therefore, single peak will be seen corresponding to sinusoid, i.e., negative frequencies are not computed.
2. The width of window is changed as the transform is computed for every single spectral component, which is probably the most significant characteristic of the wavelet transform.

The continuous wavelet transform is represented as follows:

$$C(a,b) = \int_{-\infty}^{\infty} f(t)\psi^{*}_{a,b}(t)\ dt \qquad (4.7)$$

where, C (a, b) are the coefficients of the wavelet transform, f *(t)* is the signal being analyzed and * denotes the complex conjugate of $\psi_{a,b}$. The scalogram of a signal is the squared magnitude of its wavelet transform i.e. $|C(a,b)|^2$. The locations of peaks in a scalogram provide information about the positions and duration of events in the original signal. For a two-dimensional function such as an image, this property corresponds to the ability of the CWT to provide information regarding the location and size of an object in the image. Here, $\psi_{a,b}$ is the shifted and scaled version of the mother wavelet $\psi(t)$ as given by,

$$\psi_{a,b}(t) = a^{-1/2}\psi\left(\frac{t-b}{a}\right),\ (a,b) \in R^2,\ a>0 \tag{4.8}$$

where, a is the scale (or dilation) factor, b is the translation factor and $\psi(t)$ is the mother wavelet. The scaled wavelets include an energy normalization term $(1/\sqrt{a})$, which keeps the energy (L^2-norm) of the scaled wavelet the same as the energy of the mother wavelet. To avoid the confusion often associated with terminology used in wavelet analysis, the scale factor can be described in terms of the central frequency (defined as the location of the peak of the Fourier transform) of the wavelet.

The word continuous in CWT means, that the transform operates the wavelets on the signal with continuous in scaling and shifting. During the computation, the analyzing wavelet is shifted smoothly over the full domain of the analyzed signal/function.

4.3.2 Discrete Wavelet Transform (DWT)

Calculating wavelet coefficients in CWT at every possible scale generates a very large amount of data. This disadvantage of CWT is overcome by choosing scales and positions based on powers of two, so called dyadic scales and position, which is more efficient and just as accurate. Such an analysis is called Discrete Wavelet Transform (DWT). The generation of the wavelets and calculation of the DWT are well matched to digital computer. The wavelet transform can also be expressed in discrete form

$$f(t) = A\sum_m \sum_n C_{m,n}\psi\left(\frac{t - na_0^m T}{a_0^m}\right) \tag{4.9}$$

where,

$$C_{m,n} = a_0^{-m/2} \int f(t)\psi\left(\frac{t - na_0^m T}{a_0^m}\right) dt \tag{4.10}$$

$$a = a_0^m$$

$$b = na_0^m T$$

where, T is the sampling period, A and a_0 are constants, where a_0=2 for the dyadic wavelet transform, m is depending upon the number of decomposition levels and n is depending upon the length of the signal to be decomposed.

4.3.3 Multi-Resolution Analysis (MRA)

Multi-resolution wavelet analysis allows the decomposition of a function/signal in progression of successive *approximation* and *details*, corresponding to different scales. The *approximations* are high-scale, low frequency components and the *details* are the low-scale, high frequency components of the signal. The difference between the actual signal and its approximation of order n is called its *residual*. Intuitively, the *approximation* is relatively smooth, and *detail* being composed of high frequency components. The *detail* corresponds to the difference between two successive levels of approximation.

4.3.4 Multiple-Level Decomposition

In DWT, the decomposition process can be iterated, with successive approximations being decomposed in turn, so that one signal can be broken into many lower-resolution components. This is called the *Wavelet decomposition tree*. Fig. 4.3 shows the Multi-level (three level) wavelet decomposition tree.

4.3.5 Wavelet Reconstruction

Wavelet reconstruction, or *synthesis* is the process of reconstructing the decomposed signal using a set of decomposed coefficients. The mathematical manipulation that affects synthesis is called the *inverse discrete wavelet transform* (IDWT).

4.3.6 Wavelet

A function $\psi(t)$ can be considered to be a wavelet if it is oscillatory, decaying and satisfies the following properties:

1. The function integrates (or averages) to zero:

$$\int_{-\infty}^{\infty} \psi(t)dt = 0 \tag{4.11}$$

2. It is square integrable or equivalently, has finite energy:

$$\int_{-\infty}^{\infty} |\psi(t)|^2 dt < \infty \tag{4.12}$$

3. It satisfies the admissibility condition:

$$\int_{-\infty}^{\infty} \frac{|\hat{\psi}(\omega)|^2}{|\omega|} d\omega < \infty \tag{4.13}$$

In the context of wavelet analysis, the transforming function $\psi(t)$ is called as *mother wavelet*. The term *mother* implies that the functions with different region of support that are used in the transformation process are derived from one main function or mother wavelet. In other words, the mother wavelet is a *prototype* for generating the other window functions. Different types of mother wavelets are discussed in the following paragraphs.

The simplest wavelet is *Haar* wavelet, which is a step function (Figs. 4.6(a) and 4.6(b)). Ingrid *Daubechies*, invented what are called compactly supported orthonormal wavelets. The names of the *Daubechies* family wavelets are written as *dbN*, where N is the order, and *db* is the "surname" of the wavelet. The *db1* wavelet is same as *Haar*. Figs. 4.6(c) through 4.6(p) shows the scaling and wavelet functions of the various Daubechies wavelets. In *Biorthogonal* wavelets two types of wavelet functions are used: one for decomposition and other for reconstruction instead of the same one. *Coiflets, Symlets, Morlet, Mexican Hat, Mayer* etc. are other different type of wavelets suitable for various purposes.

In this study, the Morlet function (known as Modulated Gaussian) is adopted as the analyzing wavelet because it provides smaller area of time-frequency window according to the uncertainty principle. The mother wavelet for the Morlet is given by:

$$\psi(t) = e^{i\omega_0 t} e^{-t^2/2} \tag{4.14}$$

and its Fourier transform is

$$\hat{\psi}(\omega) = \sqrt{2\pi} e^{-(\omega-\omega_0)^2/2} \tag{4.15}$$

where, ω_0 is a positive constant. Figs.4.7 (a) and (b) show the real and imaginary parts of the Morlet as well as the Fourier transform. The baby wavelets for the Morlet are:

$$\frac{1}{\sqrt{a}}\psi\left(\frac{t-b}{a}\right) = \frac{1}{\sqrt{a}} e^{i\omega_0\left(\frac{t-b}{a}\right)} e^{-\frac{1}{2}\left(\frac{t-b}{a}\right)^2} \tag{4.16}$$

Although the Morlet function does not satisfy the admissibility condition in the strict sense, it approximately satisfies the condition if ω_0 is sufficiently large. According to Flandrin, setting ω_0 between 5 to 6 (standard value 5.4285) results in the Morlet function being practically admissible. In addition, if eq. (4.14) is substituted into eq. (4.7), it is understood that the WT using the Morlet wavelet is equivalent to the Fourier transform with a Gaussian window. Therefore, the squared magnitude of the WT using the Morlet wavelet corresponds to the energy spectrum. In this study, ω_0 has been set to 2π such that the value of a is equal to the period of vibration.

4.3.7 Time-frequency resolution

The time-frequency resolution of wavelet transform can be determined from the time-frequency window associated with the wavelet. The center or mean value (t_0, ω_0) and deviations Δ_t and Δ_ω of the time-frequency window are given as follows.

$$t_0 = \int_{-\infty}^{\infty} t.\frac{|\psi(t)|^2}{\|\psi\|^2} dt \tag{4.17}$$

$$\omega_0 = \int_{-\infty}^{\infty} \omega.\frac{|\psi(\omega)|^2}{\|\psi\|^2} d\omega \tag{4.18}$$

$$\Delta_t = \left(\int_{-\infty}^{\infty} (t - t_0) . \frac{|\psi(t)|^2}{\|\psi\|^2} dt \right)^{\frac{1}{2}} \tag{4.19}$$

$$\Delta_\omega = \left(\int_{-\infty}^{\infty} (\omega - \omega_0) . \frac{|\psi(\omega)|^2}{\|\psi\|^2} dt \right)^{\frac{1}{2}} \tag{4.20}$$

where, $\psi(\omega)$ is the Fourier transform of the mother wavelet.

The center and the deviations of the scaled wavelet functions are related to those of the mother wavelet by

$$\left\{ at_0, \frac{1}{a}\omega_0 \right\} \qquad \text{and} \qquad \left\{ a\Delta_t, \frac{1}{a}\Delta_\omega \right\}$$

The time-frequency window is therefore given by

$$[b + at_0 - a\Delta_t, b + at_0 + a\Delta_t] \times \left[\frac{\omega_0}{a} - \frac{\Delta_\omega}{a}, \frac{\omega_0}{a} + \frac{\Delta_\omega}{a} \right] \tag{4.21}$$

The area of the window is independent of the scale and translation parameters, and depends only on the mother wavelet. From eq. (4.21), it is possible to see how the time and frequency resolution change with the width and height of the window. The difference between the time-frequency resolution of STFT and CWT are shown in the Fig.4.8.

4.4 NOISE SUPPRESSION

In Ultrasonic Non-destructive Evaluation (NDE), the observed ultrasonic signal $s(t)$ can be expressed as the sum of the two components.

$$s(t) = f(t) + n(t) \tag{4.22}$$

where, $f(t)$ is the signal of the defect and $n(t)$ is the noise. Noise removal is extremely important in the ultrasonic defect detection to identify the defects correctly. Optimal de-noising requires a more subtle approach called thresholding. This involves discarding only the portion of the details that exceeds a certain limit.

The main steps of the signal noise removal are:

1. Decomposition of the signal into coefficients,
2. Separation of the *approximation* and *detail* coefficients from the coefficients, and

3. Reconstruction of the de-noised signal from the *approximation* coefficients and their different levels of the noises from the *detail* coefficients.

A code for the noise suppression from the signal is available in Matlab. This gives the user options for variable Thresholding, like, fixed form thresholding, heuristic sure, rigorous sure, mini-max, penalize high, penalize medium, penalize low. It also facilitates selection of noise structure to be removed, i.e., unscaled white noise, scaled white noise and non-white noise. The signals received in the present case of laser ultrasonic set-up were found to have unscaled white noise. This option was used alongwith fixed form thresholding facility available in Wavelet toolbox (wave menu) in Matlab. All the recorded signals were de-noised before time-frequency analysis.

4.5 TIME-FREQUENCY ANALYSIS OF WAVE PROPAGATION

In this section, a brief review of the application of the wavelet transform (WT) to the time-frequency analysis of wave propagation is presented [24]. Considering two harmonic waves of unit amplitude and different frequency ω_1 and ω_2 propagating in the x-direction, given by

$$u(x,t) = e^{-i(k_1 x-\omega_1 t)} + e^{-i(k_2 x-\omega_2 t)} \tag{4.23}$$

where, k_1 and k_2 are wave numbers. Equation (4.23) can be rearranged as

$$u(x,t) = 2\cos(\Delta k x - \Delta\omega t)e^{-i(k_c x-\omega_c t)}, \tag{4.24}$$

where

$$k_c = (k_1 + k_{2)}/2,\ \omega_c = (\omega_1 + \omega_2)/2 \tag{4.25}$$

and

$$\Delta k = (k_1 - k_2)/2,\ \Delta\omega = (\omega_1 - \omega_2)/2\,. \tag{4.26}$$

If $\Delta\omega$ is sufficiently small such that $\omega_1 \cong \omega_2$, the phase velocity c_p and group velocity c_g at the frequency ω_c can be respectively defined as

$$c_p = \omega_c / k_c\ ,\ c_g = \Delta\omega / \Delta k \tag{4.27}$$

The WT of u (x, t) is given by

$$C(x,a,b) = \sqrt{a}[e^{-i(k_1 x-w_1 b)}\overline{\hat{\psi}(a\omega_1)} + e^{-i(k_2 x-\omega_2 b)}\overline{\hat{\psi}(a\omega_2)}] \tag{4.28}$$

Taking the magnitude of the WT, we obtain

$$|C(x,a,b)| = \sqrt{a}\left\{[\hat{\psi}(a\omega_1)]^2 + [\hat{\psi}(a\omega_2)]^2 + 2\hat{\psi}(a\omega_1)\hat{\psi}(a\omega_2)\cos(2\Delta kx - 2\Delta\omega b)\right\}^{1/2} \quad (4.29)$$

where, it is assumed that $\hat{\psi}(\omega)$ is a real function. Now let us consider the following two cases: (i) $\Delta\omega$ is sufficiently small and (ii) $\Delta\omega$ is sufficiently large.

(i) *The case of sufficiently small* $\Delta\omega$: In this case, u (x, t) may be considered as a wave with phase velocity c_p and group velocity c_g as shown in eq. (4.24). If $\Delta\omega$ is sufficiently small such that $\hat{\psi}(a\omega_1) \cong \hat{\psi}(a\omega_2) \cong \hat{\psi}(a\omega_c)$, we obtain

$$|C(x,a,b)| \cong \sqrt{2a}\left|\hat{\psi}(a\omega_c)\right|[1+\cos(2\Delta kx - 2\Delta\omega b)]^{1/2} \quad (4.30)$$

This result indicates that the magnitude of the WT takes its maximum value at a = $\frac{\omega_0}{\omega_c}$ and b = $\left(\frac{\Delta k}{\Delta\omega}\right)x = \frac{x}{c_g}$ on the time-frequency plane. In other words, the location of the peak on the time-frequency plane indicates the arrival time of the group velocity c_g at frequency $\omega_c = \omega_0/a$, i.e. $f = \omega_0/2\pi a$.

(ii) *The case of sufficiently large* $\Delta\omega$: In this case, a stationary vibration composed of two harmonics with frequencies ω_1 and ω_2 may be observed. The wavelet function $\psi(t)$ is localized around $\omega = \omega_0/a$. If $\Delta\omega$ is sufficiently large such that $\hat{\psi}(a\omega_1)\,\hat{\psi}(a\omega_2) \cong 0$, one can obtain

$$|C(x,a,b)| = \sqrt{a}\left\{[\hat{\psi}(a\omega_1)]^2 + [\hat{\psi}(a\omega_2)]^2\right\}^{1/2} \quad (4.31)$$

It follows that the magnitude of the WT reveals two peaks at $a_1 = \frac{\omega_0}{\omega_1}$ and $a_2 = \frac{\omega_0}{\omega_2}$ regardless of b. Therefore, two frequency components ($1/a_1$ and $1/a_2$) will be represented as two separate peaks on the time-frequency plane.

Fig. 4.1 Fourier Transform for transforming a time-domain signal to frequency-domain

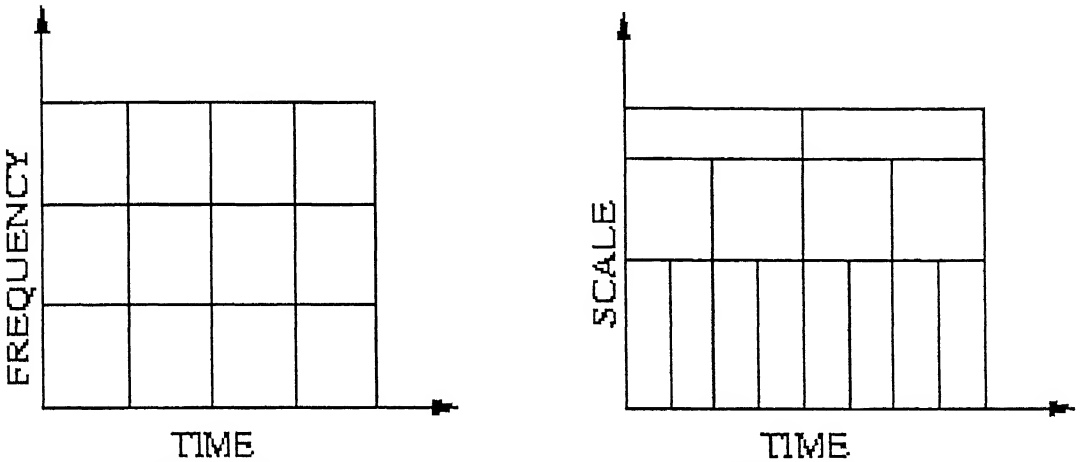

(a) STFT (Gabor) (b) Wavelet Analysis

Figs. 4.2(a-b) Short-Time Fourier Transform (Time-frequency domain), Wavelet Transform (Time-scale domain)

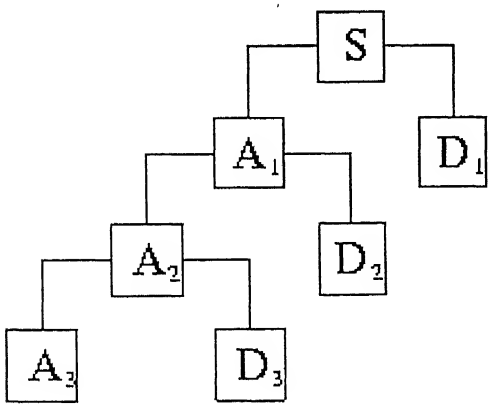

$$S = A_1 + D_1$$

$$= A_2 + D_2 + D_1$$

$$= A_3 + D_3 + D_2 + D_1$$

Fig. 4.3 Multiple-Level Wavelet decomposition tree with three-level decomposition

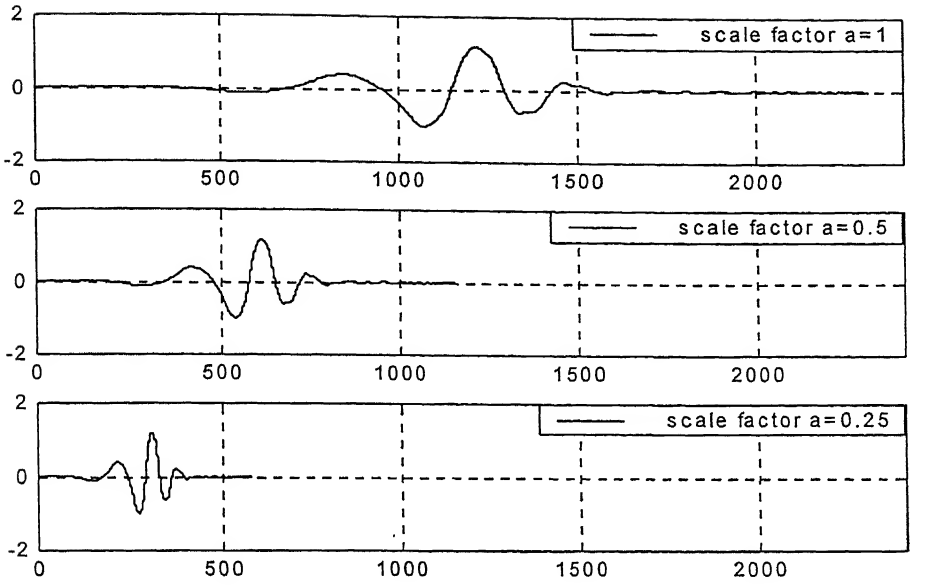

Fig. 4.4 Scaling (stretching or compression) of the wavelets with different scale factors

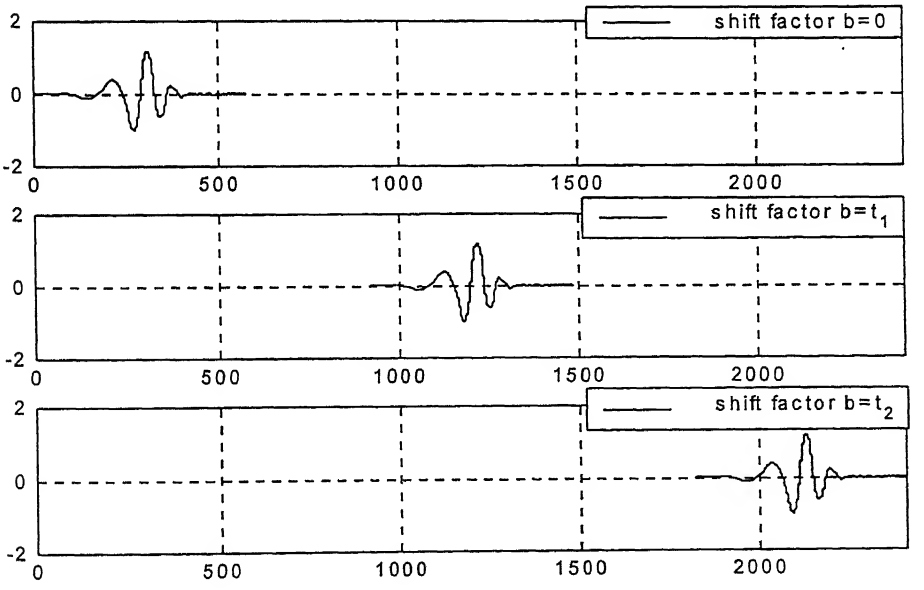

Fig. 4.5 Shifting (delaying or hastening) of the wavelets with different shift parameters

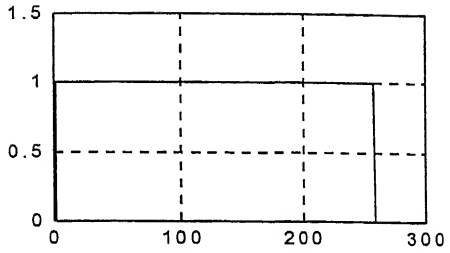

(a) db1/Haar Scaling function

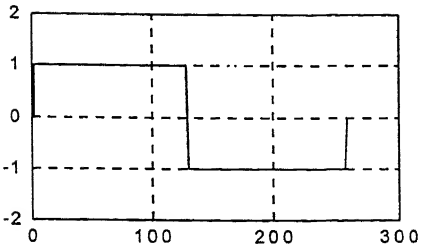

(b) db1/Haar Wavelet function

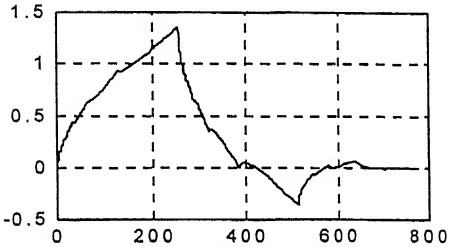

(c) db2 Scaling function

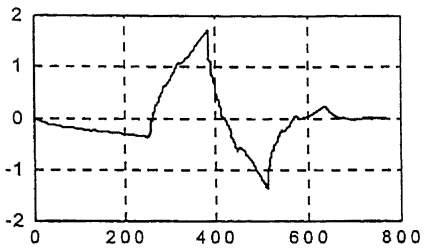

(d) db2 Wavelet function

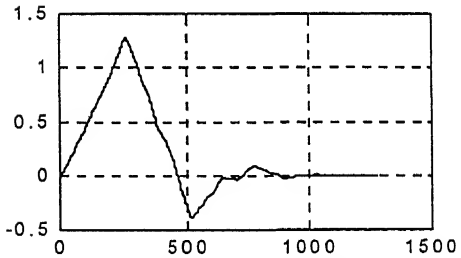

(e) db3 Scaling function

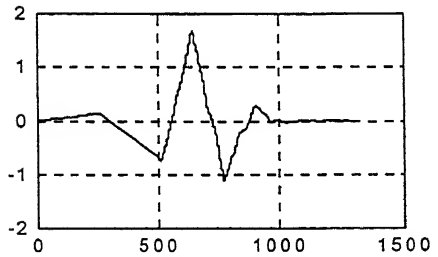

(f) db3 Wavelet function

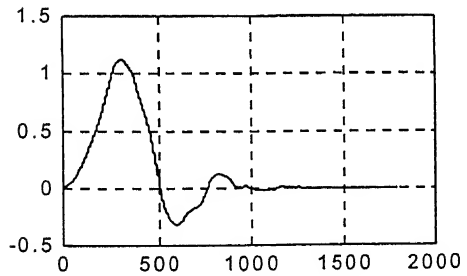

(g) db4 Scaling function

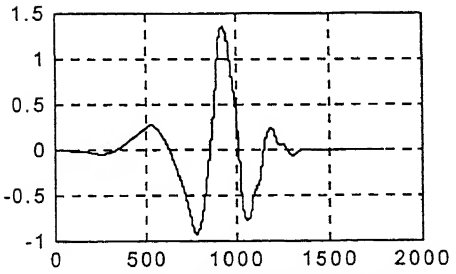

(h) db4 Wavelet function

Figs. 4.6(a-h) Different wavelets (Daubechies) scaling and wavelet functions

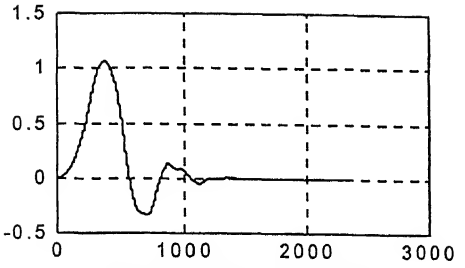

(i) db5 Scaling function

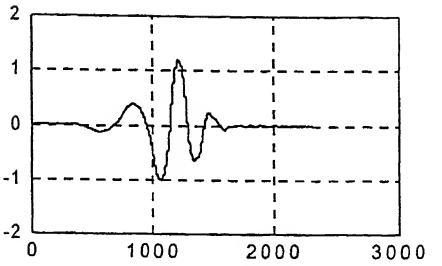

(j) db5 Wavelet function

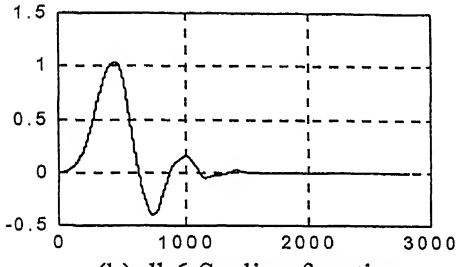

(k) db6 Scaling function

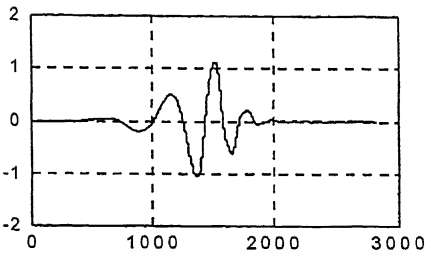

(l) db6 Wavelet function

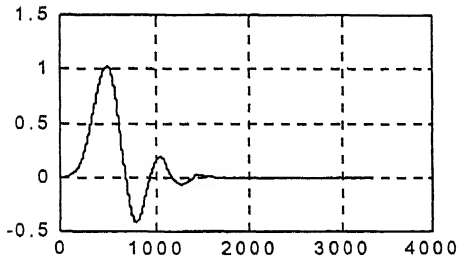

(m) db7 Scaling function

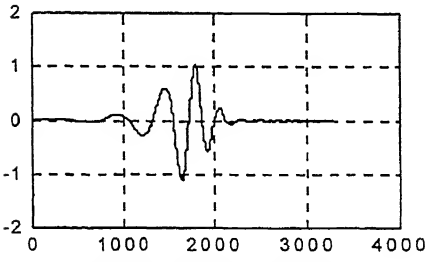

(n) db7 Wavelet function

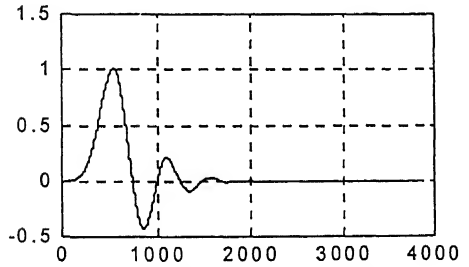

(o) db8 Scaling function

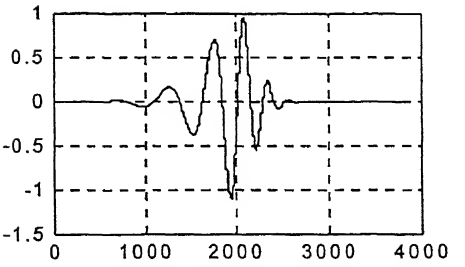

(p) db8 Wavelet function

Figs. 4.6(i-p) Different wavelets (Daubechies) scaling and wavelet functions

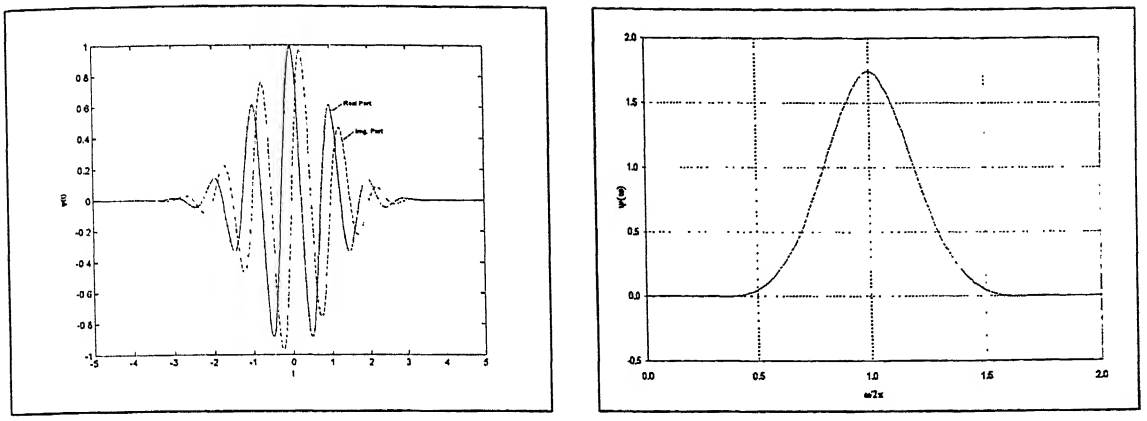

(a) (b)

Fig.4.7 (a) The Morlet function; (b) its Fourier transform when $\omega_0 = 2\pi$

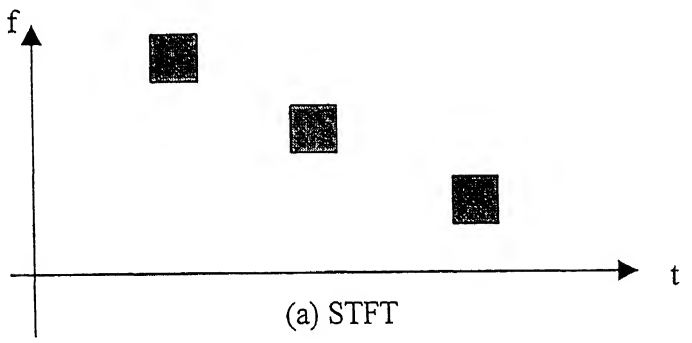

(a) STFT

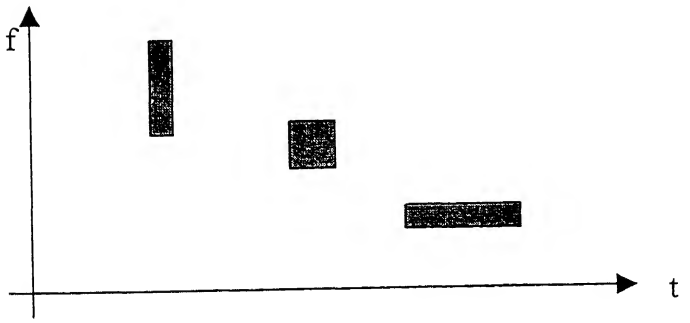

(b) CWT

Fig.4.8 Time-frequency resolution

Chapter 5

RESULTS AND DISCUSSION

In the present study, an experimental technique has been developed using an Nd: YAG pulsed laser for generation of ultrasonic waves and a He-Ne continuous laser based Heterodyne optical interferometric probe for detection of the same. Tests were conducted on pure metal specimens and composite specimens having metal inserts. Following are the results and discussion of these investigations.

5.1 EXPERIMENTAL DETAILS

Composite specimens were fabricated with artificial inclusions like metal inserts. Brass, mild steel and aluminum were used as inserts. Diagrammatic representation of composite specimens and pure metal specimens are shown in Fig.5.1 (a) and (b). The detected wave includes a pulsive noise signal induced by pulsed laser irradiation and random noise. It is generally known that the first one is inversely proportional to the intensity of the beat signal. To obtain a good signal to noise ratio of the ultrasonic signal, the signal was averaged over four readings. Figs.5.2 (a-c) show the raw signals (or noisy signals) recorded on specimens made of single metal. These raw signals were denoised using standard Wavelet Packet 1-D tool available in MATLAB using the Coiflet wavelet. Five level fixed form threshold method was used for thresholding. Threshold values for these five levels are 0.111, 0.112, 0.111, 0.114, and 0.114 respectively. The denoised signals are shown in Figs.5.3 (a-c). The raw signals recorded (using LBU) in defective and non-defective region of composite specimens are shown in Figs.5.4 (a-d). These signals were also denoised using the same MATLAB tool. Figs.5.5 (a-d) show the denoised signals recorded on composite specimens. As can be seen clearly from these signals, there is difference between the waveforms obtained from the defective and non-defective region of composite specimens. This is true for all the specimens, but not sufficient enough to give conclusive statement regarding the damage state or defects present in the specimen.

5.2 WAVELET SCALOGRAM

5.2.1 Pure Metal Specimens

The ultrasonic A-scan signals obtained from the Laser-Based Ultrasonic (LBU) set-up were analyzed by the Continuous Wavelet Transform (CWT) using the Morlet wavelet as the mother wavelet with central frequency, $\omega_0=2\pi$ (defined as the location of the peak of the Fourier transform). Normalized wavelet scalograms (as explained in Chapter 4) with projected contours of the denoised signals recorded on brass, mild steel and aluminum (3.2mm thickness) are shown in Figs.5.6 (a-c) over a frequency range of 0.2-20 MHz respectively. In these scalograms, frequency resolution is better *up to* 1 MHz and time resolution is better *above* 1 MHz. The MATLAB code, which was used to obtain these surface plots, is given in Appendix C. Maximum scalogram contour lines are clearly observed in the projected contours at lower frequencies i.e. close to 0.2 MHz. These scalograms correspond to the wave propagation (i.e. attenuation of the initial pulse) through the specimen. Figs.5.7-5.9 show the non-normalized scalograms and their 2-D contour plots to get a better identification of the shape and orientation of the maximum scalogram contour lines. These non-normalized scalograms are plotted in the decreasing order of frequency (i.e. the increasing order of dilation or scale factor) and the analysis is presented in the following sections.

5.2.2 Composite Specimens

The ultrasonic A-scan signals obtained for both defective and non-defective region of composite specimens having brass, mild steel and aluminum inserts (1mm thickness) were analyzed in the same way as pure metal specimens. The normalized scalograms with projected contours are shown in Figs.5.10 (a-d). The presence of a defect is expected to cause change in the appearance of the scalogram. This effect is visible in the surface plot, but is most readily observed in the projected contours. In non-defective region (i.e. composite area), maximum scalogram contour lines are present at higher frequencies i.e. close to 1 MHz, but in defective region maximum scalogram contour lines are present at frequencies other than 1 MHz (i.e. close to 0.5 MHz). These changes in density of contour lines over a frequency scale correspond to the wave propagation (i.e. attenuation

of the initial pulse) through the defective regions of the specimen. Alternatively, the group velocity of the signal, which is inversely proportional to the arrival time, may be reduced. This feature of the wavelet scalograms gives qualitative information regarding the presence of defects in the specimen.

From the projected contours of the scalograms of defective regions, it is clearly observed that the effect of composite (as the signals pass through composite-metal-composite region) is present at frequency scale of 1 MHz. This behaviour of the signal can be due to the presence of metal inserts inside the composite and greater thickness of composite over metal. The shape and orientation of the maximum scalogram contour lines are better seen in the non-normalized scalograms and in their 2-D contour plots. These are shown in Figs.5.11-5.14.

5.3 TIME-FREQUENCY ANALYSIS

5.3.1 Pure Metal Specimens

As composite material affects the higher frequencies (i.e. above 1 MHz), the data is analyzed with better frequency resolution above 1 MHz where as in pure metals the frequency range was 0.2-0.5 MHz. The normalized scalograms with projected contours over a frequency scale of 1-20 MHz are shown in Figs.5.15 (a-c) for pure metals (i.e. brass, mild steel and aluminum). The changes in the appearance of scalogram and changes in the density of contour lines can be seen in the surface plot, but are most readily observed in the projected contours. For a particular frequency, the value of the time for which the value of the wavelet transform (or magnitude of scalogram) is maximum, is defined as the arrival time of that frequency. As a result, by this definition of arrival time, either attenuation of a particular frequency component or a change in phase velocity can change the arrival time of certain frequencies. The combined plot of arrival time of frequencies for metal specimens is shown in Fig.5.17. This plot clearly shows a change in the arrival time of the frequencies in different metals. Arrival time corresponding to most of the frequency components of brass specimen is greater than that of mild steel and aluminum specimen. Some of the frequency components and their arrival times are listed in Table 5.1. The difference between the arrival times

corresponding to those frequency components of mild steel and aluminum specimen is not so high except at certain frequencies. This characteristic of the signal can be attributed to the material property i.e. velocity of the sound waves through the medium as given in Table 5.5. The frequency band for maximum scalogram contour lines is different for all the three samples. Table 5.2 gives the frequency band for maximum scalogram contour lines having maximum scalogram and their arrival times

From the slope of the arrival time contour of the pure metal specimens over a frequency scale of 1.2-1.6 MHz, it is clearly observed that the slope of aluminum is higher than that of brass and mild steel. The difference between the slope of brass and mild steel specimen is not so high. This characteristic of the signal can be interpreted as the material dispersion as it is known that aluminum is more dispersive than brass and mild steel.

5.3.2 Composite Specimens

5.3.2.1 Defective Region vs. Non-defective Region

The normalized wavelet scalograms with projected contours of the denoised recorded signals corresponding to the defective and non-defective region of composite specimens are shown in Figs.5.16 (a-d) over a frequency scale of 1-20 MHz having better frequency resolution close to 1 MHz. Changes in the appearance of scalogram and changes in the density of contour lines can be clearly seen in the surface plot, but are most readily observed in the projected contours. For comparison of defective areas with the non-defective areas, the arrival time of frequencies for composite specimens are plotted in Figs.5.18 (a-c). These plots clearly show change in the arrival time of frequencies. The arrival time of certain frequencies are given in Table 5.3 for better comparison. It can also be seen in these plots that the slope over a frequency scale can characterize the type of material. Changes in the arrival time slope over a frequency scale indicate the variation of wave propagation velocity with respect to frequency through the defective regions of the specimen. This characteristic of the signal can be interpreted as dispersion in the time domain. The larger arrival time slope over a frequency scale indicates that the signal is more dispersive in nature. This effect is clearly observed in the arrival time plots.

5.3.2.2 Changing Insert Metal

The normalized scalograms with projected contours of the insert zone signals are shown in Figs.5.16 (a-c) for brass, mild steel and aluminum inserts respectively. It can be clearly seen that the shape and orientation of the maximum scalogram contour lines are not same for all metal inserts (i.e. brass, mild steel and aluminum). For comparison of different metal insert zones, the combined plot of arrival time of frequencies is shown in Fig.5.18 (d). This plot clearly shows the change in the arrival time of frequencies. Arrival time corresponding to most of the frequency components of brass insert zone is greater than that of mild steel and aluminum insert zone. Some of the frequency components and their arrival times are listed in Table 5.3. The difference between the arrival times corresponding to those frequency components of mild steel and aluminum insert zone is not so high except at certain frequencies. This characteristic of the signal is almost same as pure metal specimens. The frequency band for maximum scalogram contour lines is also different for all the three zones. Table 5.4 gives the frequency band for maximum scalogram contour lines and their arrival times. It can also be seen in the combined arrival time plot that the slope over a frequency scale of 1.2-1.6 MHz is not same for all metal inserts. The slope of aluminum insert zone is higher than that of brass and mild steel insert zone and the difference between the slope of brass and mild steel insert zone is not so high. Interestingly, however, this characteristic of the signal (almost same as pure metal specimens), which could be interpreted as dispersion in the time domain, is not simple material dispersion but is related to the amplitude rather than the phase velocity characteristics of the signal.

5.4 WAVE COMPONENTS AT AND OFF EPICENTRE

To find a method by which the arrival of compression and shear wave components can be determined, the ultrasonic waves arriving at a few neighbouring locations were recorded. Due to limitation of the set-up, instead of moving the He-Ne laser, the approximately 1mm diameter pulsed laser source was systematically moved across the surface of 3.2 mm thick aluminum specimen as shown in Fig.5.19 (a). The signals recoded for different off-epicentre distances (i.e. 0, 0.5, 1.1 and 1.7 mm) are shown in Figs.5.20 (a-d). The non-normalized wavelet scalograms projected onto the time-scalogram plane are shown

in Figs.5.21 (a-d). The scalogram corresponding to a particular time and frequency is the square of the magnitude of wavelet transform. P and S waves are the combination of frequencies. So, it is not possible to identify the P and S waves conclusively from the scalogram plots. The first P-wave peak is supposed to arrive at a time of 0.6 μsec from the trigger point (knowing that the P-wave velocity in aluminum is 5160 m/sec and the thickness of the specimen is 3.2mm). The amplitudes of this peak is plotted for the above distances in Fig.5.22 (a). From the plot, it is clearly observed that the amplitude of the P-wave is fairly constant around epicentre. The small variation at neighbouring locations may be due to source size, near field effects, etc. Fig.5.22 (b) shows the S-wave amplitudes as a function of off-epicentre distance. From the plot, it is clearly seen that the S-wave amplitude is very small (approximately zero) around epicentre.

5.5 ANGLE DEPENDENT WAVE COMPONENTS

Although a very large number of ultrasonic applications involve the propagation of elastic waves perpendicular to the source surface such as thickness measurements and planar flaw detection, there are other areas where beam at an angle may be more appropriate. Therefore, to investigate the angular dependence (or directivity) of P and S waves, experimental data was collected in which the aluminum specimen was rotated with respect to the incident laser in a fixed direction as shown in Fig.5.19 (b). The signals recorded for different angles (i.e. 0^0, 30^0, 45^0 and 60^0) are shown in Figs.5.23 (a-d). Figs.5.24 (a-d) show the non-normalized wavelet scalograms projected onto the time-scalogram plane. In this section, it is also not possible to identify the P and S waves conclusively from the scalogram plots. The amplitudes of P-wave for the above orientations are plotted in Fig.5.25 (a). It is clearly seen that the form of the directivity is a lobe centred on an orientation of approximately 45^0. In other words, the amplitude of P-wave is maximum around 45^0. Fig.5.25 (b) shows the S-wave amplitudes as a function of angle of incidence. From the plot, it is clearly seen that the form of the directivity is a very narrow lobe centred on an orientation of 45^0. In other words, the amplitude of S-waves on either side of 45^0 angle is very small (approximately zero). Thus, although the epicentre is useful in studying the physics of thermoelastic source, other orientations are likely to be more useful in the context of applications of the technique.

Table 5.1 Arrival times of frequencies for pure metal specimens in μsec

Metal	1.0 MHz	1.2 MHz	1.6 MHz	2.3 MHz	4.1 MHz
Brass	2.0	2.0	2.8	3.8	0.6
MS	1.8	1.4	2.2	3.4	3.2
Al	1.6	1.0	2.0	1.8	1.4

Table 5.2 Frequency band for maximum scalogram contour lines for pure metal specimens

Metal	Frequency band (MHz)	Time (at central value)
Brass	1.02-1.18	2.0 μsec
MS	1.0-1.05	1.8 μsec
Al	1.6-1.8	2.0 μsec

Table 5.3 Arrival times of frequencies for composite specimens in μsec

Region	1.0 MHz	1.2 MHz	1.6 MHz	2.3 MHz	4.1 MHz
Brass Insert	4.6	5.0	5.6	6.2	4.6
MS Insert	2.2	2.6	2.8	2.4	4.6
Al Insert	2.0	2.8	4.6	2.4	4.4
Non-insert	3.2	4.0	5.0	4.6	2.8

Table 5.4 Frequency band for maximum scalogram contour lines for composite specimens

Region	Frequency band (MHz)	Time (at central value)
Brass Insert	1.0-1.14	4.6 μsec
MS Insert	1.2-1.3	2.8 μsec
Al Insert	1.3-1.4	3.6 μsec
Non-insert	1.02-1.1	3.4 μsec

Table 5.5 Material properties

Material	Density (kg/m^3)	Elastic Modulus (Gpa)	Longitudinal Vel. (m/s)
Aluminum	2700	72	5160
Steel	7800	200	5060
Brass	8400	100	3450

All the dimensions are in mm.

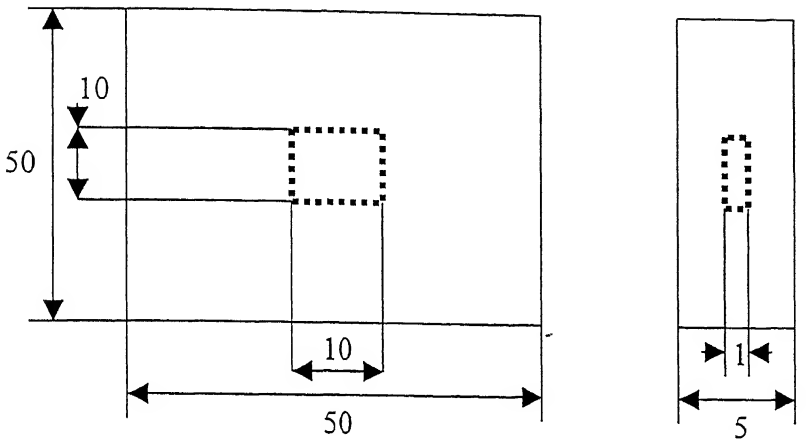

Fig.5.1 (a) Diagrammatic representation of composite specimen having metal insert

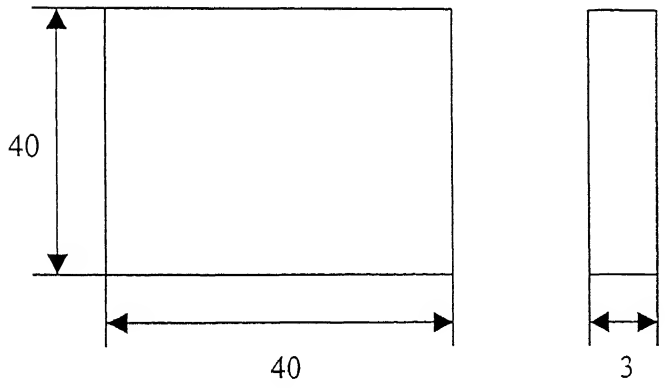

Fig.5.1 (b) Diagrammatic representation of pure metal specimen

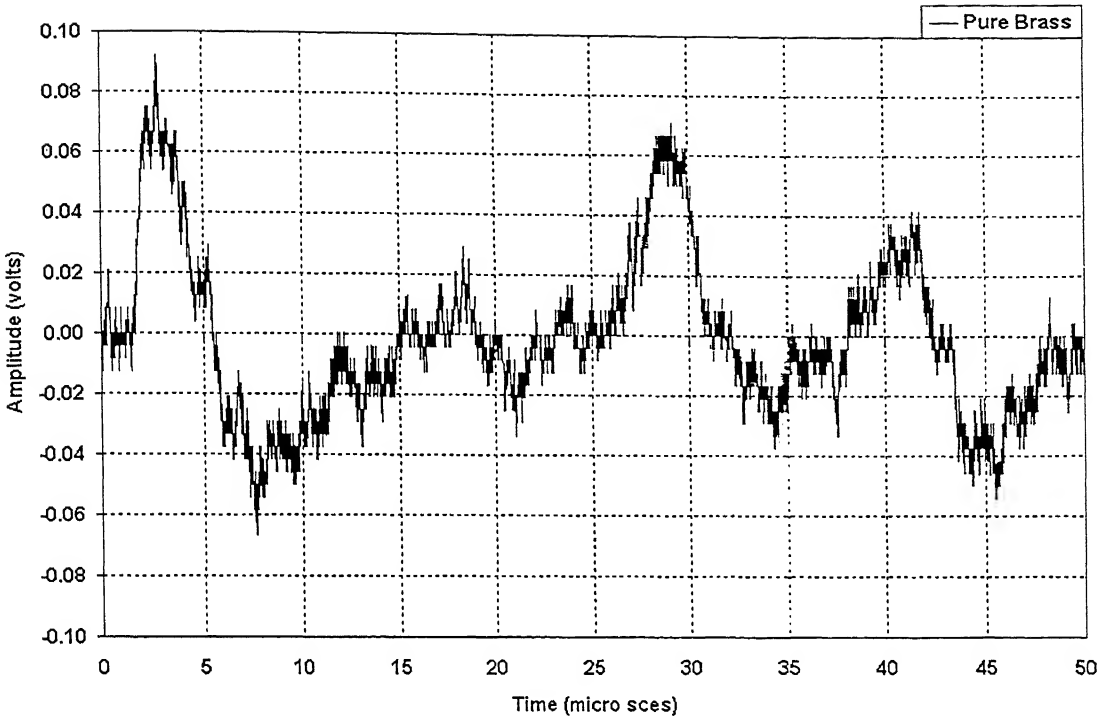

Fig.5.2 (a) Raw signal recorded in pure Brass

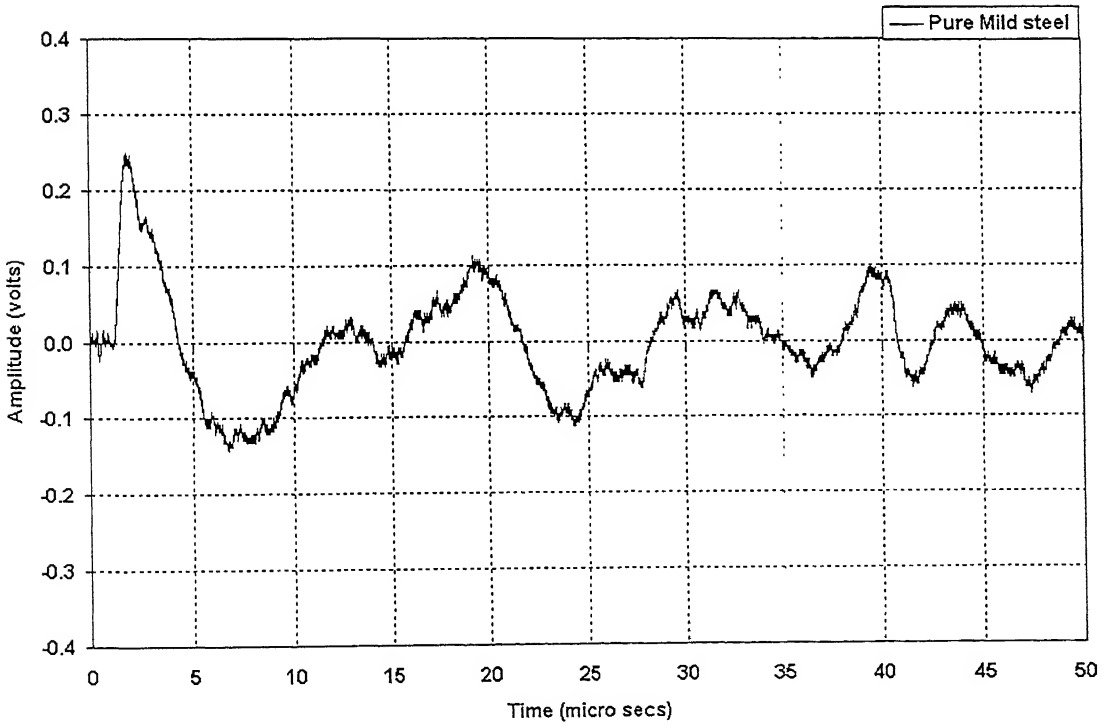

Fig.5.2 (b) Raw signal recorded in pure Mild-steel

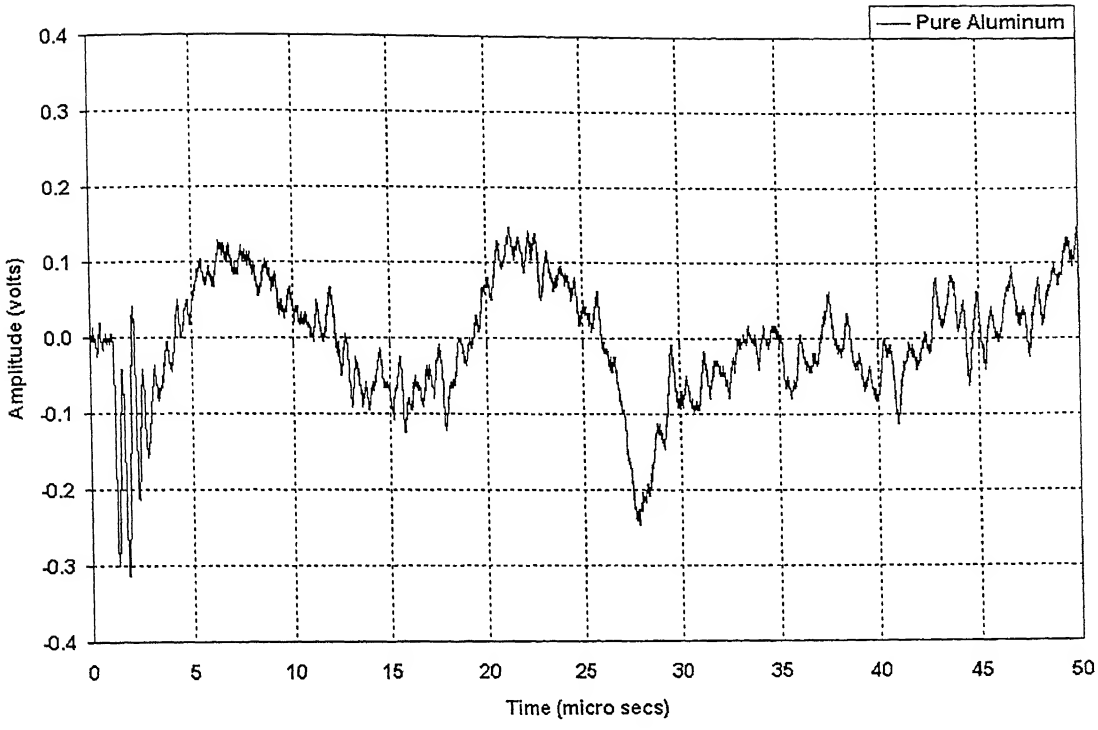

Fig.5.2 (c) Raw signal recorded in pure Aluminum

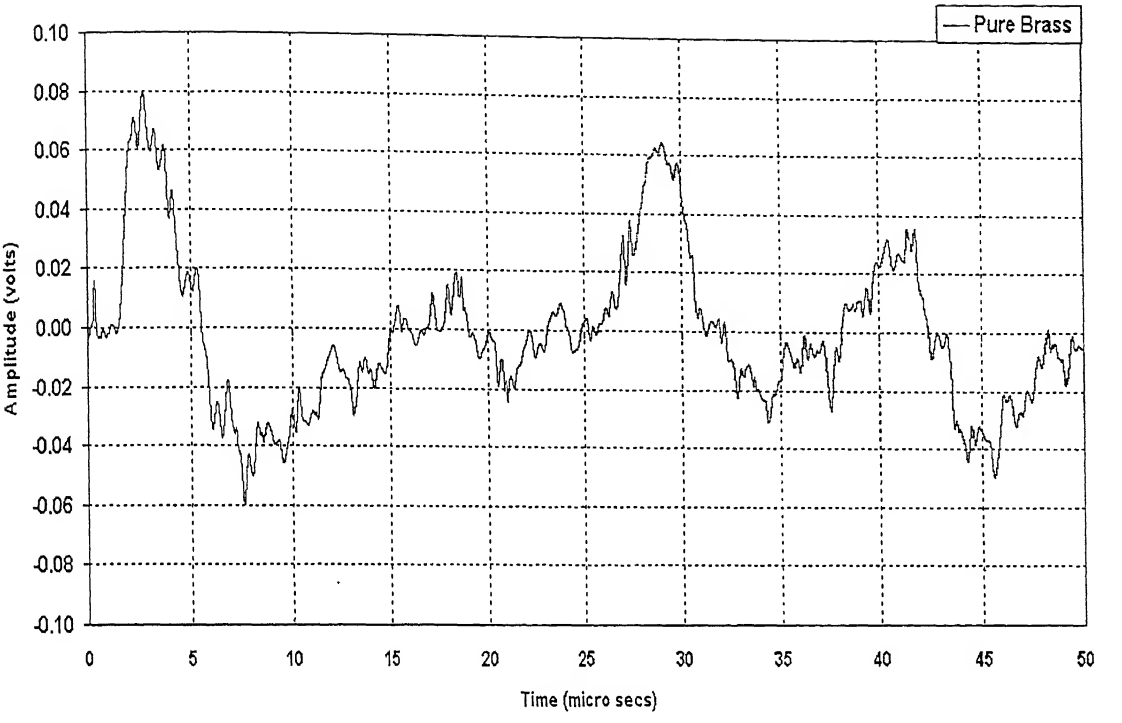

Fig.5.3 (a) Denoised signal recorded in pure Brass

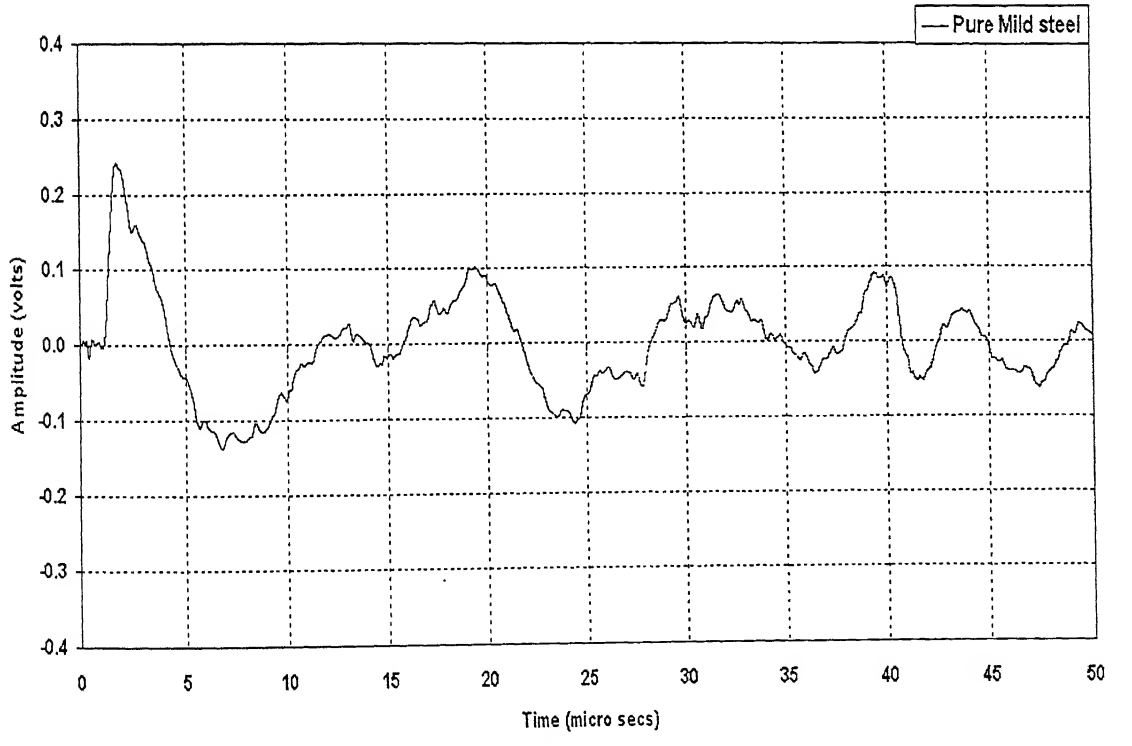

Fig.5.3 (b) Denoised signal recorded in pure Mild-steel

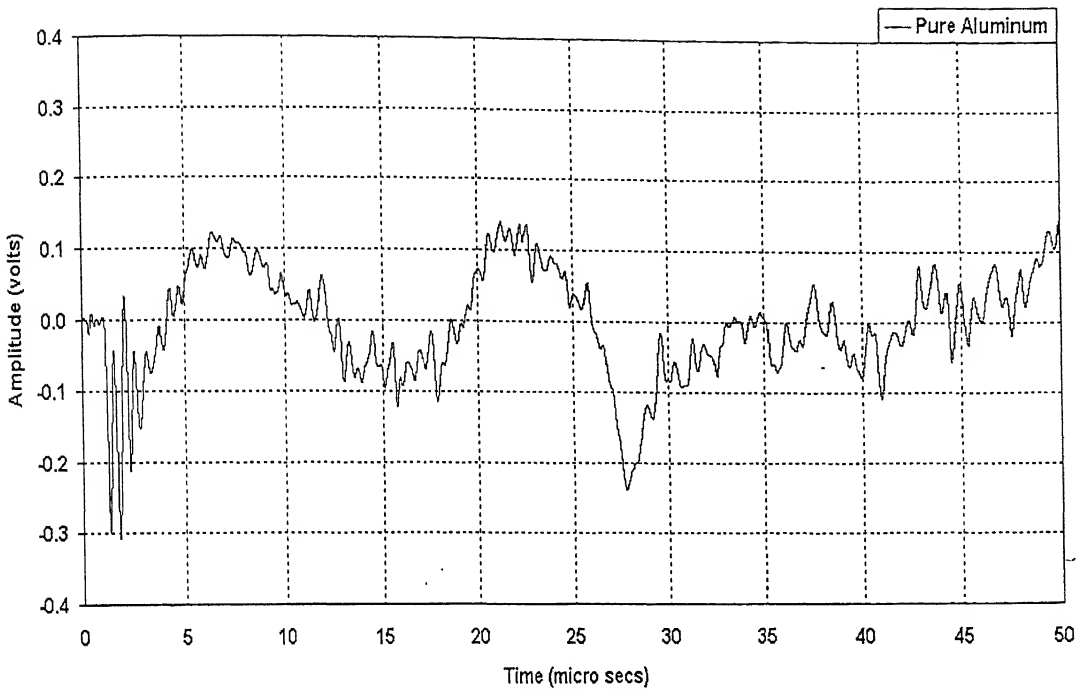

Fig.5.3 (c) Denoised signal recorded in pure Aluminum

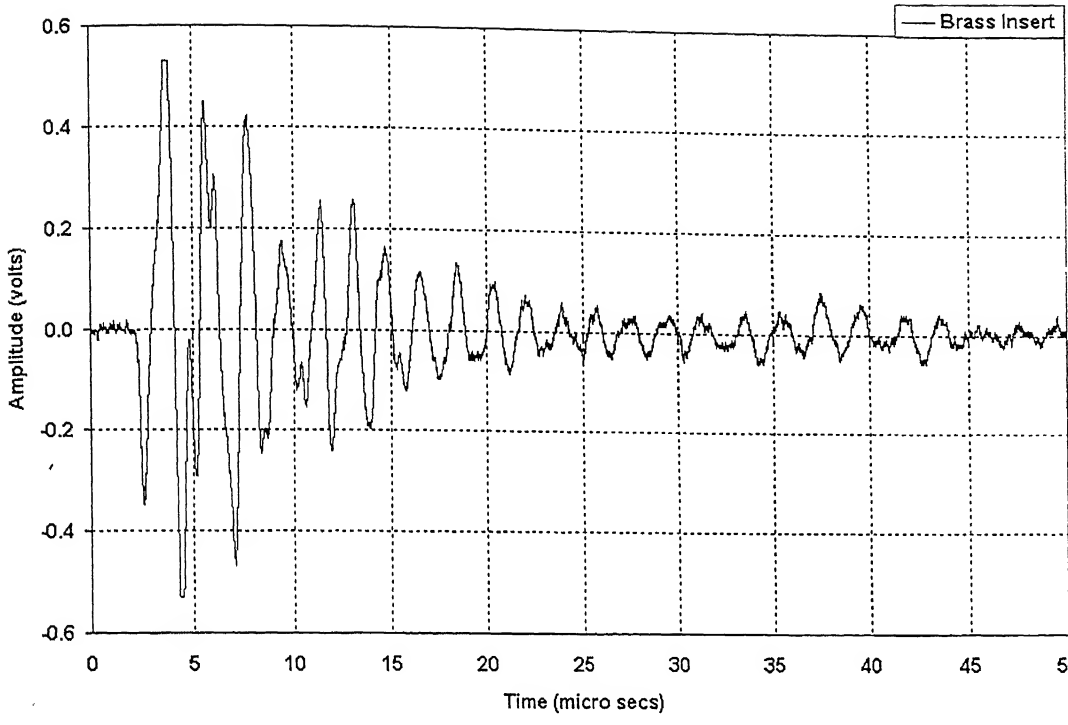

Fig.5.4 (a) Raw signal recorded in Brass insert zone

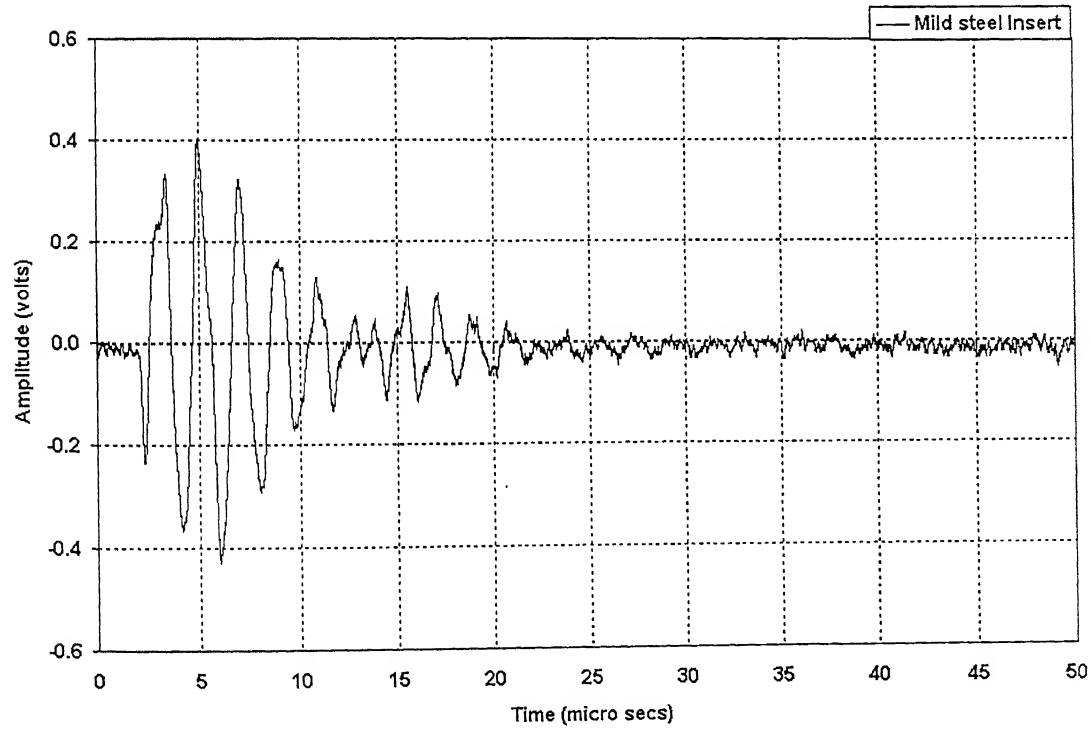

Fig.5.4 (b) Raw signal recorded in Mild-steel insert zone

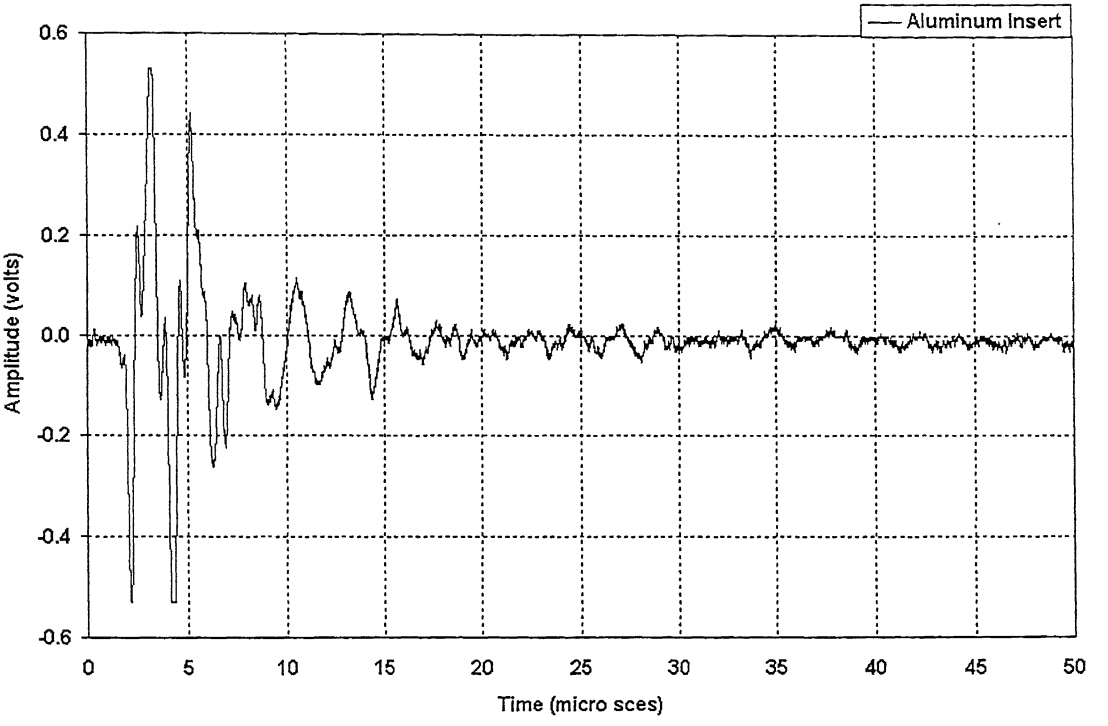

Fig.5.4 (c) Raw signal recorded in Aluminum insert zone

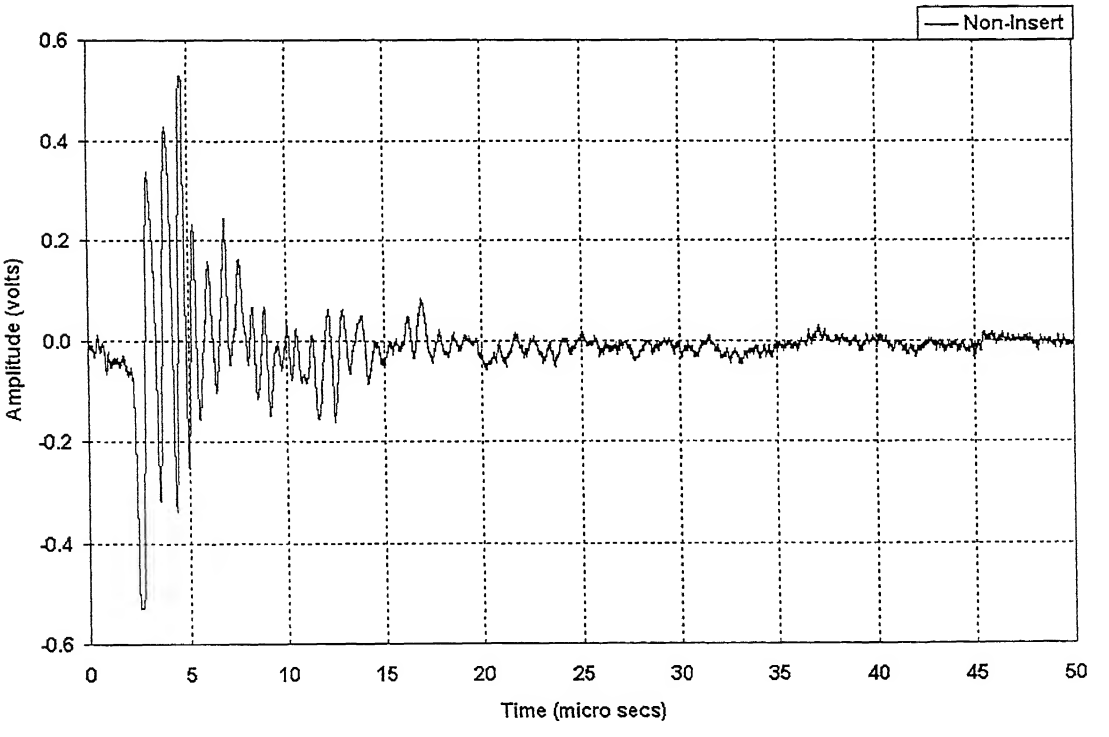

Fig.5.4 (d) Raw signal recorded in Non-insert zone

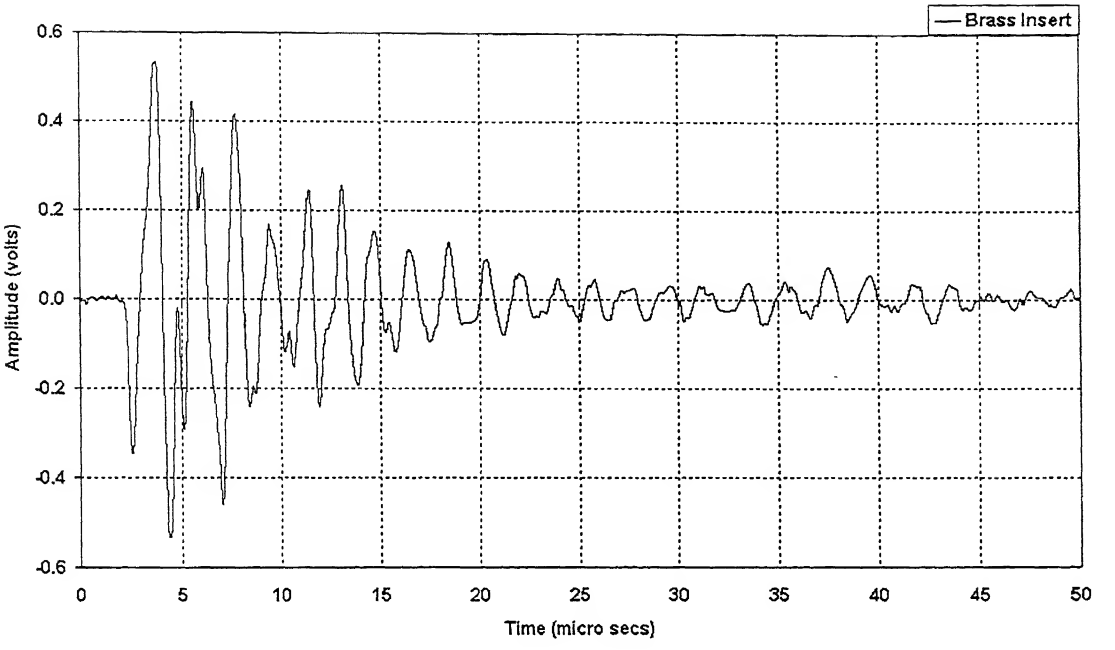

Fig.5.5 (a) Denoised signal recorded in Brass insert zone

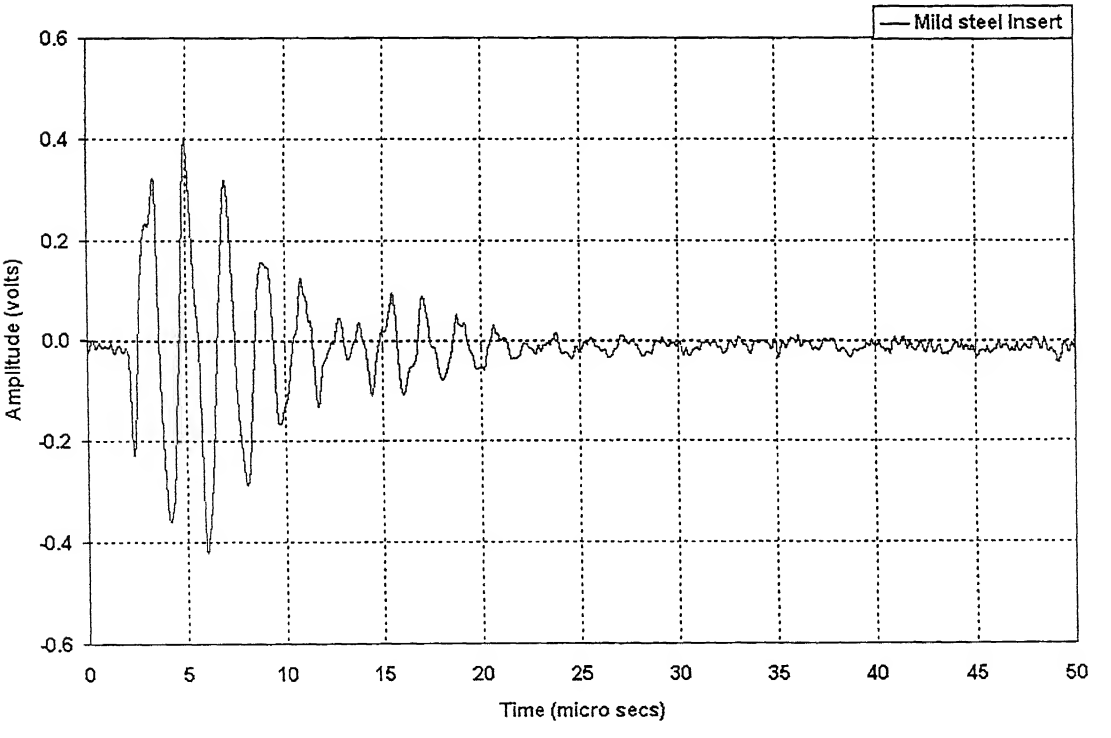

Fig.5.5 (b) Denoised signal recorded in Mild-steel insert zone

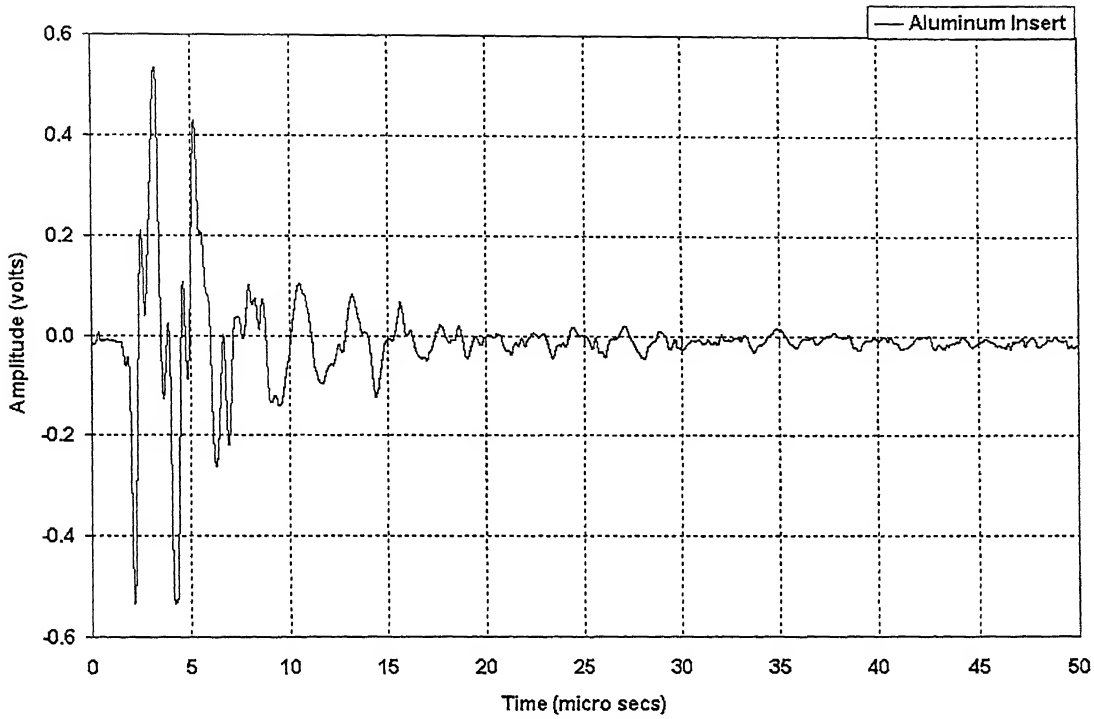

Fig.5.5 (c) Denoised signal recorded in Aluminum insert zone

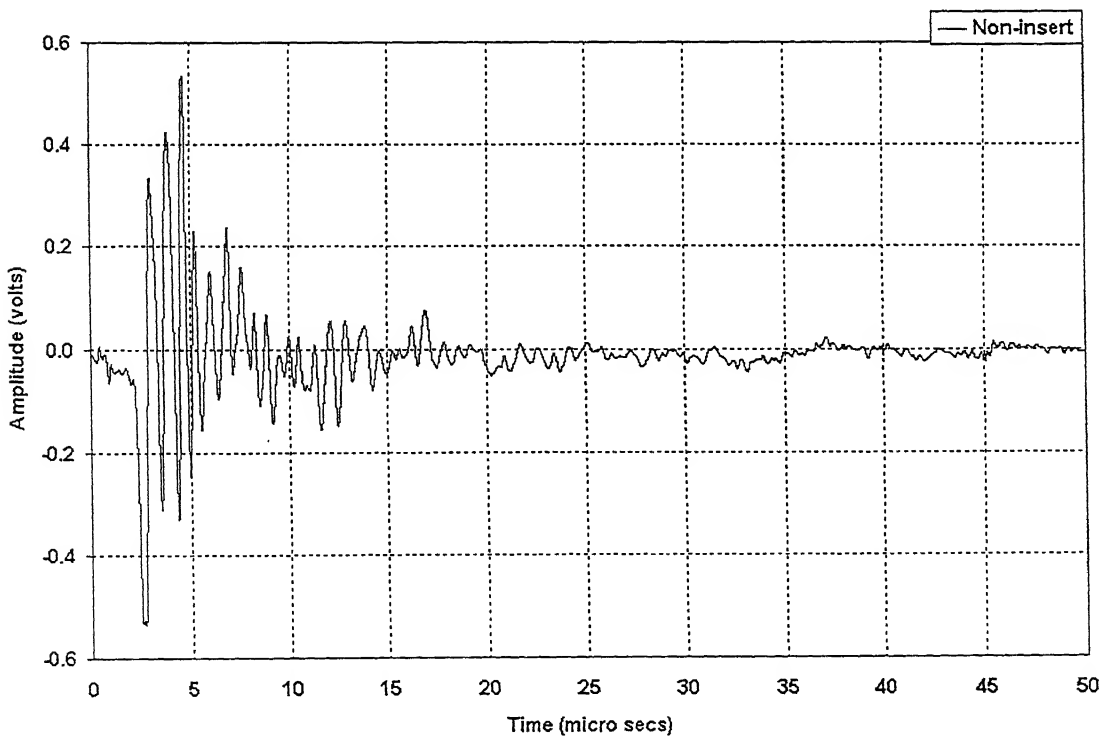

Fig.5.5 (d) Denoised signal recorded in Non-insert zone

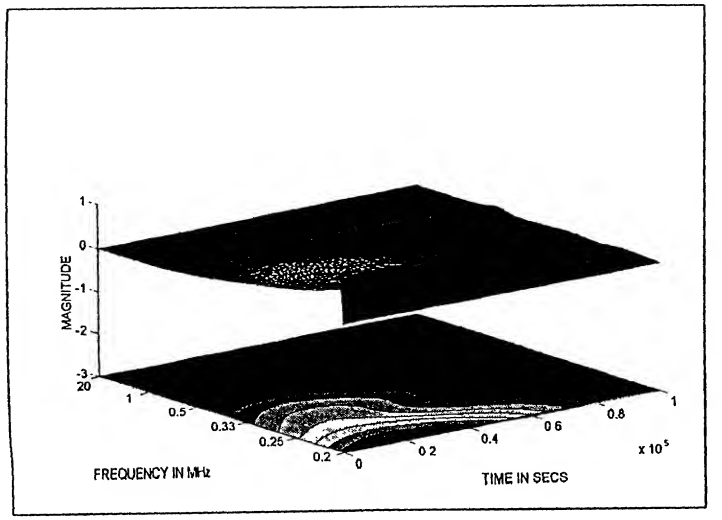

(a) Pure Brass

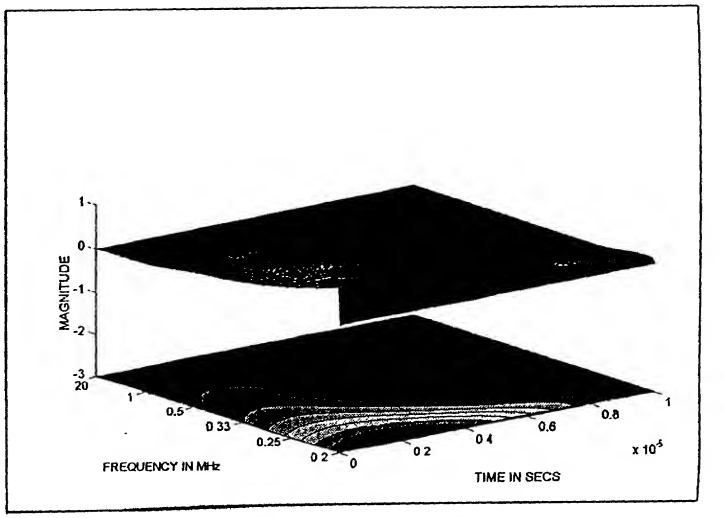

(b) Pure Mild steel

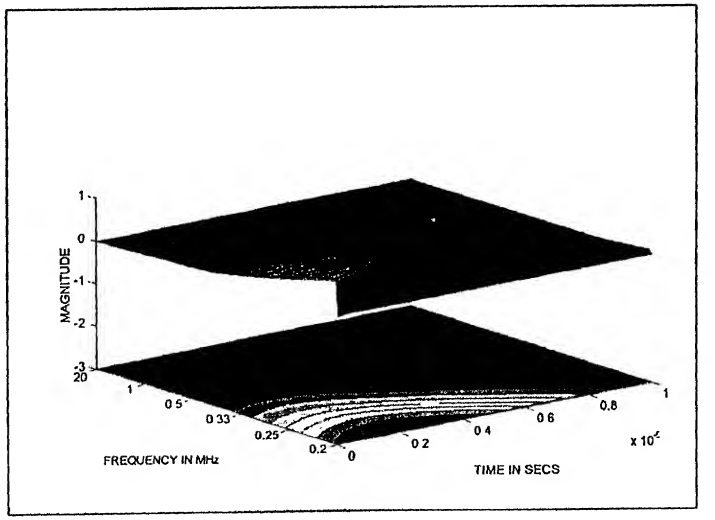

(c) Pure Aluminum

Fig.5.6 Normalized scalograms with projected contours produced for pure metals (0.2-20 MHz)

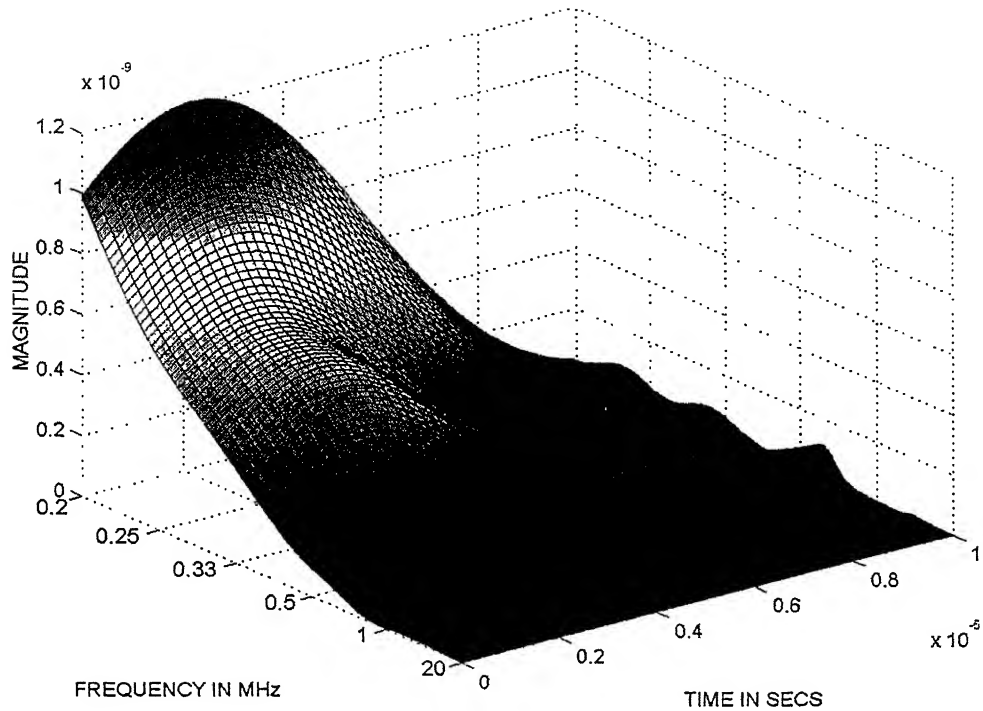

Fig.5.7 (a) Non-normalized scalogram produced for pure Brass

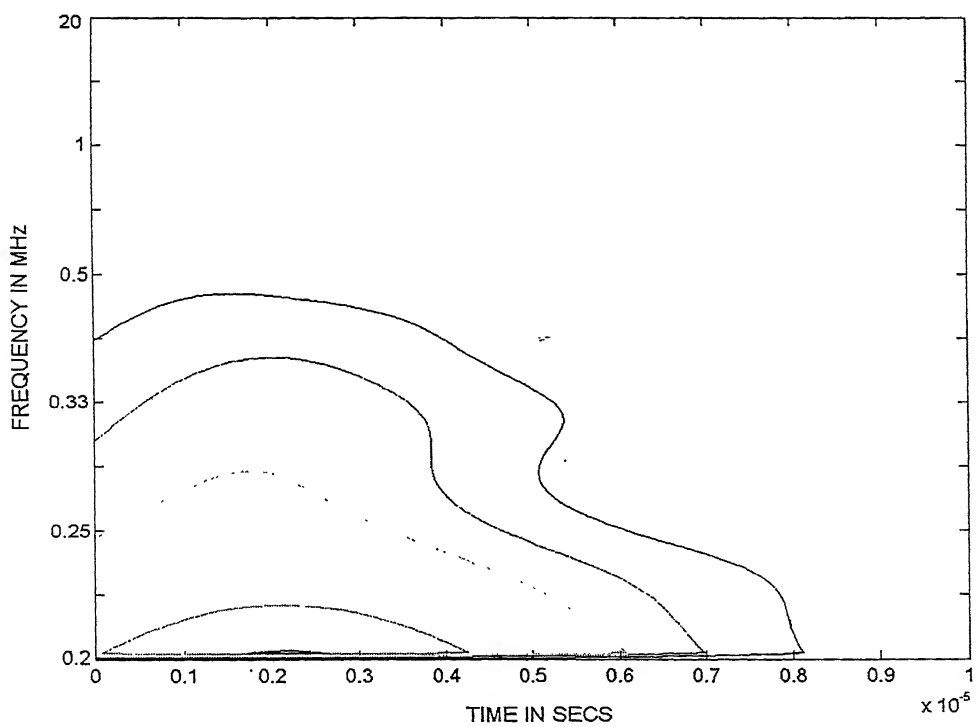

Fig.5.7 (b) Projected contours of non-normalized scalogram produced for pure Brass

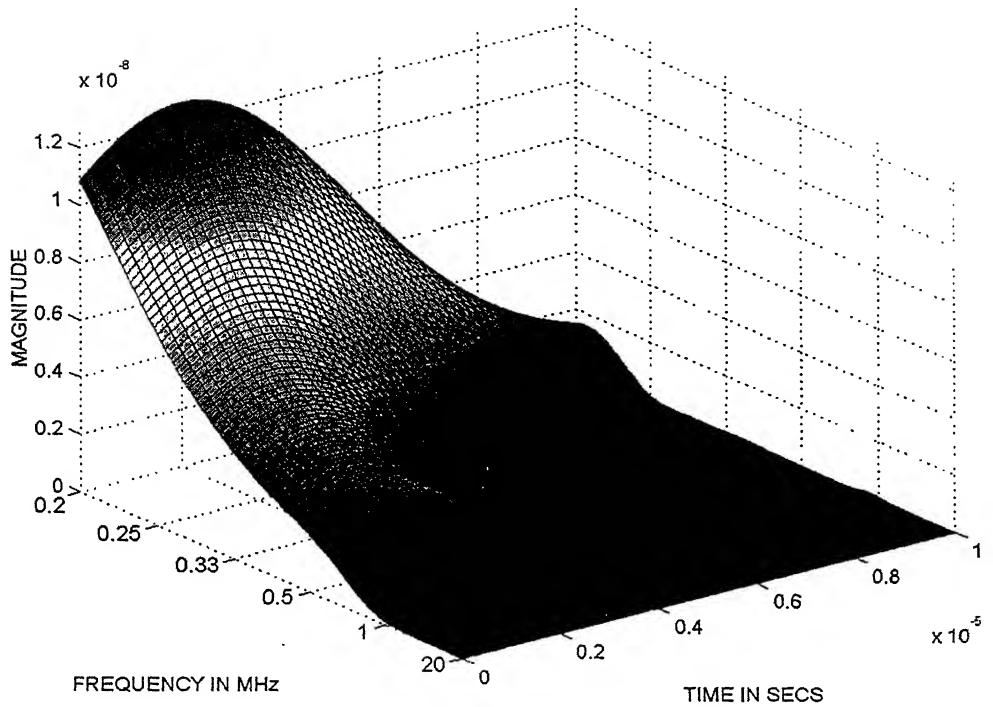

Fig.5.8 (a) Non-normalized scalogram produced for pure Mild steel

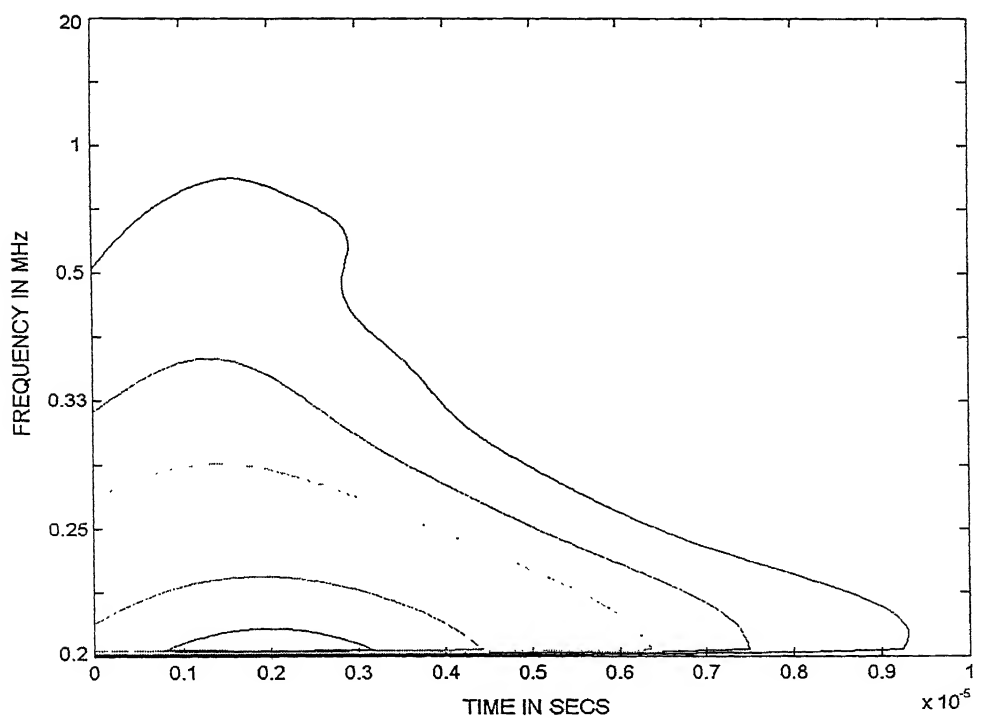

Fig.5.8 (b) Projected contours of non-normalized scalogram produced for pure Mild steel

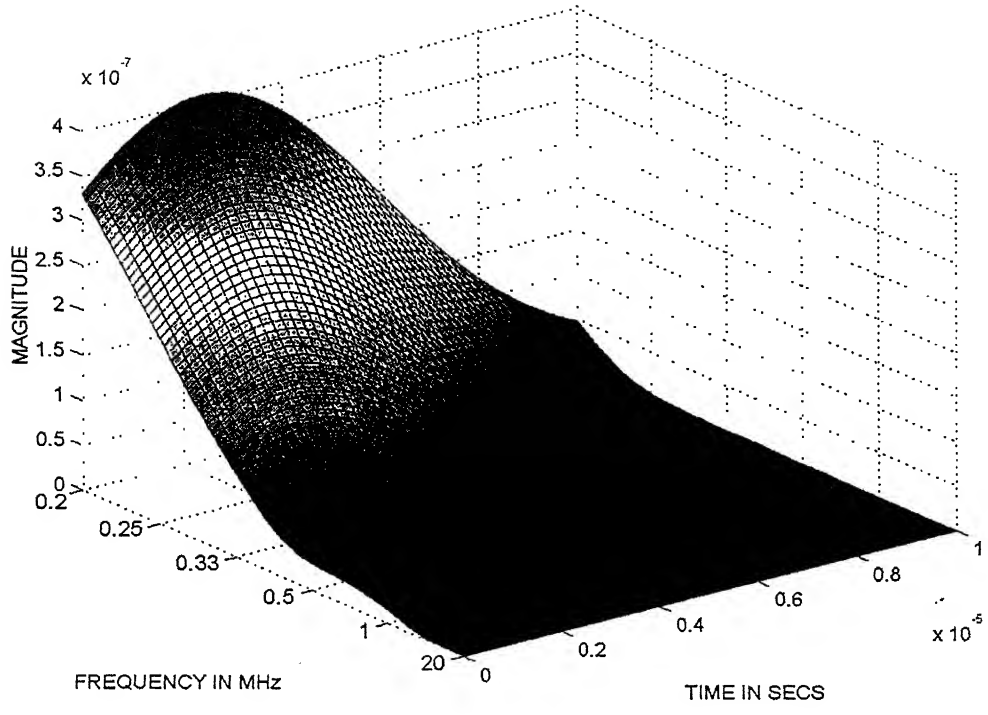

Fig.5.9 (a) Non-normalized scalogram produced for pure Aluminum

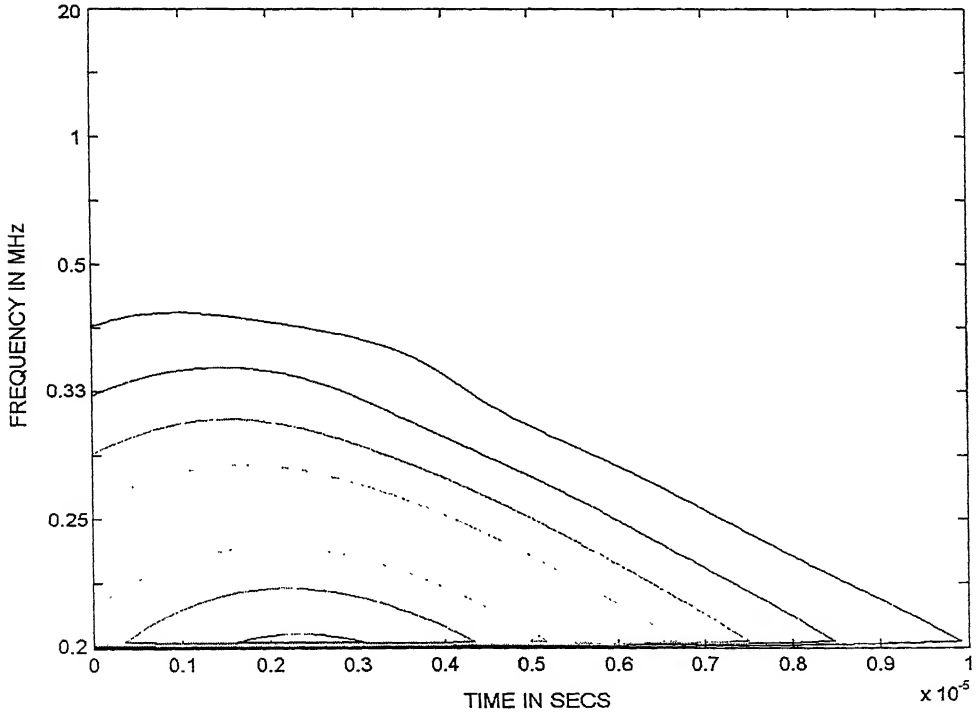

Fig.5.9 (b) Projected contours of non-normalized scalogram produced for pure Aluminum

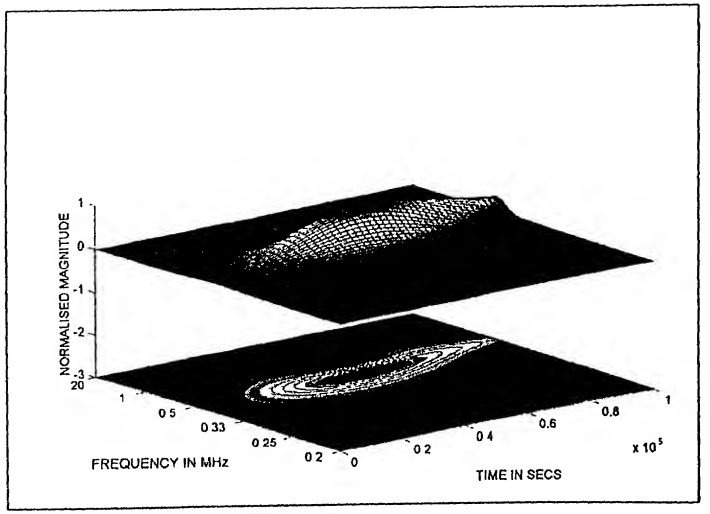

(a) Brass Insert Zone

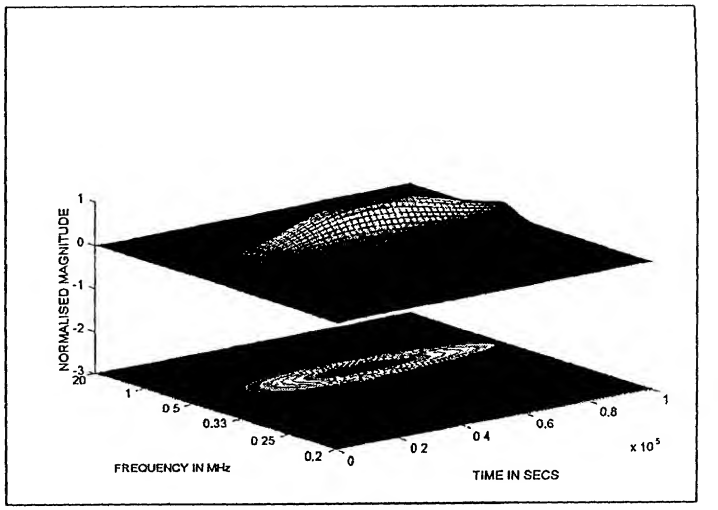

(b) Mild steel Insert Zone

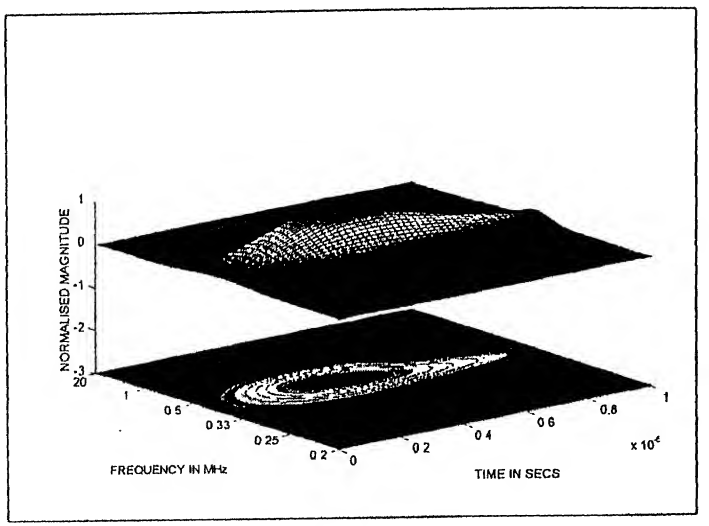

(c) Aluminum Insert Zone

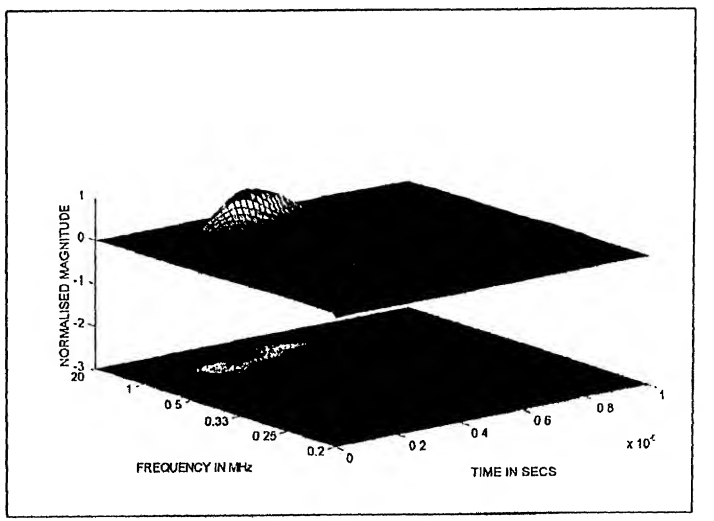

(d) Non-insert Zone

Fig.5.10 Normalized scalograms with projected contours produced for composite specimens (0.2-20 MHz)

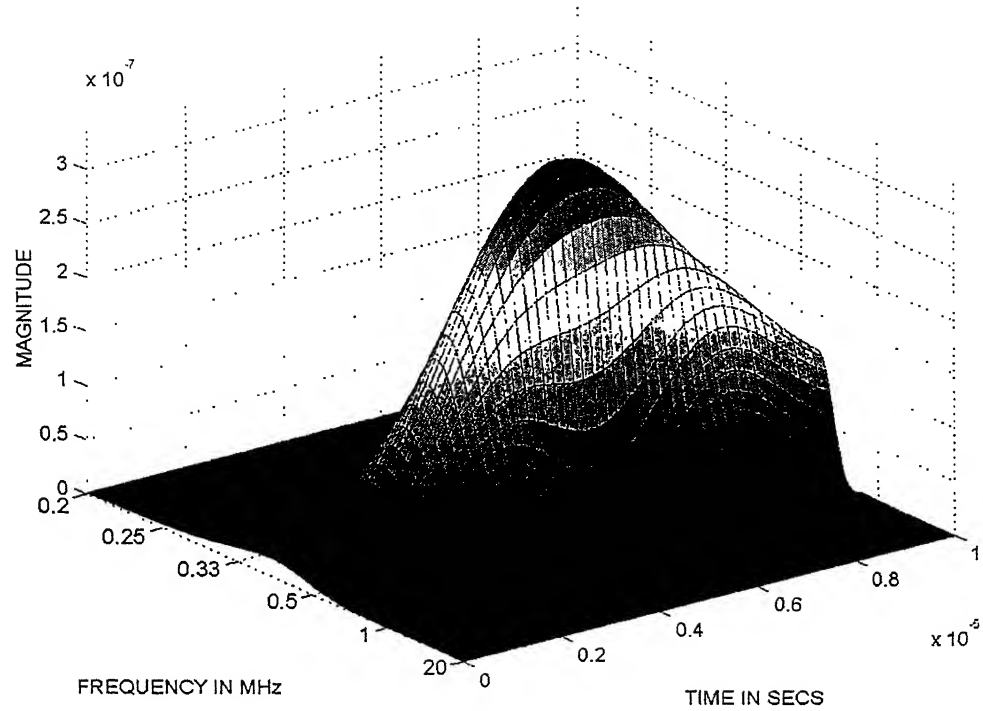

Fig.5.11 (a) Non-normalized scalogram produced for Brass insert zone

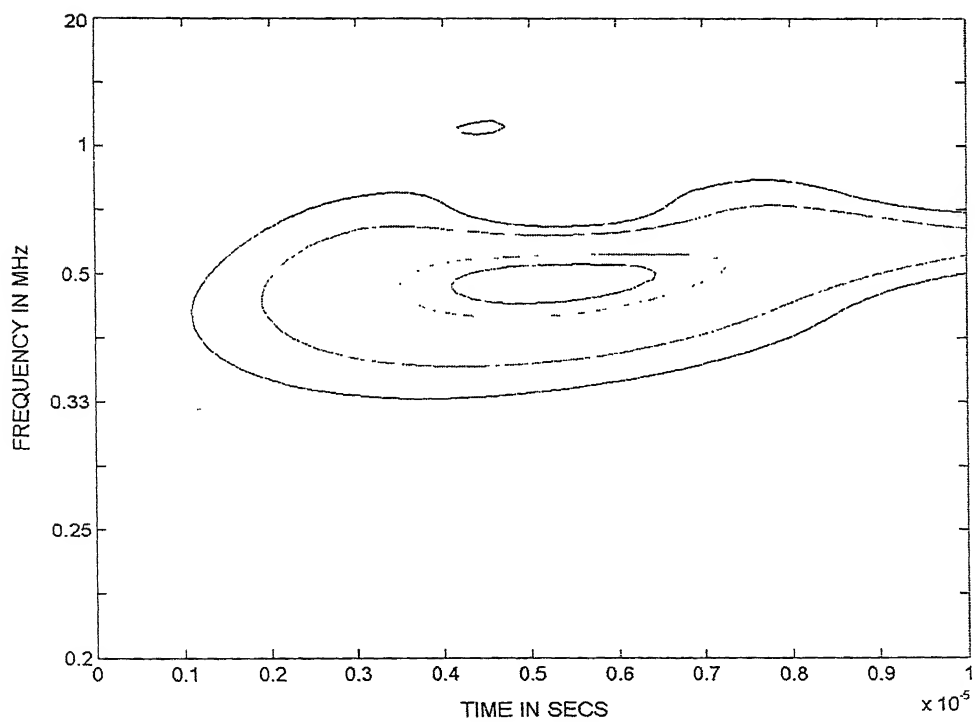

Fig.5.11 (b) Projected contours of non-normalized scalogram produced for Brass insert zone

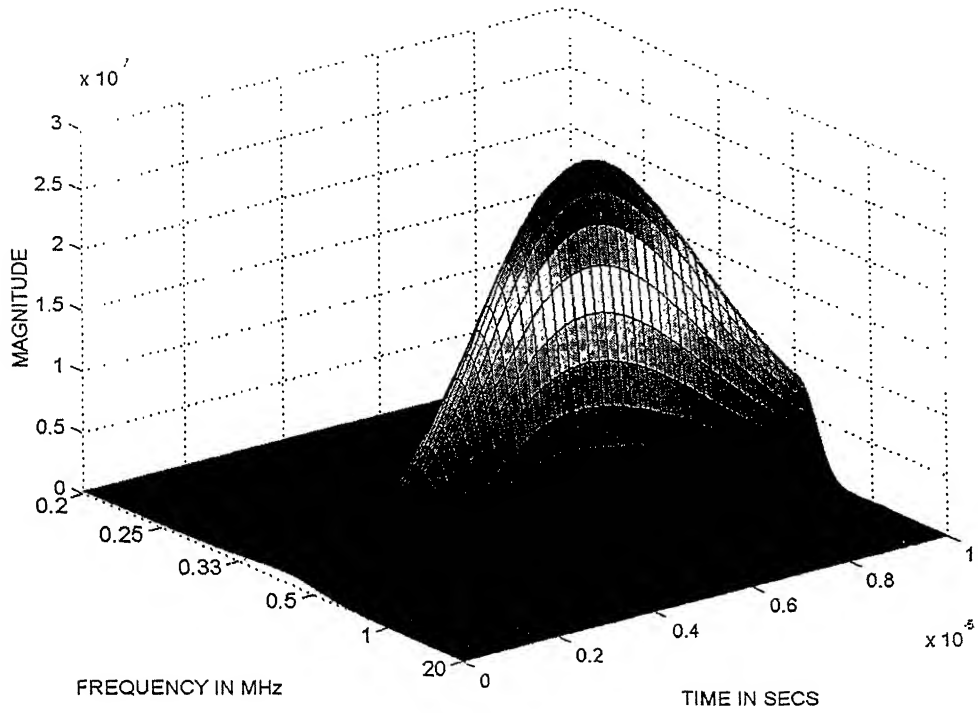

Fig.5.12 (a) Non-normalized scalogram produced for Mild steel insert zone

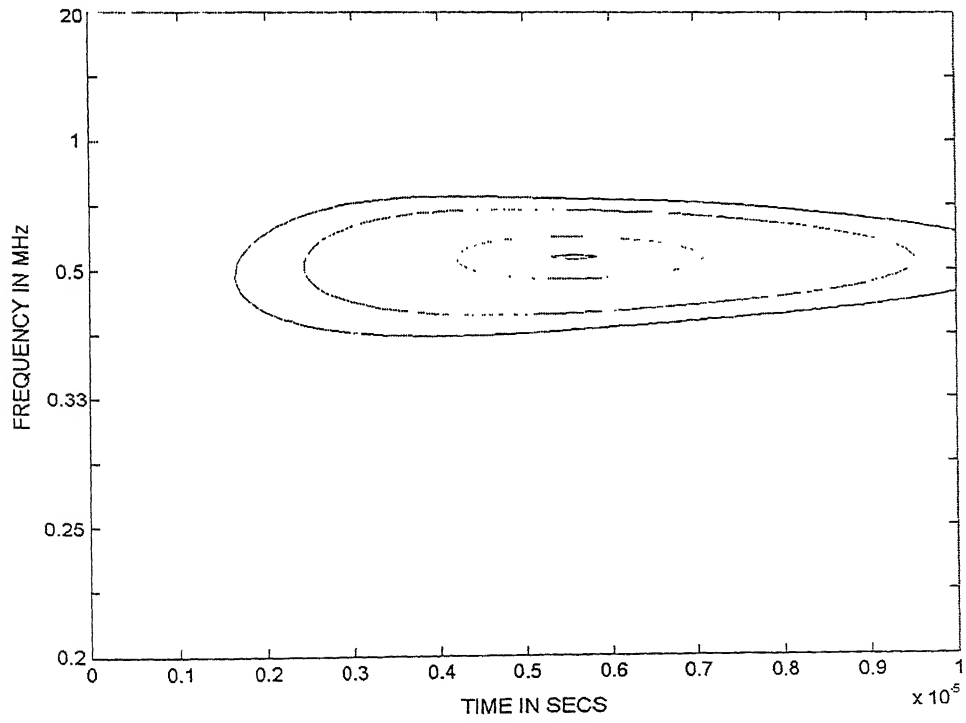

Fig.5.12 (b) Projected contours of non-normalized scalogram produced for Mild steel insert zone

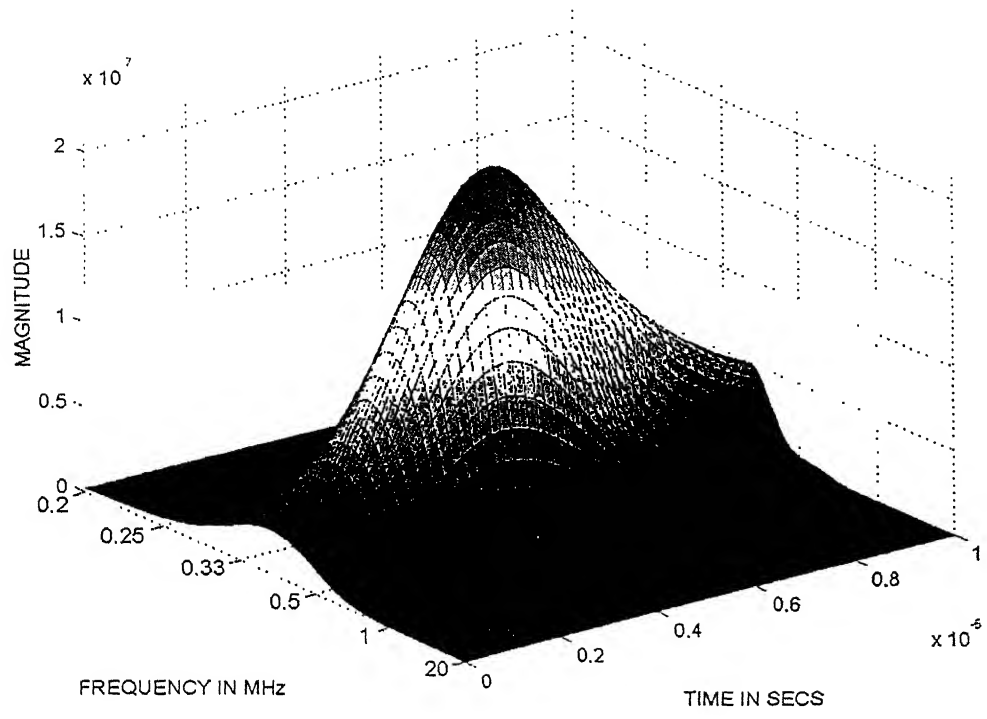

Fig.5.13 (a) Non-normalized scalogram produced for Aluminum insert zone

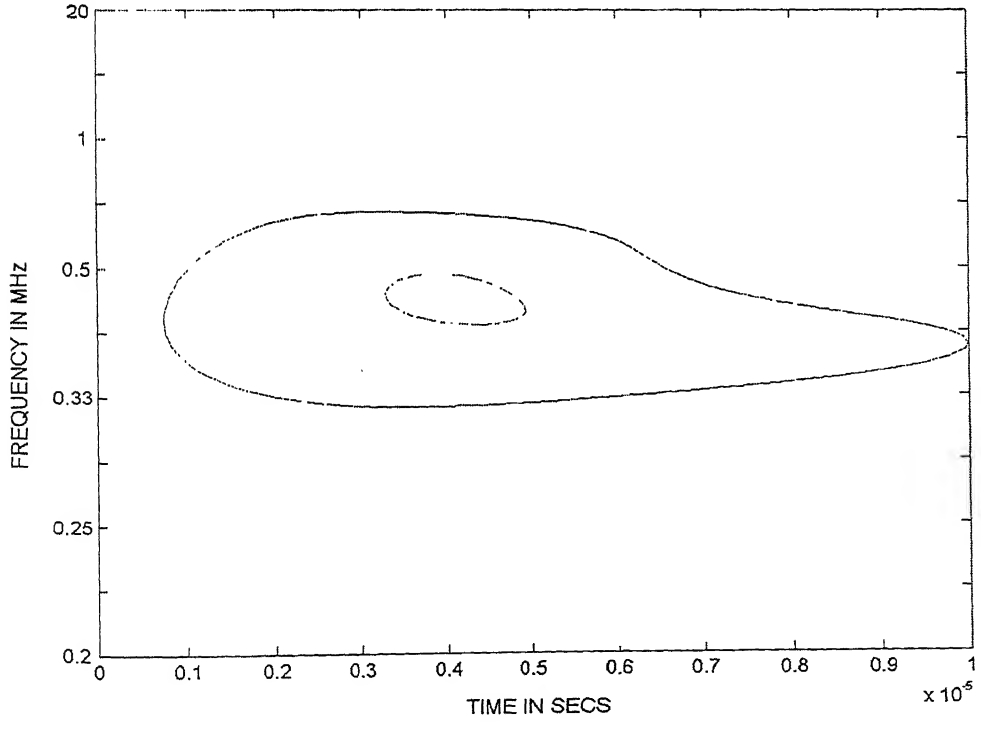

Fig.5.13 (b) Projected contours of non-normalized scalogram produced for Aluminum insert zone

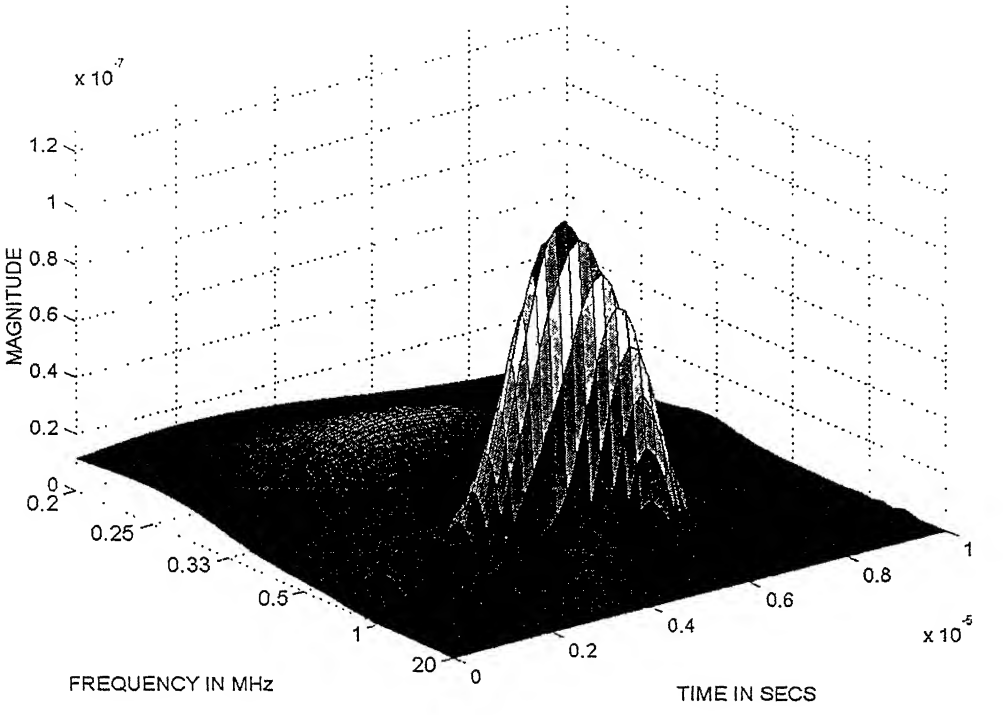

Fig.5.14 (a) Non-normalized scalogram produced for non-insert zone

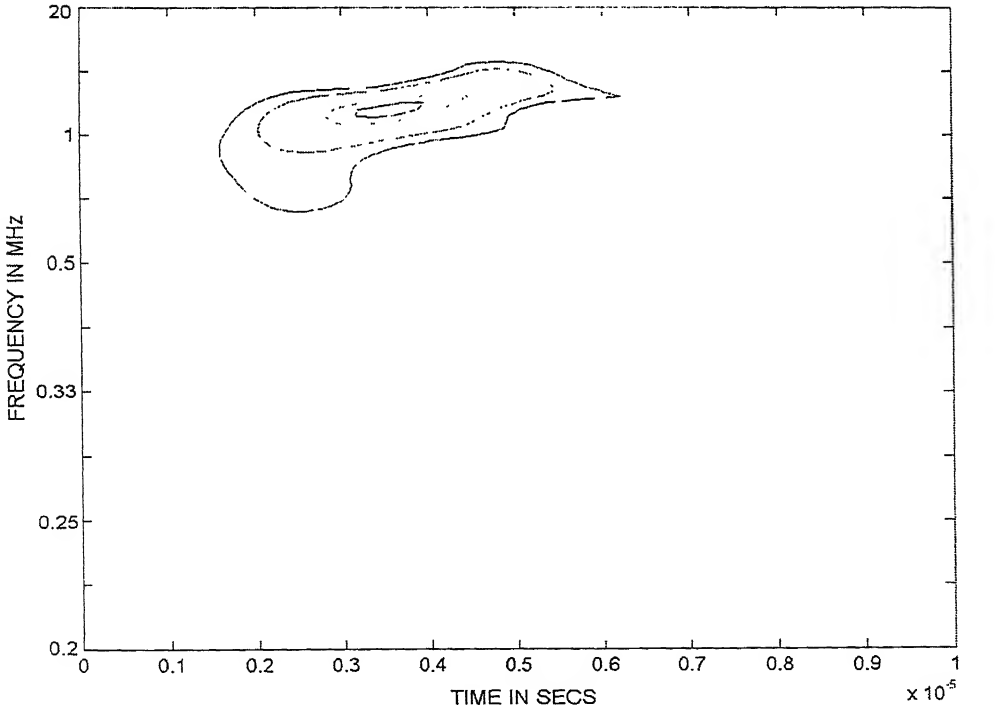

Fig.5.14 (b) Projected contours of non-normalized scalogram produced for non-insert zone

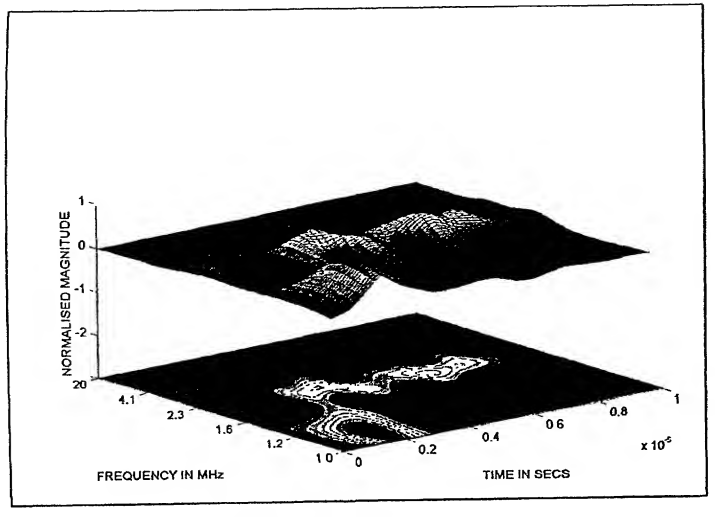

(a) Pure Brass

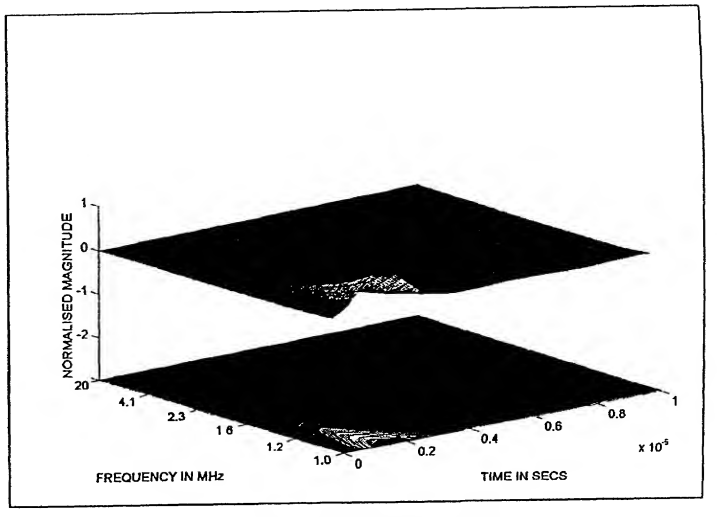

(b) Pure Mild steel

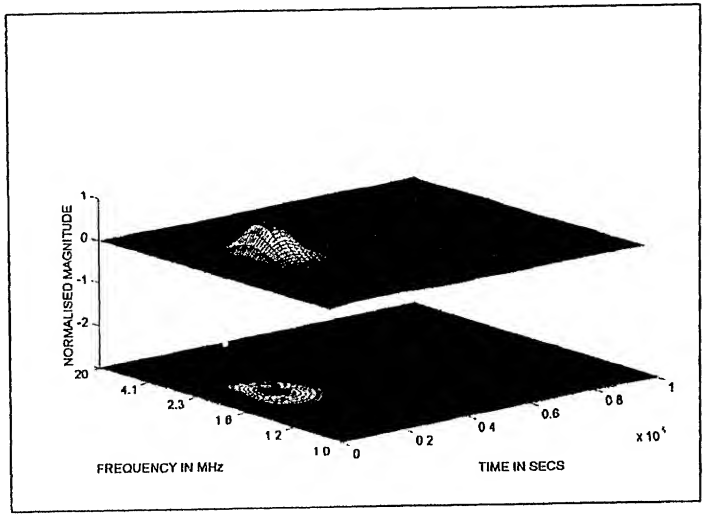

(c) Pure Aluminum

Fig.5.15 Normalized scalograms with projected contours produced for pure metals (1-20 MHz)

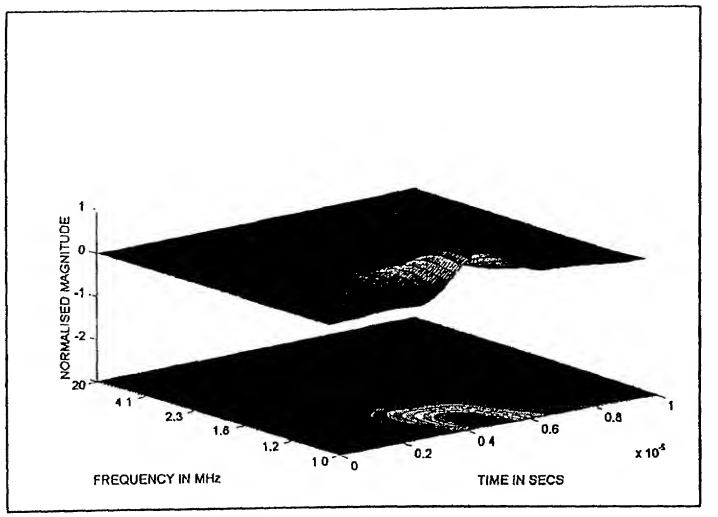

(a) Brass Insert Zone

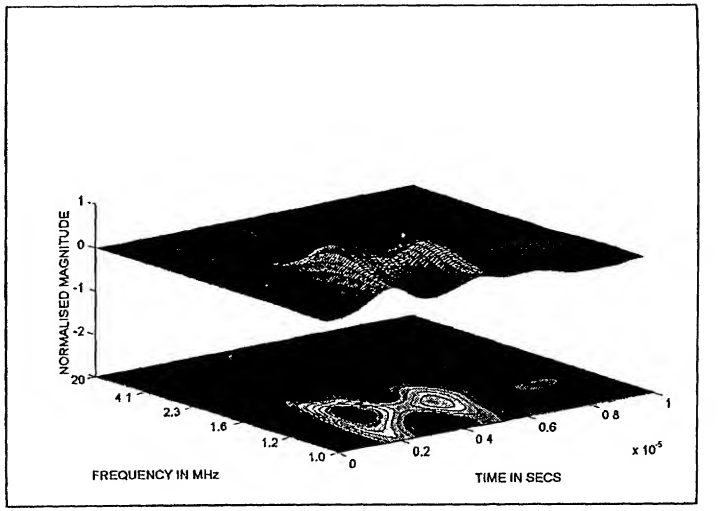

(b) Mild steel Insert Zone

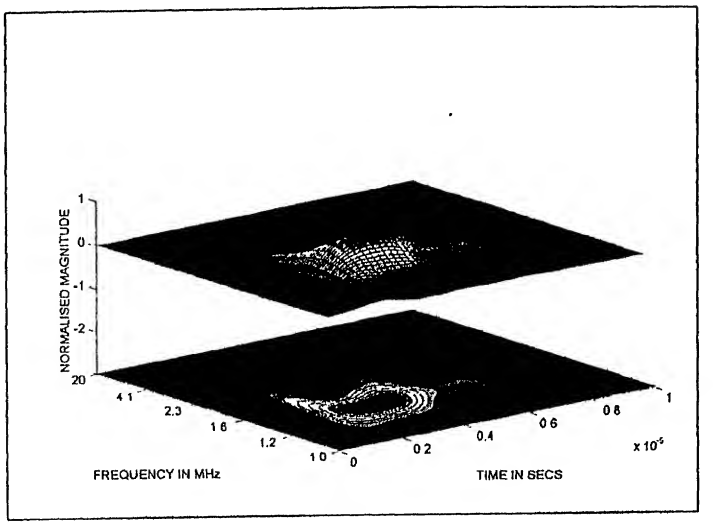

(c) Aluminum Insert Zone

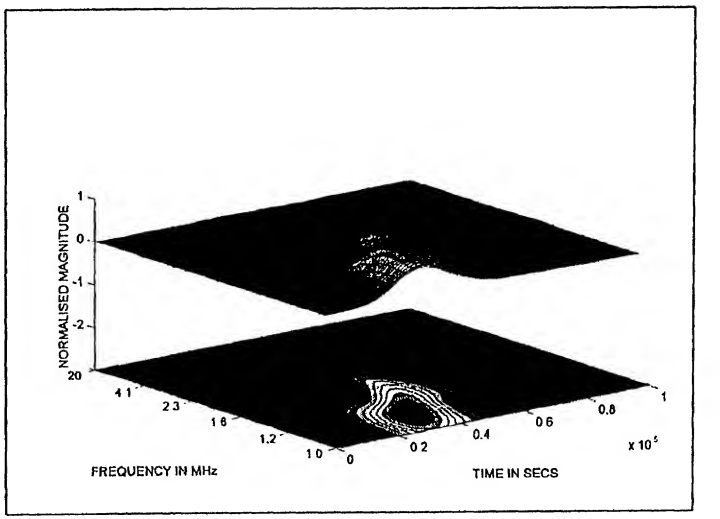

(d) Non-insert Zone

Fig.5.16 Normalized scalograms with projected contours produced for composite specimens (1-20 MHz)

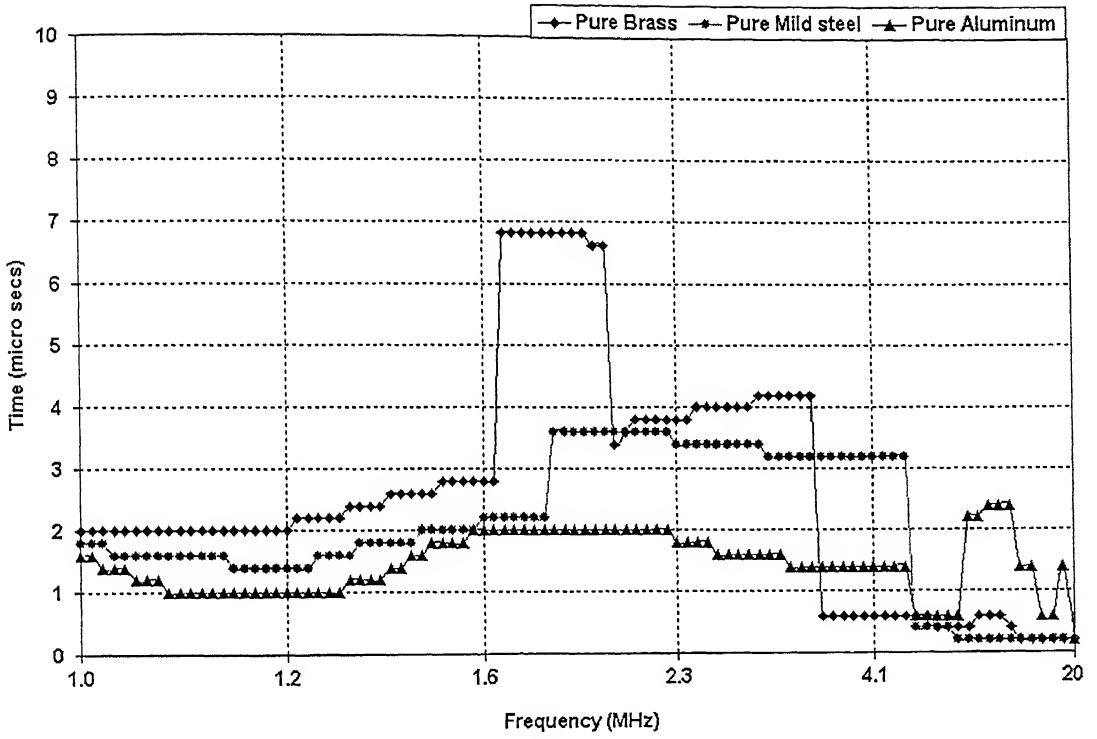

Fig.5.17 Combined plot of arrival time of frequencies for pure metals

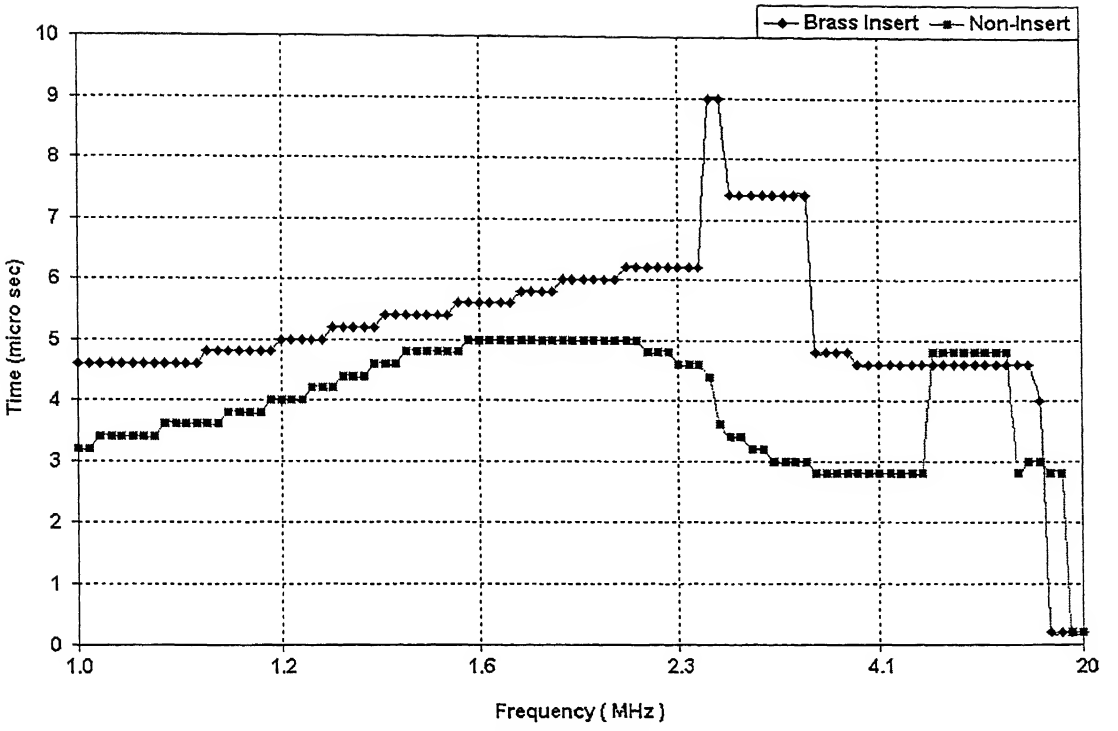

Fig.5.18 (a) Arrival time of frequencies for Brass insert sample

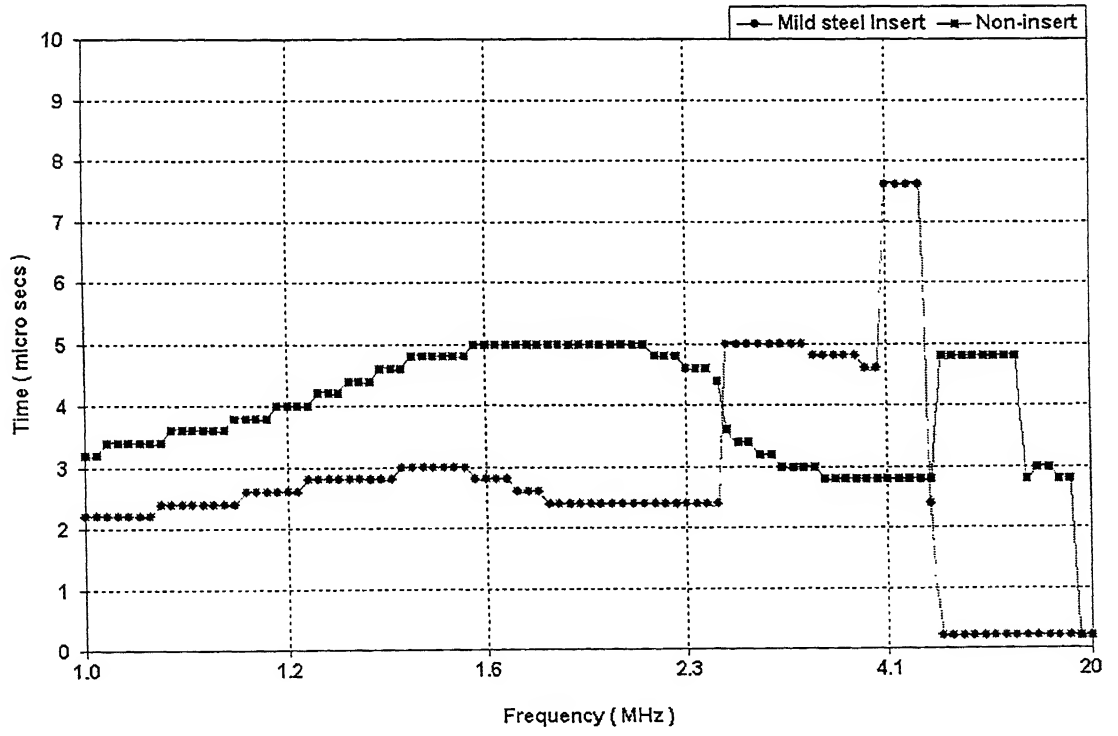

Fig.5.18 (b) Arrival time of frequencies for Mild steel insert sample

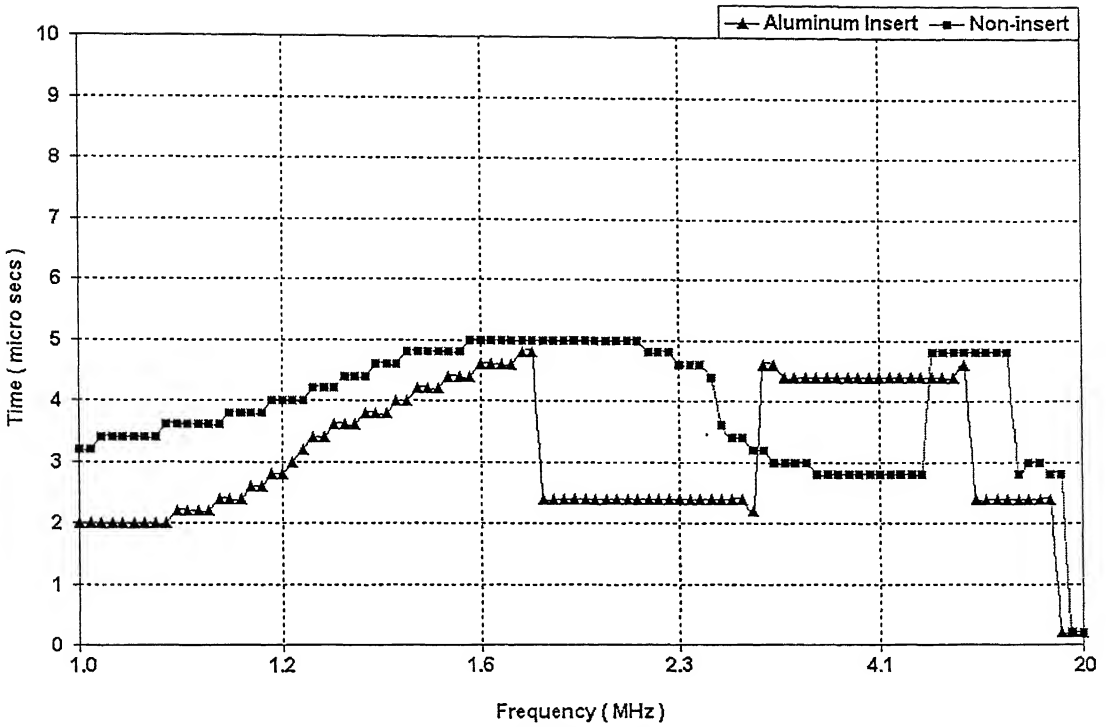

Fig.5.18 (c) Arrival time of frequencies for Aluminum insert sample

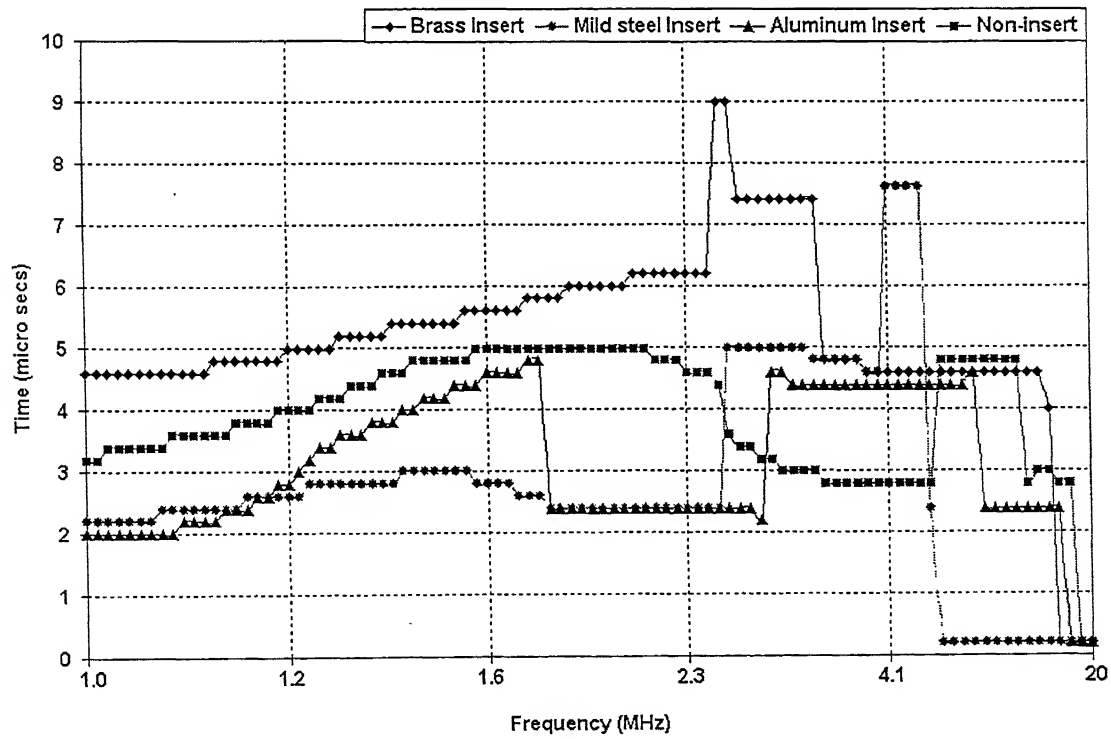

Fig.5.18 (d) Combined plot of arrival time of frequencies for composite samples

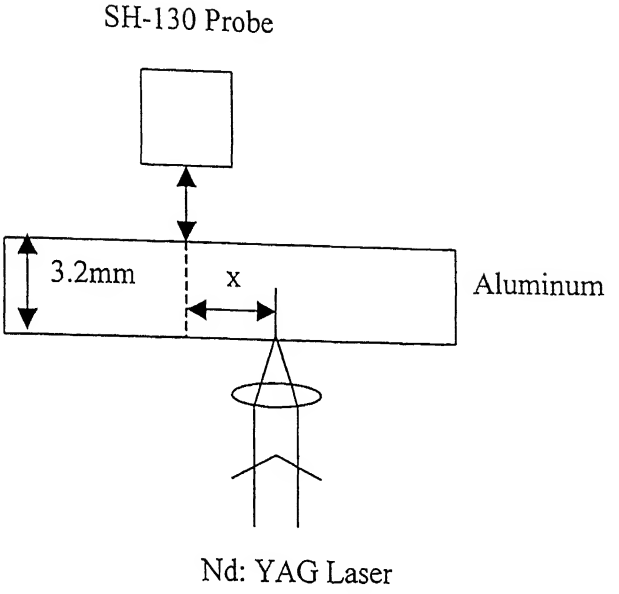

Fig.5.19 (a) Experimental set-up to obtain data at small distances off epicenter in Aluminum

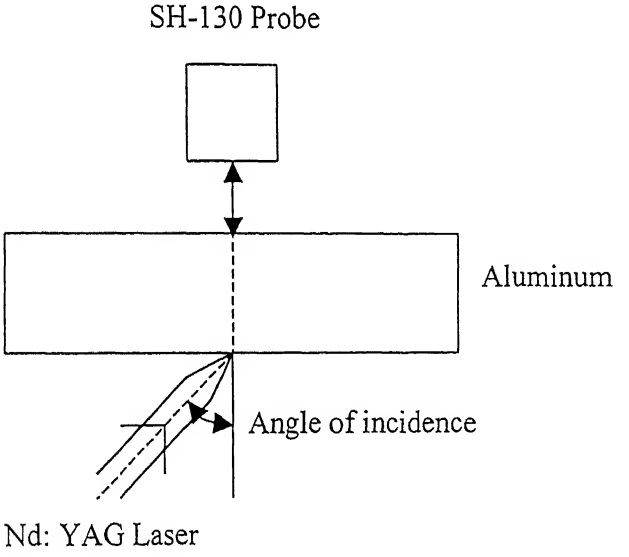

Fig.5.19 (b) Experimental set-up to obtain data at different angles in Aluminum

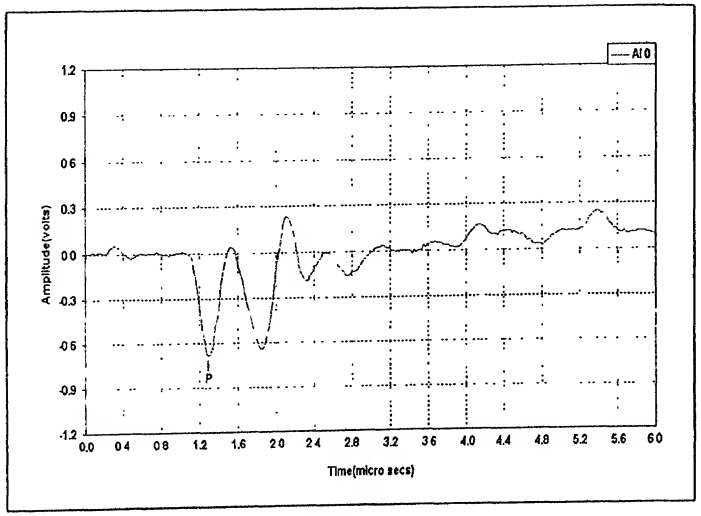

(a) 0mm

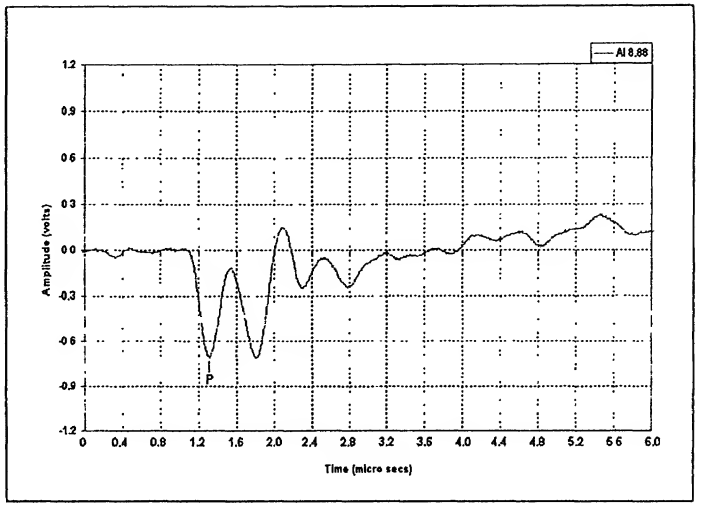

(b) 0.5mm

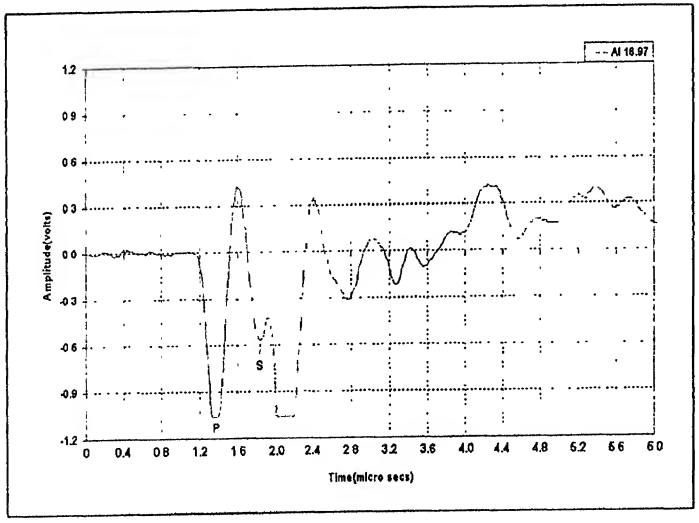

(c) 1.1mm

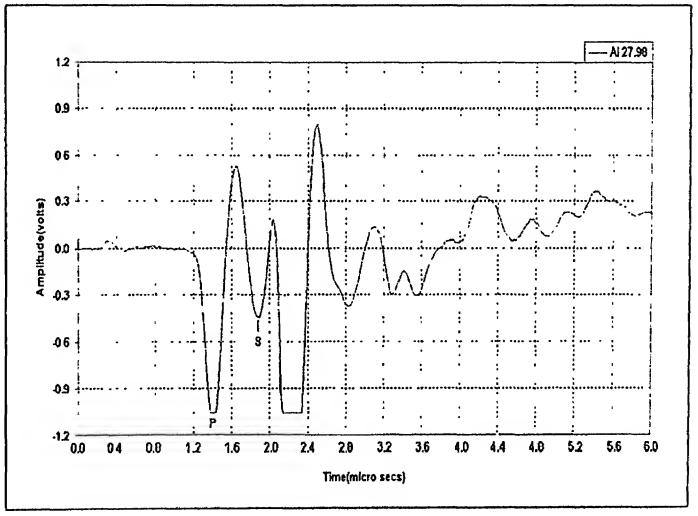

(d) 1.7mm

Figs.5.20 (a-d) Signals recorded at small distances off epicentre in aluminum

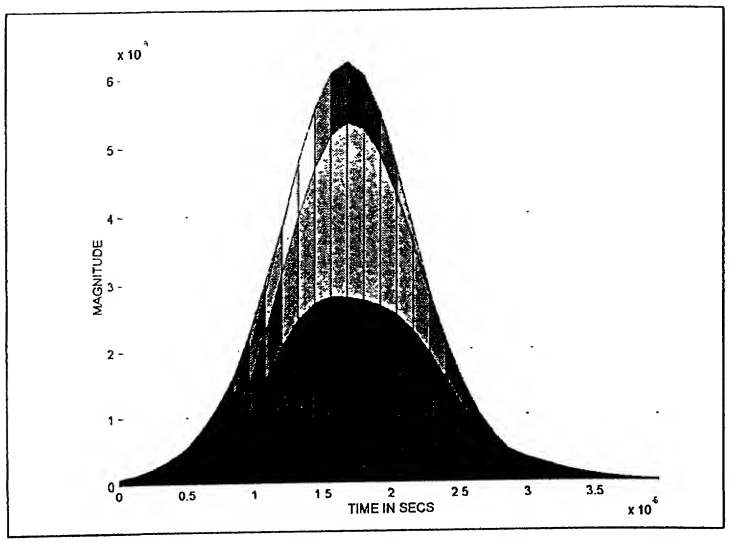

(a) 0mm

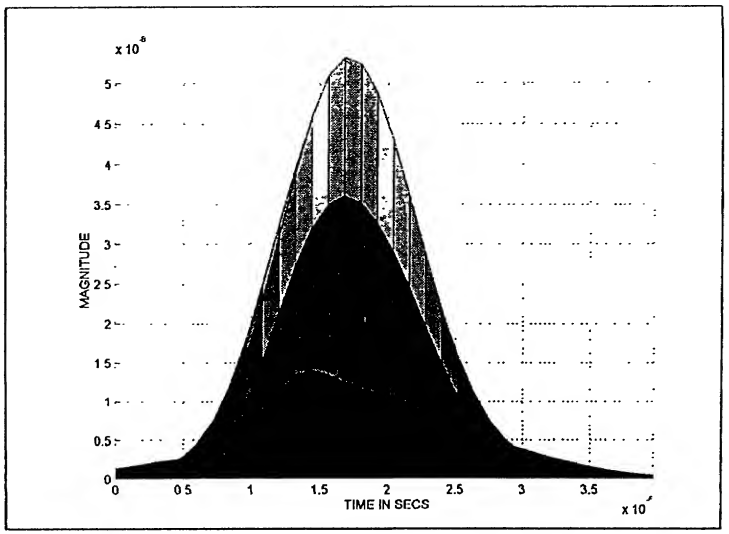

(b) 0.5mm

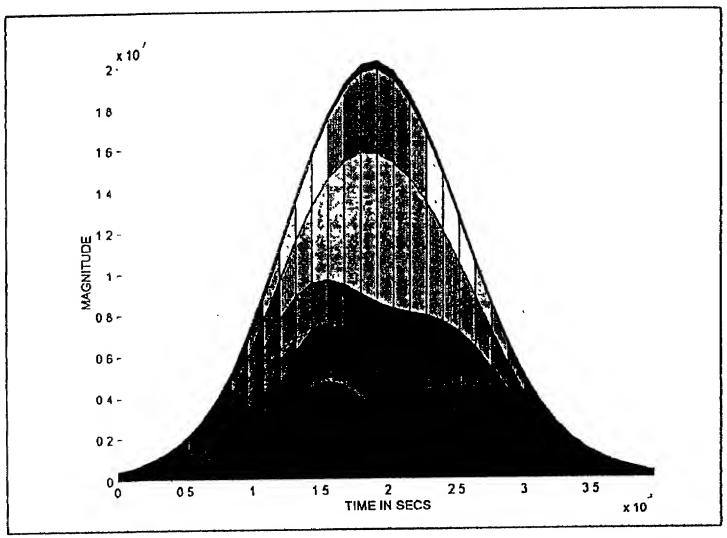

(c) 1.1mm

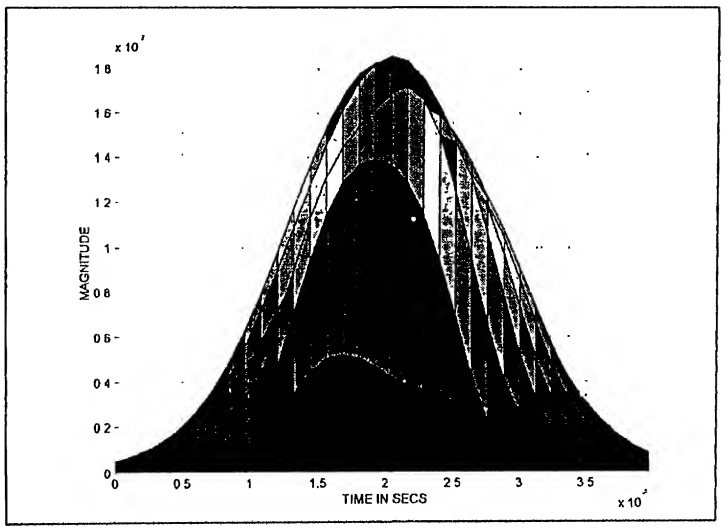

(d) 1.7mm

Figs.5.21 (a-d) Projected non-normalized scalograms on time-scalogram plane for different off-epicentre distances

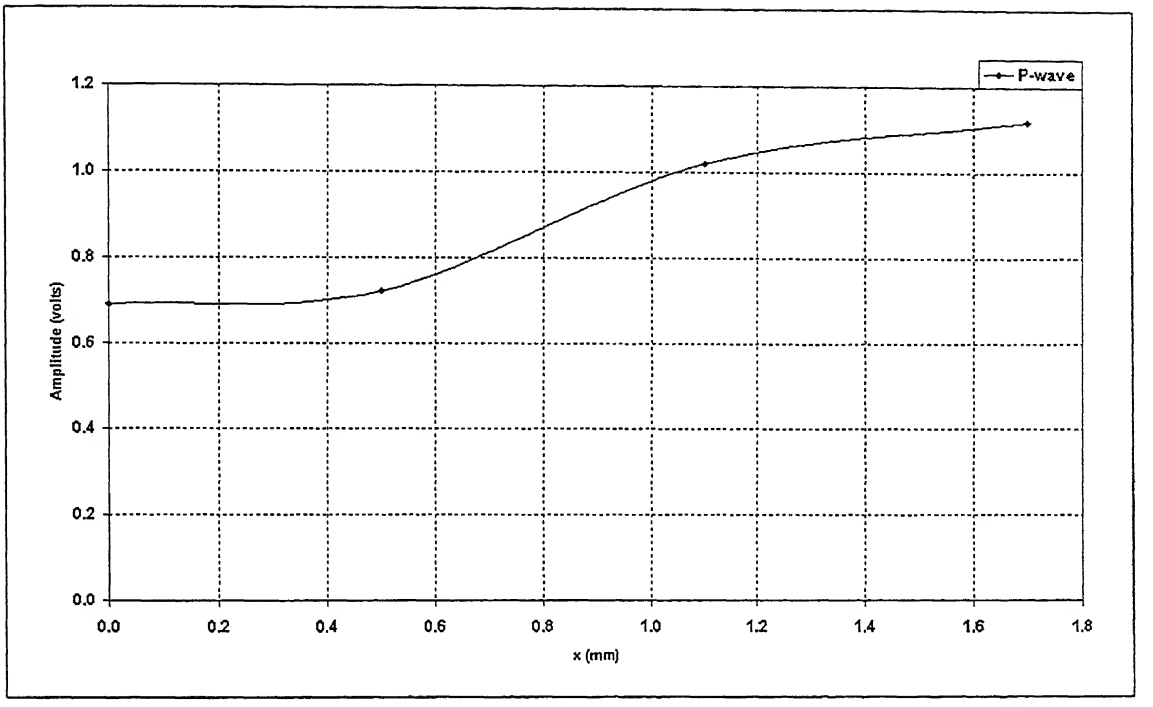

(a) P-wave

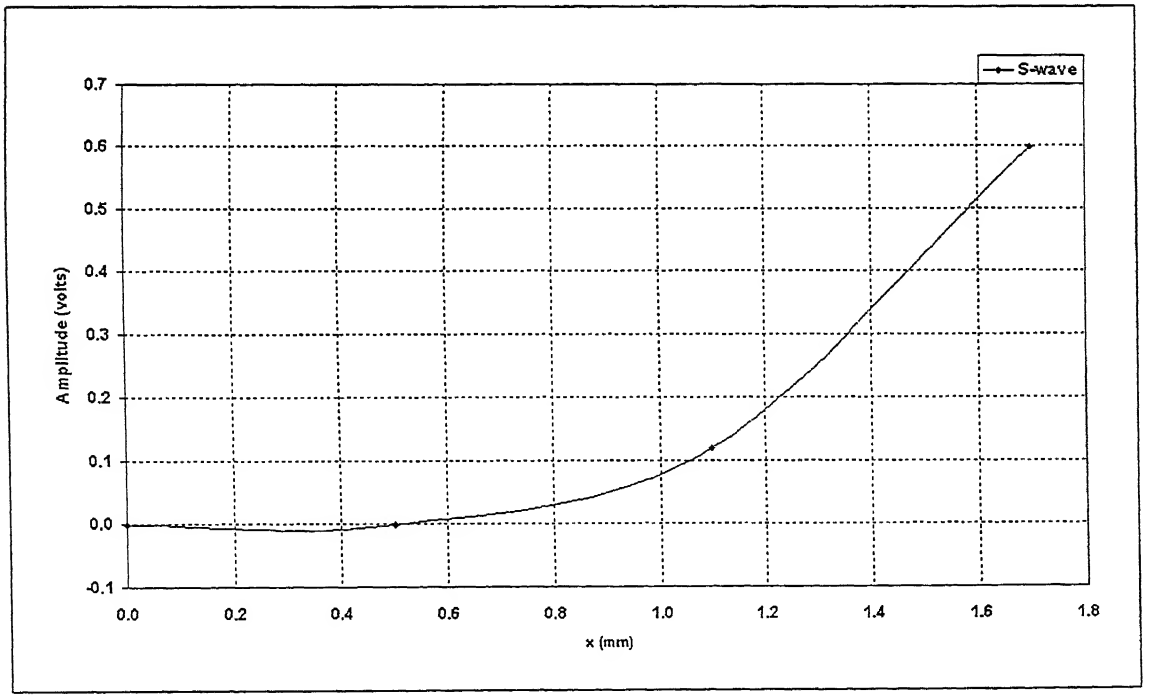

(b) S-wave

Figs.5.22 (a-b) Far-field P and S wave amplitudes in Aluminum as a function of distance (x) off epicentre

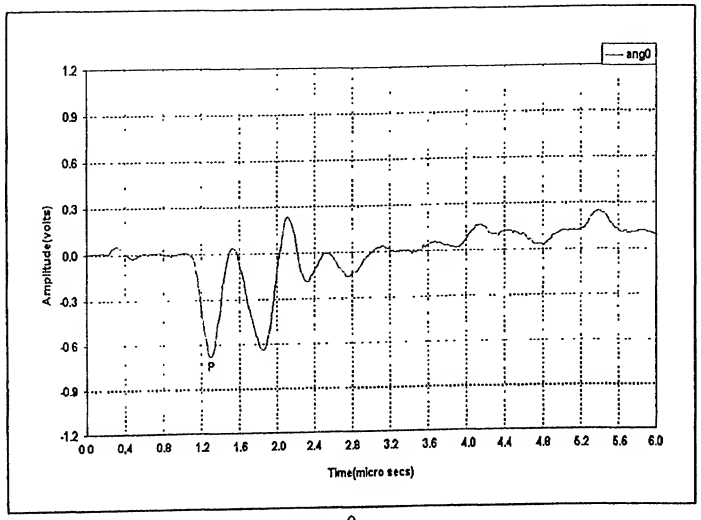

(a) 0^0

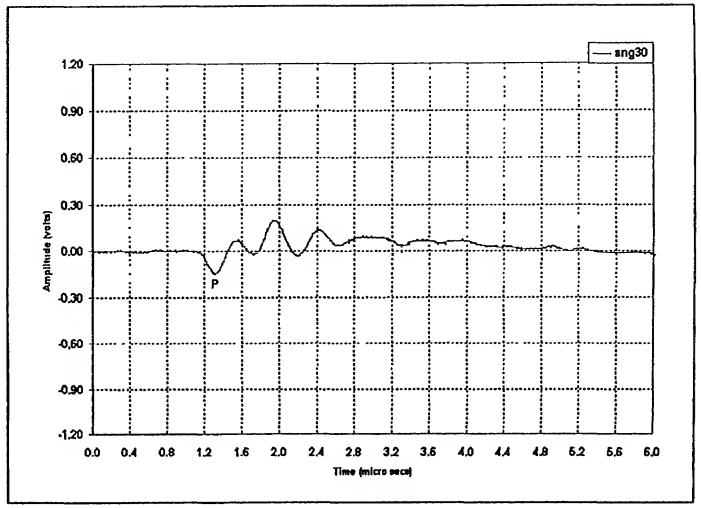

(b) 30^0

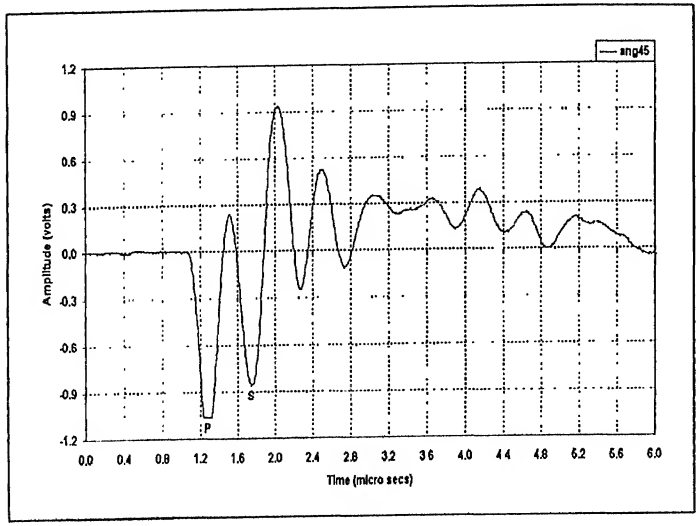

(c) 45^0

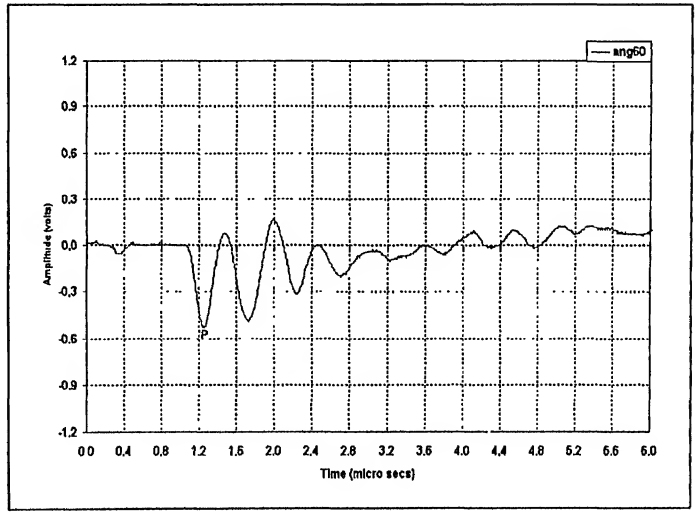

(d) 60^0

Figs.5.23 (a-d) Signals recorded for different orientations at epicentre in aluminum

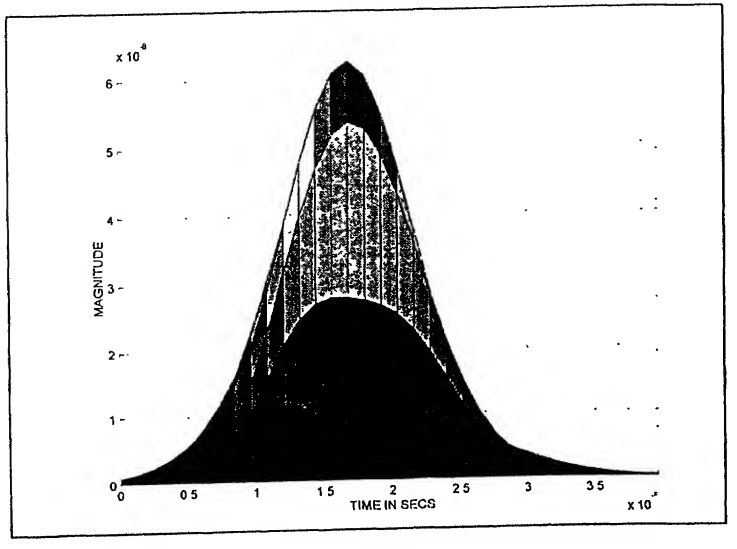

(a) 0^0

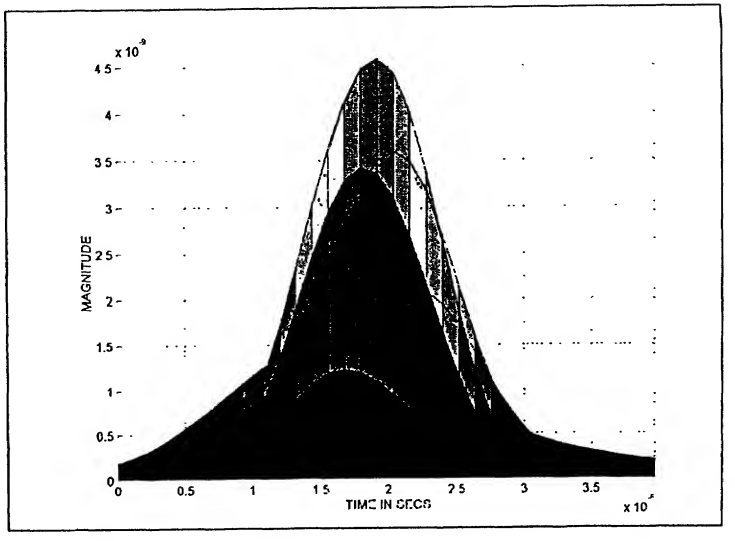

(b) 30^0

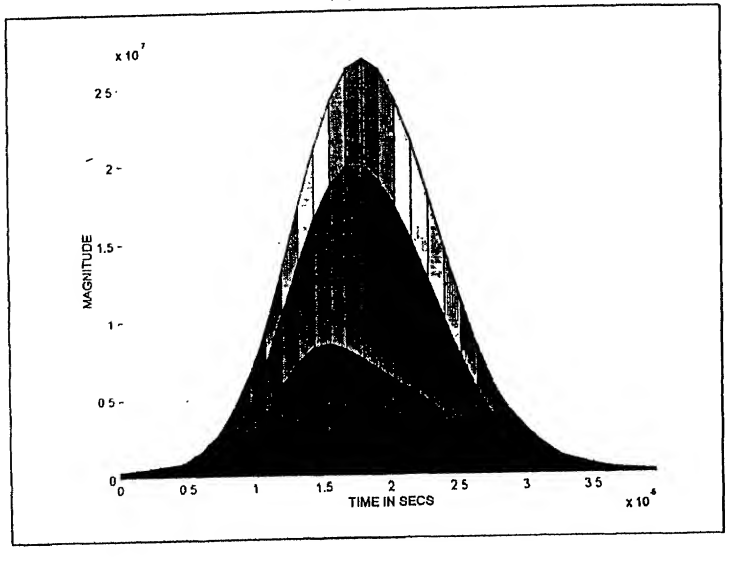

(c) 45^0

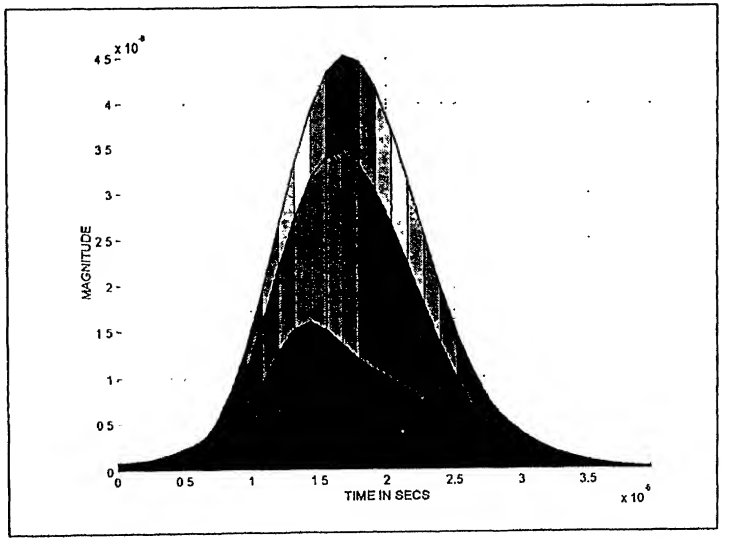

(d) 60^0

Figs.5.24 (a-d) Projected non-normalized scalograms on time-scalogram plane for different orientations

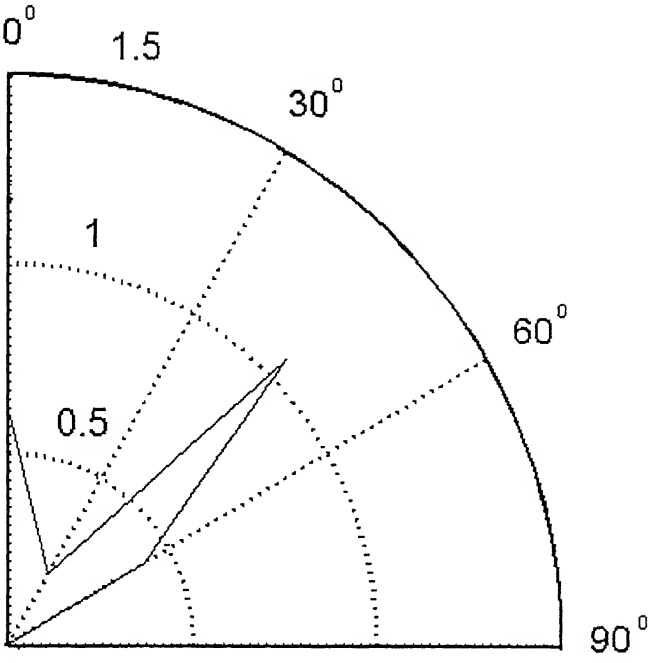

Fig.5.25 (a) P-wave amplitudes in aluminum as a function of angle of incidence

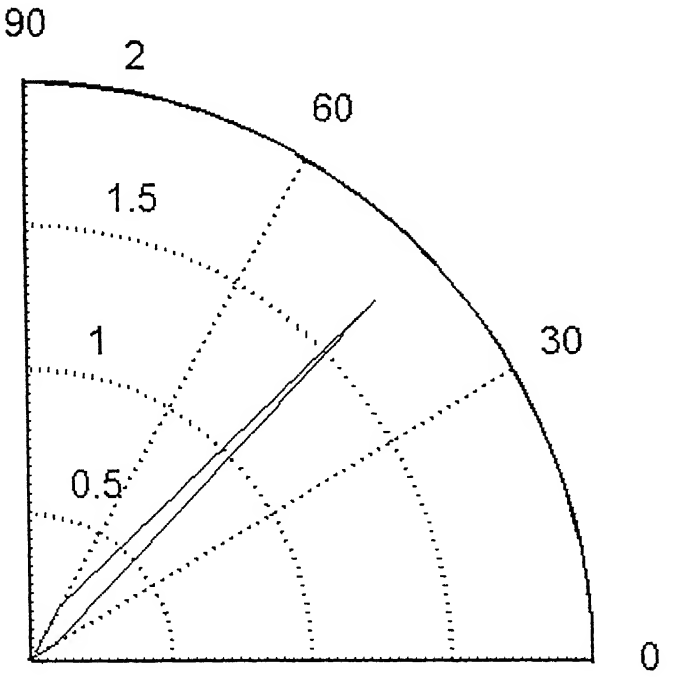

Fig.5.25 (b) S-wave amplitudes in aluminum as a function of angle of incidence

Chapter 6

CONCLUSIONS AND SCOPE FOR FUTURE WORK

6.1 CONCLUSIONS

In the present study of ultrasonic wave propagation in composite materials, a laser-based ultrasonic set-up consisting of an Nd: YAG pulsed laser for ultrasonic generation and a He-Ne laser-based Heterodyne optical interferometric probe for detection has been used. Artificially implanted defective composite specimens have been scanned using this set-up and the recorded signals are analyzed by wavelet transform (WT) with the Morlet wavelet. Based on the results obtained, the following conclusions are drawn:

(1) The wavelet transform with the Morlet wavelet is an effective tool for analyzing the wave propagation phenomena in composite materials. The WT provides an appropriate resolution for a wide range of frequency.

(2) The inspection of scalograms can reveal differences in the arrival time contours or frequency/amplitude characteristics, which indicate the presence of defects. Metal inserts in composite specimens have been identified by using the attenuation of high frequency components of the signal and the slope of the arrival time of a narrow band (i.e. 1-2-1.6 MHz) of the signal.

(3) The arrival times of P and S wave components in a signal can be identified from the known velocity of P and S waves in the material and the distance travelled through the material. The arrival times and amplitudes of P and S wave components have been identified in aluminum for different off-epicentre distances and for different angle of incidences for better application of the technique.

6.2 SCOPE FOR FUTURE WORK

(1) More experimental work on ultrasonic data collection of several material systems is necessary for any conclusive statement.

(2) Based on the results obtained from the arrival time contours, automation of the defect detection may be implemented.

(3) The method may be employed to damage identification and analysis of failures in composite laminates subjected to other tests.

(4) The potential of the phase of the signal in the wavelet domain may be explored.

References

[1] Krautkramer J. and Krautkramer H. "*Ultrasonic Testing of Materials*", 4th edition Springer-Verlag, New York, 1990.

[2] Neslroth J.B., Rose J.L., Bashyam M. and Subramanian K. "Physically based ultrasonic feature mapping for anomaly classification in composite materials", *Materials Evaluation*, 1985, Vol. 43, pp. 541-546.

[3] Rose J.L. "Elements of a feature-based ultrasonic inspection system", *Materials Evaluation*, 1984, Vol. 42, pp. 210-218.

[4] Datta D. "A Methodology in Ultrasonic NDE for identification and reconstruction of defects in fiber composites", *Ph.D. Thesis*, September 1995, Department of Mechanical Engineering, Indian Institute of Technology, Kanpur.

[5] Sarin P.S. "Development of laser-based ultrsonic Non-destructive testing", *M.Tech. Thesis*, January 2002, Department of Mechanical Engineering, Indian Institute of Technology, Kanpur.

[6] Daliraji G. "Experimental characterization of laser-based ultrasonic system", *M.Tech. Thesis*, February 2002, Department of Mechanical Engineering, Indian Institute of Technology, Kanpur.

[7] Scruby C.B. and Drain L.E. "*Laser Ultrasonics: Techniques and Applications*", Adam Hilger Bristol, Philadelphia, New York, 1990.

[8] Monchalin J.P. "Optical detection of ultrasound", *IEEE Transactions on Ultrasonics, Ferroelectrics, and Frequency control*, 5 September 1986, Vol. UFFC-33, No. 5, pp. 485-499.

[9] Corbel C., Guillois F., Royer D., Mathias A. Fink, and Rene DE Mol, "Laser-generated elastic waves in carbon-epoxy composites", *IEEE Transactions on Ultrasonics, Ferroelectrics, and Frequency Control*, November1993, Vol. 40, No. 6, pp. 710-716.

[10] Huang J., Nagata Y., Krishnaswamy S. and Achenbach J. D. "Laser Based Ultrasonics for flaw detection", *Ulrasonics Symposium IEEE* 1994, pp. 1205-1209.

[11] Castagnede B., Deschamps M., Mottay E. and Mourad A. " Laser impact generation of ultrasound in composite materials", April 1994, *Acta Acustica*, Vol. 2, pp. 83-93.

[12] Jeong H. "Analysis of plate wave propagation in anisotropic laminates using a wavelet transform", *NDT&E International* 2001, Vol. 34, pp. 185-190.

[13] Legendre S., Goyette J., and Massicotte D. "Ultrasonic NDE of composite material structures using wavelet coefficients", *NDT&E International* 2001, Vol. 34, pp. 31-37.

[14] Cho H., Ogawa S. and Takemoto M. "Non-Contact laser ultrasonics for detecting sub-surface lateral defects", *NDT&E International* 1996, Vol. 29, No. 5, pp.301-306.

[15] Yamawaki H., Saito T., Fukuhara H., Masuda C., Tanaka Y. "Non-contact ultrasonic imaging of sub-surface defects using a laser-ultrasonic technique", *J. Appl. Phys.*, May 1996, Vol. 35, pp. 3075-3079.

[16] Carlo F.M. "Independent component analysis and feature extraction techniques for NDT Data", *Materials Evaluation*, January 2000, pp. 85-92.

[17] Monchalin J.P., Neron C., Bussiere J.F. "Laser-ultrasonics: from the laboratory to shop floor", http://www.ultraoptec.com/

[18] Rathore S.K., Kishore N.N., Munshi P. and Arnold W. "Defect location and sizing using Laser-Based Ultrasonics (LBU)", Submitted for publication.

[19] Chan Y.T. "*Wavelet Basics*", Kluwer Academic Publishers. USA, 1995.

[20] Chui C.K. "*An Introduction to Wavelets*", San Diego, CA: Academic Press, 1992.

[21] Mallat S. "*A wavelet tour of signal processing*", 2nd Edition, San Diego, CA: Academic Press, 1999.

[22] Flandrin P. "*Time-Frequency/Time-scale Analysis*", Academic press, USA, 1999.

[23] Kishimoto K., Inoue H., Hamada M. and Shibuya T. "Time-frequency analysis of dispersive waves by means of wavelet transform", *J. Applied Mechanics*, December 1995, Vol. 62, pp. 841-846.

[24] Suzuki H., Kinjo T., Hayashi Y., Takemoto M. and Ono K. "Wavelet transform of acoustic emission signals", *J. Acoustic Emission*, 1996, Vol. 14, pp. 69-84.

[25] Abbate A., Koay J., Frankel J., Schroeder S.C. and Das P. "Signal detection and noise suppression using a wavelet transform signal processor: application to ultrasonic flaw detection", *IEEE Transactions on UFFC*, January 1997, Vol. 44, No.1, pp. 14-26.

[26] Safizadeh M.S., Lapine B.A., Forsyth D.S. and Fahr A. "Time-Frequency analysis Of pulsed eddy current signals", *Journal of Nondestructive Evaluation*, June 2001, Vol. 20, No. 2, pp. 73-86.

[27] Gaul L., Hurlebaus S. and Jacobs L.J. "Localization of a synthetic acoustic emission source on the surface of a fatigue specimen", *Research in Non-destructive Evaluation* (2001), pp. 105-117.

[28] Peterson M.L., Srinath S., Lambert T., Woodham D. and Schuller M. "Wavelet display of dispersion in concrete using Paul and Morlet wavelets", *Non-destructive Testing and Evaluation*, August 1998, Vol. 13, pp. 151-169.

Appendix A

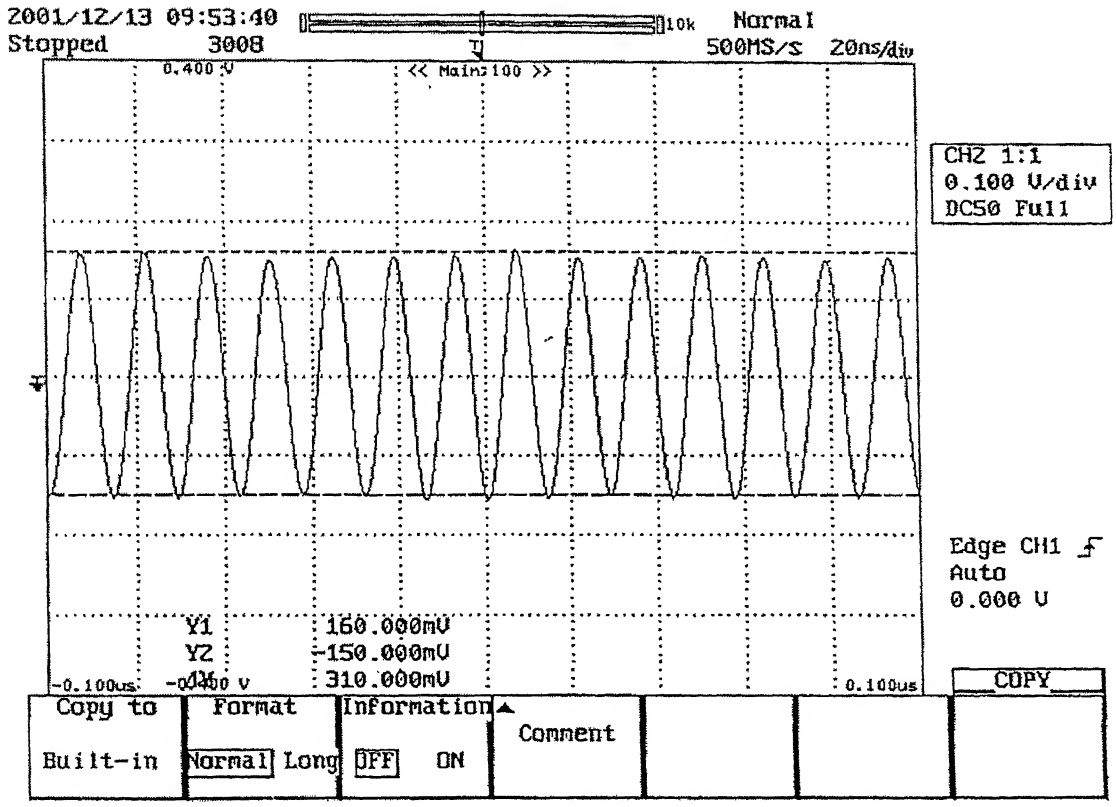

Photo Detector output measured without going through the Signal Processor.

Appendix B

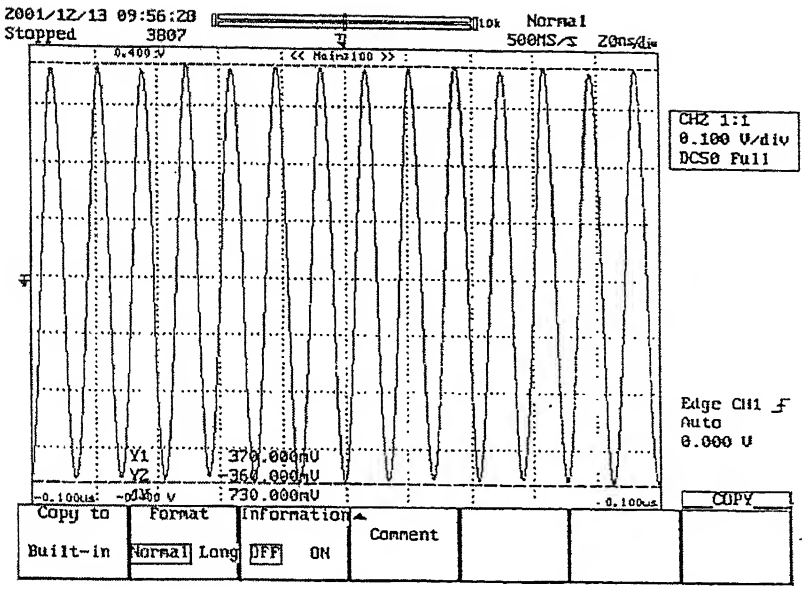

Output taken through the Signal Processor with the Automatic Gain Control switched ON

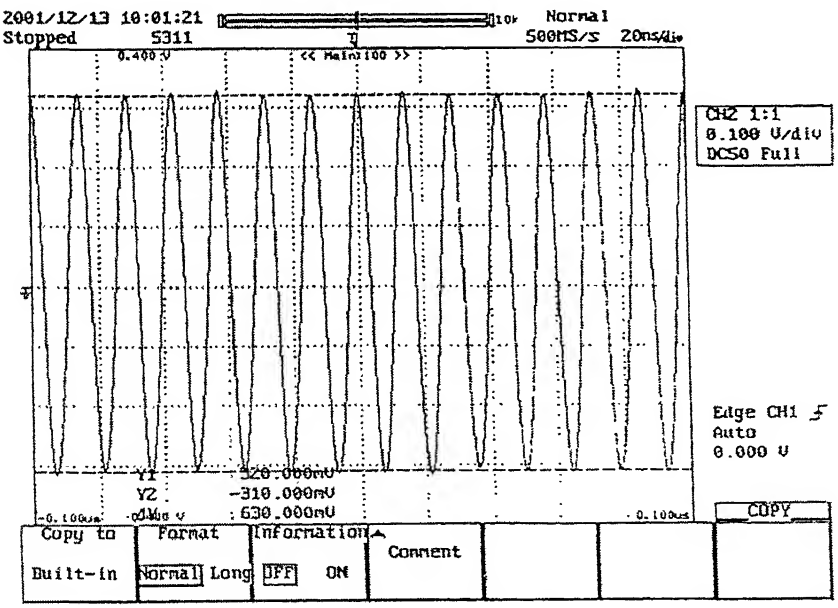

Output taken through the Signal Processor with the Automatic Gain Control switched ON after making adjustments available in the Signal-Processing Unit in order to set it to 630mv

Appendix C

% Matlab Program for 3-D Wavelet Scalogram plot and its projected contour

```
close all;
clear all;
%% Plotting real and imaginary part of the Morlet function
n=0;
for t=-5:0.01:5
   n=n+1;
   f(n)=exp(-t^2/2)*cos(2*pi*t);
   f1(n)=exp(-t^2/2)*sin(2*pi*t);
   y(n)=t;
end
plot(y,f,'k',y,f1,'b')
grid on
%% Reading the signal
FID=fopen(input('Enter the file name\n','s'));
 x= fscanf(FID,'%f',3000);
 %time=4.99e-9:4.99e-9:(0.5*4.99e-6);
 %time=4.99e-9:4.99e-9:4.99e-7;
 %time=4.99e-9:4.99e-9:4.99e-6;
 %time=4.99e-9:4.99e-9:9.98e-6;
 time=4.99e-9:4.99e-9:14.97e-6;
 %time=2e-8:2e-8:6e-5;
 %time=4.99e-9:4.99e-9:24.95e-6;
 %time=4.99e-9:4.99e-9:4.99e-5;
 kkk=length(time);
%% Input of scaling parameter
 i=[];
 for a=0:0.05e-6:5e-6
 %for a=0:0.12e-6:6e-6
 %for a=0:0.12e-6:24e-6
  i=[i;a];
 end
maxy=max(i);
normalisedi=i/maxy;
ii=length(i);
%% Input of translation parameter
j=[];
   %for b=0:9.98e-7:2.994e-5
   for b=0:2e-7:1e-5
   %for b=0:2e-6:1e-4
     j=[j;b];
  end
     jj=length(j);
```

```
%% Calculation of WT
W=zeros(ii,jj);
v=zeros(ii,jj);
for l=1:jj
 for k=1:ii
  aa=i(k);
  bb=j(l);
   if aa < 0
    z(k,l)=0;
   elseif aa == 0
     z(k,l)=0;
   else
    psi=zeros(kkk,1);
    ipsi=zeros(kkk,1);
    for kk=1:kkk
     psi(kk)= psi(kk)+exp(-((time(kk)-bb)/aa)^2/2)*cos(2*pi*(time(kk)-bb)/aa);
     ipsi(kk)= ipsi(kk)+exp(-((time(kk)-bb)/aa)^2/2)*sin(2*pi*(time(kk)-bb)/aa);
     %psi(kk)= psi(kk)+exp(-((time(kk)-bb)/aa)^2/2)*cos(5.43*(time(kk)-bb)/aa);
     %ipsi(kk)= ipsi(kk)+exp(-((time(kk)-bb)/aa)^2/2)*sin(5.43*(time(kk)-bb)/aa);
    end
%% Numerical Integration
    %W(k,l)=W(k,l)+2e-8*sum(x.*psi);
    %v(k,l)=v(k,l)+2e-8*sum(x.*ipsi);
    %W(k,l)=(1/sqrt(aa))*(W(k,l)-0.5*2e-8*(x(1)*psi(1)+x(kkk)*psi(kkk)));
    %v(k,l)=(1/sqrt(aa))*(v(k,l)-0.5*2e-8*(x(1)*ipsi(1)+x(kkk)*ipsi(kkk)));
    W(k,l)=W(k,l)+4.99e-9*sum(x.*psi);
    v(k,l)=v(k,l)+4.99e-9*sum(x.*ipsi);
    W(k,l)=(1/sqrt(aa))*(W(k,l)-0.5*4.99e-9*(x(1)*psi(1)+x(kkk)*psi(kkk)));
    v(k,l)=(1/sqrt(aa))*(v(k,l)-0.5*4.99e-9*(x(1)*ipsi(1)+x(kkk)*ipsi(kkk)));
%% Calculation of Scalogram (i.e. magnitude of WT)
    z(k,l)=W(k,l)*W(k,l)+v(k,l)*v(k,l);
   end
 end
end
mmaxi=max(z);
mmaxz=max(mmaxi)
[rrow,ccolumn]=find(z==mmaxz)
sscale=i(rrow)
ttime=j(ccolumn)
ffrequency=1/sscale
%% Conversion of time-scale representation to time-frequency representation
zz=zeros(ii,jj);
     for counter=1:ii
        for counter1=1:jj
           zz(counter,counter1)=zz(counter,counter1)+z(ii-counter+1,counter1);
        end
```

```
    end
    zzz=zeros(1,jj);
    zzz(1,:)=z(1,:);
    zzz=[zzz;zz];
    [nr,nc]=size(zzz);
    zzz(nr,:)=[];
%% Calculation of arrival time of frequencies
    maxi=max(zzz');
     col=[];
     for ct=2:201
        [rr,cc]=find(zzz==maxi(ct));
        col((ct-1))=cc;
     end
     coll=col';
     save pb1t coll -ascii;
     maxz=max(maxi)
     %[row,column]=find(zzz==maxz)
     %scale=i(row)
     %time=j(column)
     %frequency=1/scale
     normalisedz=zzz/maxz;
     %subplot(2,1,1)
%% Plotting 3-D surface
     axes('position',[.1  .165  .8  .6])
     surf(j,normalisedi,normalisedz)
     %surf(j,normalisedi,zzz)
     axis([0 inf 0 inf -3 1])
     title('WAVELET SCALOGRAM');
     xlabel('TIME IN SECS');
     ylabel('FREQUENCY IN MHz');
     zlabel('NORMALISED MAGNITUDE');
     grid off
     %axis('off')
%% Plotting projected contours
     axes('position',[.1  0  .8  .6])
     %hold on
     %subplot(2,1,2)
     contourf(j,normalisedi,normalisedz)
     %meshgrid(j,normalisedi);
     %contour3(zzz),view(0,90)
     %colorbar('h')
     view(3)
     axis('off')
     %colorbar('horiz')
```